Biophysics of Encapsidated DNA States in Viruses and their Role for Infectivity

by

Ting Liu

Submitted in partial fulfillment of the requirements for the
degree of Doctor of Philosophy

from

Carnegie Mellon University
Department of Biological Sciences
Pittsburgh, Pennsylvania

Aug.1st, 2016

Committee in charge:

Professor Alex Evilevitch, Chair
Professor Marcel Bruchez,
Professor Philip LeDuc,
Professor Gordon Rule
Professor Russell Schwartz

TABLE OF CONTENTS

LIST OF FIGURES

LIST OF TABLES

ACKNOWLEGEMENTS

I would like to give a huge appreciation to my doctoral advisor Dr. Alex Evilevitch, for all of his tremendous inspirations, insight, encouragement, patience, and dedication for taking me on a student and researcher during the past six years. It was truly my honor and blesses to be a student of Alex. I would also like to extend my thanks to all the coworkers in the group, Dr. Dong Li, Dr. Udom Sae-Ueng, Dr. Dave Bauer, Krista Freeman, Adi Das and Kaitlin Hamilton. I would also like to thank Dr. Carlos Catalano, Dr. Ulf Olsson, Dr. Marcel Bruchez, Dr. Fred Homa, Dr. Bernard Roizman, who have generously hosted me in their lab for a significant length of research. In addition, I would like to thank the members of my dissertation committee, Dr. Gordon Rule, Dr. Russell Schwartz, Dr. Marcel Bruchez, Dr. Philip LeDuc. All of them have provided unique insights that assisted me and provoked crucial questions during my research and this thesis. I would also like to thank Dr. Bruce McWilliams and the university for a generous gift of the McWilliams Presidential Fellowship I had from 2015 to 2016. Last and most special, I would like to thank my family, especially my dearest parents, my grandparents for their love, encouragement, and support.

Chapter 3, is a reprint of the material as it appears in: Liu T, Sae-Ueng U, Li D, Lander GC, Zuo X, Jönsson B, Rau D, Shefer I, Evilevitch A. "Solid-to-fluid-like DNA transition in viruses facilitates infection." Proc Natl Acad Sci USA. 111(41), 2014. The dissertation author was a primary researcher and co-first author of this paper. The AFM part of this work, done by Dr. Udom Sae-Ueng, was not presented in this thesis. The SXAS part of this work, was co-performed with Dr. Dong Li. The work was done with collaborator Dr. Xiaobing Zuo at Argonne National Lab, APS, for synchrotron x-ray studies.

Chapter 4, is a reprint of the material as it appears in: Li D, Liu T, Zuo X, Li T, Qiu

X, Evilevitch A. “Ionic switch controls the DNA state in phage λ” Nucleic Acids Res. 43(13), 2015. The dissertation author was a primary researcher and co-first author of this paper. All the SAXS work done in this Chapter was performed with Dr. Dong Li. The work was done with collaborator Dr. Xiaobing Zuo at Argonne National Lab, APS, for synchrotron x-ray studies.

Chapter 5, is a reprint of materials as it appears in a manuscript we prepared to submit. “Solid-to-fluid like DNA transition in the capsid controls heterogeneity of DNA ejection dynamics from phage.” The dissertation author was a primary researcher and author of this paper.

Chapter 6, is a reprint of materials as it appears in a manuscript we prepared to submit. “Osmotic pressure inhibits HSV-1 genome translocation into nucleus.” The dissertation author was a primary researcher and author of this paper. The work was done with collaborator Dr. Marcel Bruchez, Dr. Yi Wang at Carnegie Mellon University for fluorescence imaging, Dr. Bernard Roizman, Dr. Te Du at University of Chicago for quantitative PCR studies.

VITA

2009 Bachelor of Science, Zhejiang University

2009 Master of Science, University of Nebraska-Lincoln

2016 Doctor of Philosophy, Carnegie Mellon University

Publications

D. Li*, T. Liu*, X. Zuo, T. Li, X. Qiu, A. Evilevitch,"Ionic switch controls the DNA state in phage λ". Nucleic Acids Research, 2015, Jun 19.

T. Liu*, U. Sae-Ueng*, D. Li*, G. Lander, X. Zuo, B. Jönsson, D. Rau, I. Shefer, A. Evilevitch, "Solid-to-Fluid DNA Transition in Viruses Facilitates Infection". PNAS, 2014, Sep 30.

U. Sae-Ueng, T. Liu, C. Catalano, J. Huffman, F. Homa, A. Evilevitch, "Major capsid reinforcement by a minor protein in herpesviruses and phage". Nucleic Acids Research 2014, Jul 22.

ABSTRACT OF THE DISSERTATION

Biophysics of Encapsidated DNA States in Viruses and their Role for Infectivity

by

Ting Liu

Doctor of Philosophy in Biological Sciences

Professor Alex Evilevitch, Chair

Viruses typically consist of three fundamental components, a genetic material, either DNA or RNA; a protein shell, termed as the capsid; and in the case of many eukaryotic viruses, a third part made of lipid-coat and glycoproteins, known as the envelope. Viral replication cycles start with the delivery of its genetic material into the host cell cytoplasm or nucleoplasm, thus viral infectivity largely depends on its ability to: (i) effectively and efficiently translocate the genome into the host and (ii) protect its genome prior to infection and between rounds of replication. The main goal of this doctoral thesis is to understand how viral particles regulate its infectivity through altering its genome's physical states under different conditions, i.e. temperatures, ionic strength, osmotic pressure.

First, it was investigated that ejection of genome into its host is controlled by encapsidated genome states. In many double-stranded DNA bacterial viruses and herpesviruses, the tightly packaged and highly condensed DNA molecule is trapped in a glassy state with restricted molecular motion. The viral genome undergoes a solid-to-fluid-like disordering transition to increase its mobility or fluidity, which facilitates genome release. *Second,* it was shown that this structural transition strongly depends on physical parameters such osmotic pressure, temperature and ionic condition. Thus viral particle only gains the infectivity under right physical surroundings. There is striking evidence that the intra-capsid DNA transition can be switched "on" and "off" by mimicking those

medium conditions optimized and non-optimized *in vivo*.

All work in the first two steps was done on bacteriophages or type-1 herpes simplex virus (HSV-1) and viral DNA ejection was triggered by incubation with purified portal-binding receptor proteins or portal-targeted trypsin solutions. *Last*, the idea of tuning viral DNA states by physical parameters was applied to an advanced system reconstituted with isolated cellular nuclei and cytosol, in which HSV-1 were shown be docked onto nuclear membrane through nuclear pore complexes (NPC). DNA translocation into nucleoplasm was effectively inhibited by increasing osmotic pressure in the surrounding solution. These experiments entailed quantifying t he thermodynamics of DNA ejections from viral particles via calorimetric assays, structural studies of viral genome states via solution small-angle x-ray scattering, visualizing and quantifying DNA translocation process via fluorescence and electron microscopy imaging, in combination with real-time quantitative PCR methods. Results of these studies shed light on how viral particles regulate its genome infectivity and stability, as references for broad-spectrum anti-viral medicine research and development.

CHAPTER 1 INTRODUCTION

1.1 A touch of physical virology

Despite simplicity in structure, viruses exhibit extreme complexity in the sense of diversity and high mutation rates of genetic materials (*9*). One of the most often asked questions in healthcare is how many viruses on earth and more relevantly, how many out there are infectious to human. Yet there are no systematic and rigorous estimates of total viral diversity, a recent statistical study suggested a minimum number of 320,000 mammalian viral species (*10*). A typical anti-viral therapy would be exclusively developed against one viral species and aims to interrupt a target stage in viral replication cycles. For example, anti-Human immunodeficiency virus (HIV) drug "maravioc" acts by binding to the human cellular receptor of HIV and blocks the entry of the viruses; another important category of anti-HIV drugs are the nucleoside reverse transcriptase inhibitors (NRTI) which target blocking the HIV genome replication step (*11*). Because of the high biochemical specificity in these antiviral agents, they fail when virus mutates, known as "viral resistance". It was estimated that there are nearly 1016 HIV genomes existed today and very likely there might be HIV virions resistant to every one of the current therapies (*12*).

This highlights the motivation of physical virology, which seeks to define the less specified physical mechanisms in virion stability, maturation and replication (*13*). As the interest is in the general physical characteristics, viral systems of different evolutionary origins can be investigated and compared in this study, e.g. bacteriophage λ as an example of prokaryotic virus and type-1 human herpes simplex virus (HSV-1) as an example of eukaryotic virus. Results of this study may serve as new insights for broad-spectrum anti-viral medicines.

1.2 Phage λ and HSV-1

Both λ and HSV-1 contain double-stranded (ds-) DNA as their genetic material. A wild type (wt) λ is made of an icosahedral capsid of triangulation number T = 7 (*2*) and a genome of 48,502 bp (16.5 μm in geometric length). The capsid head is 63 nm in diameter with 1.8-4.1 nm thickness (*2*, *5*) (Figure 1.1). λ capsid is composed of 415 copies of the gpE protein (40 kDa) and 405-420 copies of the decoration protein (gpD, 11.4 kDa) at three-fold axes (*1*, *5*).

Unlike λ, HSV-1 consists of an outer membrane envelope decorated by glycoprotein spikes. Inside the lipid membrane there is an additional layer made of tegument proteins (*4*) and an isometric capsid of triangulation number T = 16. During maturation, HSV-1 forms three capsid types (A-, B-, C- capsid) (*7*), only one of which (C-form) is fully packaged with viral DNA. HSV-1 C capsid is 125 nm in diameter, with a shell thickness of 15 nm (*1*, *4*) (**Figure 1.1**). The capsid is made of major protein VP5 (149 kDa), decorated with: (i) a triplex formed by two copies of VP23 (34 kDa) and one copy of VP19c (50 kDa) at each three-fold axis; (ii) a theterodimer formed by UL17 (75 kDa) and UL25 (63 kDa) at each five-fold axis (*3*, *6*, *8*).

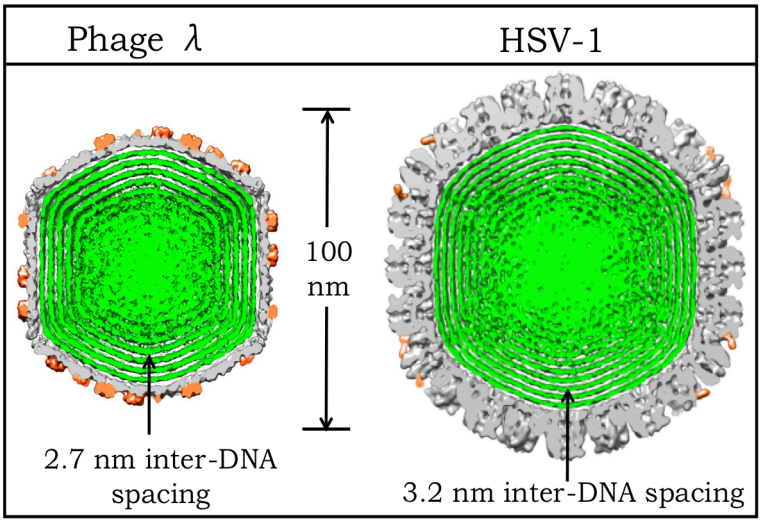

Figure 1.1 Comparison of λ capsid and HSV-1 capsid (DNA-filled). Both structures from cross-section of 3D-EM re-construction of viral particles (*1*). λ is 63 nm (with ~2-4 nm thickness) in dia-meter and HSV-1 is 125nm (with 15nm thickness). DNA inter-axial spacing is 2.7 nm in λ and 3.2 nm in HSV-1. λ genome is 48.5 kbp (16 μm) and HSV-1 genome is 152 kbp (52 μm) (*1-8*).

1.3 Forces on viral DNA inside capsid

Double stranded (ds-) DNA viruses package their genome to an extreme density, at about 500 mg/mL (*14*). Packaged DNAs are in a liquid crystal phase of hexagonally ordered structure. No other known biological system packaged DNA to similar density. Figure 1.2 shows three typical scenarios where DNA is subject to tight packing (*15*) in biological contents. Notice that in the first two scenarios where DNA was locally looped mediated by transcription factors (TFs) or condensed around histones, DNA was locally severely bent to a scale much smaller than its persistence length of 50nm (150bp) calculated using $\xi_p = \kappa/k_BT$ (where κ is the flexural rigidity of the polymer and k_BT defines the thermal energy scale)(*15*, *16*). The persistence length of DNA was defined as the scale over which DNA polymer could be spontaneous bent due to thermal fluctuations(*16*). Bending of DNA to a length scale much shorter than its persistence length (as shown in Figure 1.2A and 1B) would result a maximization of energy penalty due to DNA curvature.

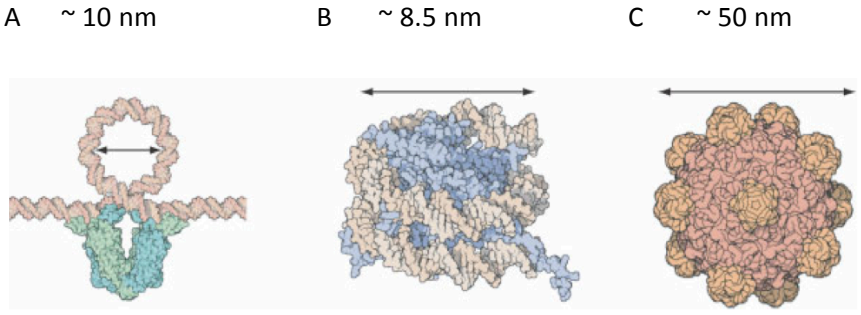

Figure 1.2 Examples of tightly bent DNA in biological contents: (A) DNA looping mediated by TFs; (B) DNA condensing in nucleosome. (C) DNA packaging in bacteriophages.

Genome structure in bacteriophages, on the other hand (Figure 1.2C), is a different scenario. A good number of ds-viruses have icosahedral capsid shells; most icosahedral viral capsids have diameters in the range of 30-100 nm, which means that the edge as well as the circumscribed radius would be 10 nm and longer. Viral genome is confined in this icosahedral container and its bending energy is dependent on the topology they adopt to fill the inside volume. Theoretical models were proposed as early as 1970s suggesting that DNAs were packaged to fit in these

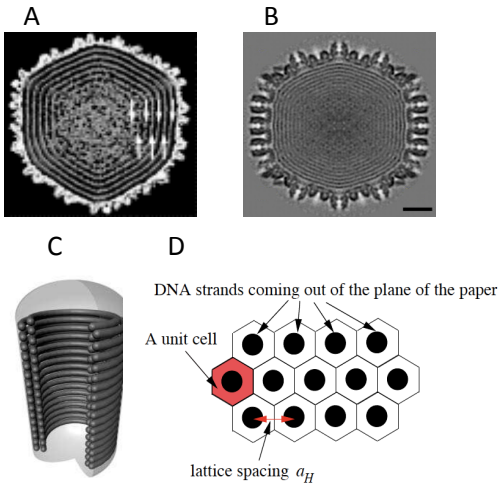

Figure 1.3 Viral DNA structure inside icosahedral capsid shells. (A) Central section of the three-dimensional reconstruction of phage P22 showing the concentric shells, the arrowheads indicate DNA toroid (18); (B) Central section of C-capsids with filled DNA of HSV-1 (19); (C) Inverse-spool model of packaged DNA inside viral capsid; (D) Hexagonal lattice formation by the DNA spool inside the capsid, black dots indicate side-cross section of viral DNAs (17).

icosahedral capsids either in the topology of "wound into a spool (can be interpreted as toroid with an angle to the asymmetric portal) " or "liquid crystal with hairpin defects (can be interpreted as toroid with hairpin defects to circumvent the asymmetric portal)" (*17-19*). Contemporary model of DNA topology inside the capsid was build upon cryo-electron microscopy (cryo-EM) experimental data, suggesting that DNAs adopt "inverse-spool" geometry (*20*, *21*), which means that viral DNA was axially wrapped in concentric shells of a hexagonal toroidal structure with its leading end (first end into the host cell during infection) either extending into the narrow portal channel or being cross-linked to the tail (see Figure 1.3 for visualization of encapsidated DNA structure) (*22*). The energy penalty of DNA curvature for encapsidated viral genomes is small for peripheral DNA loops (as shown in Figure 1.2). However, towards the core region of packaged DNA structure, acute bending of DNA happens, in the extend similar to TFs mediated acute DNA looping and packed nucleosome DNA. This change in bending forces was critical to induce a DNA transition, as revealed in later Chapter 2, where DNA has to re-organize itself to minimize the bending energy, leaving the core region disordered in a non-loop-like structure.

The interaxial DNA-DNA spacing of ds-DNA viral genome in a completely filled icosahedral capsid shell was estimated to be in the range of 20-30 Å, which means

that viral genomic DNA is at crystalline density (Figure 1.3) (7, 23). Unlike other biological systems where DNA is condensed (e.g. sperm DNA or chromosome DNA) and the repulsive interaction between DNA strands were offset by positively

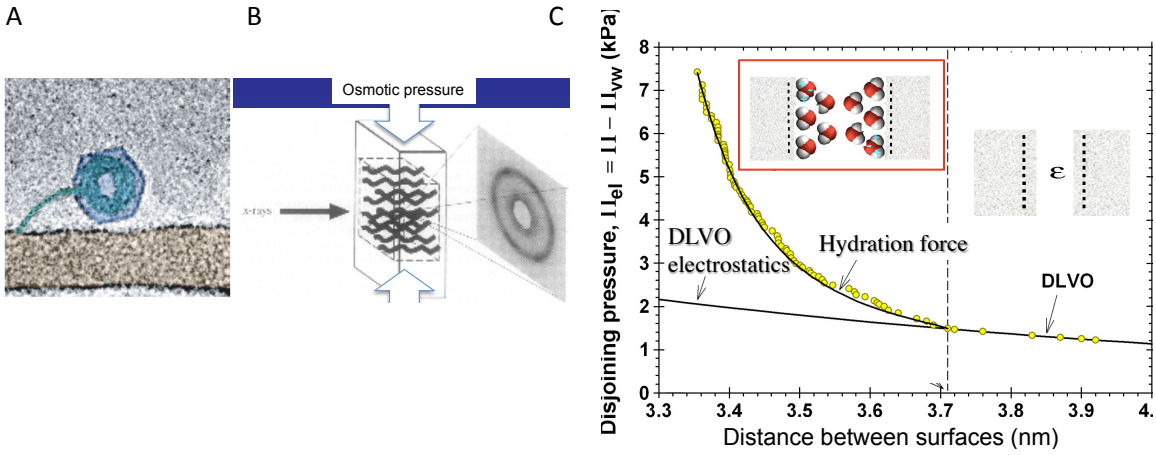

Figure 1.4 Hydration forces. (A) Cryoelectron micrograph of toroidally condensed DNA, note that DNA only occupies about 50-60% of the inner capsid volume and the rest of volume is occupied by water molecules (23); (B) The osmotic stress (OS) method to measure hydration forces: in this setup, linear polymers is equilibrated with a reservoir solution containing water and other small solutes, as well as a stressing polymer that is exluded from it. The excluding polymer controls the OS on the polymer phase and the spacing between polymers is measured using X-ray diffraction (6), generally it is perceived that when d_s is approaching around 20 to 30 Å, the corresponding OS represents the hydration forces in the system (22); (C) Pressure-distance curve using experimental setup shown in 3b, it can be seen that hydration force has a characteristic exponential repulsion which can not be explained by electro-static theories (6).

charged protruding residues of interacting proteins, viral genomic DNAs do not live in such a friendly neighborhood with counterion-charged mates.

The electrostatic interactions resulted from adjacent DNA strands have been identified as the dominant contributors to the internal pressure and internal energy of virus particles till the discovery of hydration forces (21, 24). Hydration forces, also named water structuring forces or water perturbation forces, can be understood as the energetic consequences of perturbing water layers structure as

two hydrated surfaces approach. As water forms hydrogen-bonded networks, the structuring of water layer by polar or nonpolar groups on a macromolecular surface is organized to have preferred orientations; however these organized water layers would be perturbed when two surfaces of macromolecules are brought into close proximity, the change in hydration energy of approaching molecules are defined as hydration forces (*25*, *26*). Hydration forces were discovered in force (or osmotic pressure) versus surface separation measurements in colloidal system with a characteristic exponential hydration-like repulsion (see Figure 1.4B and C), it is now generally accepted that when the distance between two surfaces (ds) approaches 20 to 30 Å or lower, hydration forces would dominate other electrostatic or electro-dynamic interactions (*26*, *27*). Considering DNA inside viral genome that has an interaxial spacing experimentally measured to be around 20-30 Å, it is in fact in a range where the dominant energy contributions are from hydration forces and in this particular setup, hydration force can be understood as the force required to remove a molecule of water from the vicinity of condensed DNA toroid to the bulk solution. It should be noted that DNA only occupies about 50-60% of the inner capsid volume in most viruses with icosahedral head geometry (Figure 1.4A); the rest of the inner capsid volume is occupied by bulk solution that consist of water molecules and small ions that are interchangeable between inside and outside of the capsid shells (*28*).

1.4 DNA in and out, who is the player

As a summary of what is being discussed in last section, the viral DNA molecule exerts a large internal pressure on the capsid due to: (i) Interaxial repulsive forces between neighboring DNA strands of extreme proximity (Figure 1). (ii) Acute bending force rising from intracapsid genome condensing (*29*). Bending of DNA to a length scale much shorter than its persistence length (42 ± 5 nm due to thermal fluctuation (*30*)) would result a maximization of energy penalty due to DNA curvature. (iii) Additional hydration forces by removal of water molecules from

their hydration layers between DNA helices (*31*).

The internal pressure had been experimentally confirmed for λ (*32*), SPP1 (*33*), T5 (*34*) and in HSV-1 (*35*). The estimated intracapsid pressure value is 20 atmosphere (atm) (*32*) in λ and 18 atm in HSV-1 C-capsid (*35*). The pressure was shown to be crucial for driving DNA ejection and counterpoising of this internal pressure by introducing osmolytes around external side of capsids result in complete suppression of genome ejection (*29*, *32*, *35*, *36*). Figure 1.2 shows similar pressure-driven ejection mechanism in λ and in HSV-1. Upon docking onto receptors on cellular (λ) or pore complexes on nuclear (HSV-1) membranes, DNA ejections are triggered in which highly condensed genome are released into the host content.

On the other hand, other physical parameters play as the counterpart in the ejection process. In vitro studies show polyamine spermidine can condense DNA segments to a similar degree as encapsidated viral DNA (*37*, *38*). These spermidine-condensed DNAs exhibit hexagonal order with restricted fluidity (*39*). It was illustrated experimentally (*40*, *41*) and theoretically (*42*) that frictional force between tightly-packed DNA segments would control the speed of ejection. Observations that ejection speed starts slow and gradually reaches maximum in the intermediate stage also supported the relationship between DNA density in the capsid and its friction (*43*).

However during viral infection, high DNA mobility is required to enable fast genome translocation. In bacteriophages, genome translocation step was reported to be highly efficient, in seconds scale into physiological buffer containing receptors and in minutes scale into living bacterial cells (*43*, *44*). The precise mechanism of viral DNA ejections remains largely unknown. During the ejection of phage T5 genome, T5 DNA undergoes a series of phase transitions. These DNA transitions introduce the necessary fluidity to the original constrained DNA state (*45*). But this

still does not explain the fast flow of DNA in the initial stage of genome ejection (*43*), as DNA was still in solid-like hexagonal phase and the frictional force was calculated to be highest (*43*).

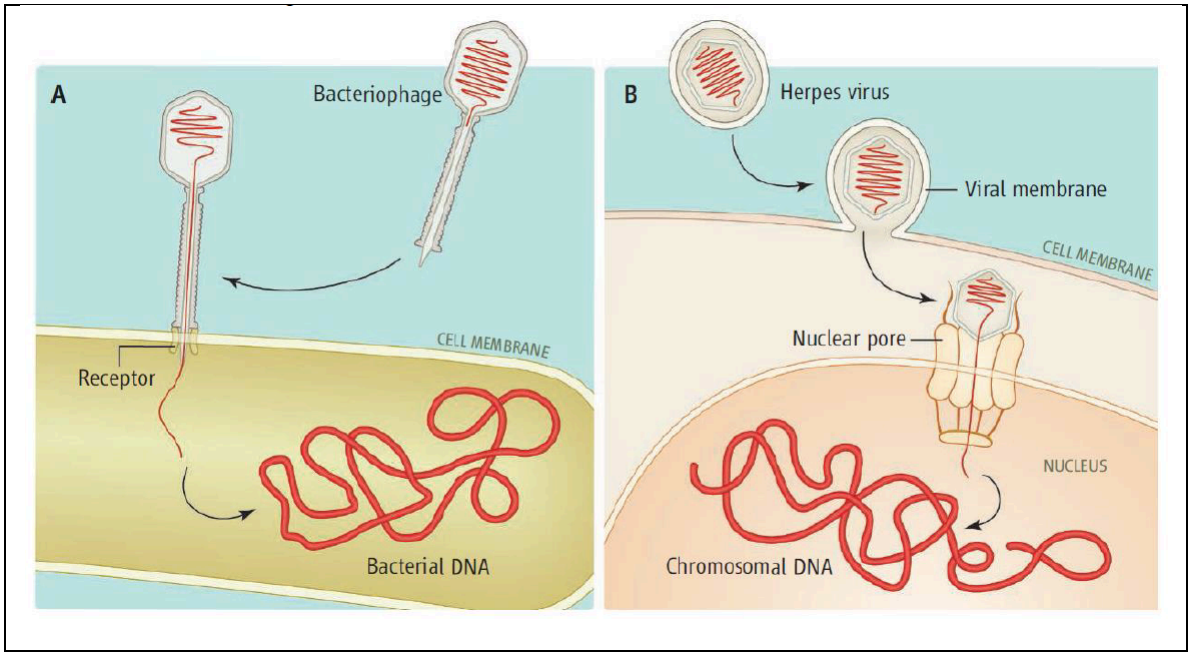

Figure 1.5 Cartoon illustration of DNA ejection process in λ (A) and in HSV-1 (B). λ ejects its genome into cytoplasm in comparison of HSV-1 genome releases into nucleoplasm. Image reproduced from Gelbart WM and Knobler CM, Science 2009 (*46*).

1.5 HSV-1 docking onto nuclear NPC

As mentioned in part 1.2, unlike λ, HSV-1 is an enveloped virus. HSV-1 entries the host cell by fusion of its lipid envelope with the plasma membrane (Figure 1.5A) and rapidly releases its capsid (with partial tegument proteins attached) into the cytosol (*47*). The capsid is then transported to proximity of nucleus via microtubule networks and docked specifically at the nuclear pore complexes (NPCs) (Figure 1.6). The EM images of the infection process using whole-cell fixation indicates that HSV-1 capsids start to appear at the nuclear pores at 2 h post-infection and within 4 h timeframe, 60% of those penetrated have successfully accumulated onto the nuclear

membrane (48). Once docked, HSV-1 genome rapidly releases into nucleoplasm, leaving empty capsids that are eventually released into the cytosol (48, 49) (Figure 1.6C). Interactions between HSV-1 capsid and NPC is specific, experiments show that HSV-1/2 ICP27 protein interact directly with the core nucleoporin Nup62 (50). Association between viral ICP27 and NPC-Nup62 also provides additional binding sites at the nuclear pore for ICP27 shuttling, while competing and inhibiting host cellular transport pathways (50).

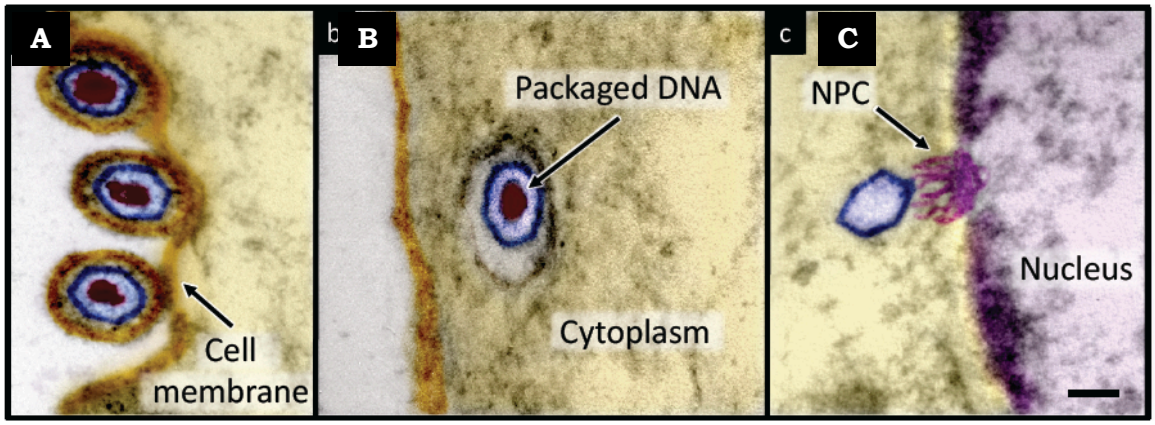

Figure 1.6 HSV-1 viral infection imaged by EM. After adsorbtion (A), the virions enter the cytoplasm of the host cell (B) and eventually docked onto the NPC on nuclear membrane (C). Figure reproduced from Bauer DW et al., JACS 2013 (35).

1.6 Core questions answered in this thesis

In this doctoral thesis, through careful experimental design and utilization of a variety of biophysical tools (Chapter 2), we aim to investigate the central problems of (i) How viral DNA transits into a state of higher fluidity and mobility during infection (Chapter 3 and 4), as challenges were proposed and stated in the introduction part 1.3. (ii) How particle regulates and adapts its genome state in response to different physical environments to maintain stability and gain mobility (Chapter 4 and 5). With all these core questions answered, we extend the biological contexts of these problems by applying physical parameters to a constructed isolated nuclei system, in which HSV-1 capsids were docked onto nuclear, we

showed that osmotic pressure outside the nuclei is effective in inhibiting DNA releases via nuclear pore and into the nucleoplasm (Chapter 6).

References for Chapter

1. U. Sae-Ueng *et al.*, Major capsid reinforcement by a minor protein in herpesviruses and phage. *Nucleic acids research* **42**, 9096-9107 (2014).
2. T. Dokland, H. Murialdo, Structural transitions during maturation of bacteriophage lambda capsids. *Journal of molecular biology* **233**, 682-694 (1993).
3. W. W. Newcomb *et al.*, Structure of the herpes simplex virus capsid. Molecular composition of the pentons and the triplexes. *Journal of molecular biology* **232**, 499-511 (1993).
4. Z. H. Zhou, D. H. Chen, J. Jakana, F. J. Rixon, W. Chiu, Visualization of tegument-capsid interactions and DNA in intact herpes simplex virus type 1 virions. *Journal of virology* **73**, 3210-3218 (1999).
5. F. Yang *et al.*, Novel fold and capsid-binding properties of the [lambda]-phage display platform protein gpD. *Nature structural & molecular biology* **7**, 230-237 (2000).
6. Z. H. Zhou *et al.*, Seeing the herpesvirus capsid at 8.5 A. *Science* **288**, 877-880 (2000).
7. B. L. Trus *et al.*, Allosteric signaling and a nuclear exit strategy: binding of UL25/UL17 heterodimers to DNA-Filled HSV-1 capsids. *Molecular cell* **26**, 479-489 (2007).
8. S. K. Cockrell, M. E. Sanchez, A. Erazo, F. L. Homa, Role of the UL25 protein in herpes simplex virus DNA encapsidation. *Journal of virology* **83**, 47-57 (2009).
9. E. Nurmemmedov, M. Castelnovo, E. Medina, C. E. Catalano, A. Evilevitch, Challenging packaging limits and infectivity of phage lambda. *Journal of molecular biology* **415**, 263-273 (2012).
10. S. J. Anthony *et al.*, A strategy to estimate unknown viral diversity in mammals. *MBio* **4**, e00598-00513 (2013).
11. J. A. Levy, HIV pathogenesis: 25 years of progress and persistent challenges.

AIDS **23**, 147-160 (2009).

12. S. J. Flint, American Society for Microbiology., *Principles of virology*. (ASM Press, Washington, DC, ed. 3rd, 2009).
13. A. M. Wen, P. H. Rambhia, R. H. French, N. F. Steinmetz, Design rules for nanomedical engineering: from physical virology to the applications of virus-based materials in medicine. *J Biol Phys* **39**, 301-325 (2013).
14. I. J. Molineux, D. Panja, Popping the cork: mechanisms of phage genome ejection. *Nat Rev Microbiol* **11**, 194-204 (2013).
15. H. G. Garcia *et al.*, Biological consequences of tightly bent DNA: the other life of a macromolecular celebrity. *Biopolymers* **85**, 115-130 (2007).
16. D. H. Boal, *Mechanics of the cell*. (Cambridge University Press, Cambridge, UK ; New York, 2002), pp. xiv, 406 p.
17. S. C. Riemer, V. A. Bloomfield, Packaging of DNA in bacteriophage heads: some considerations on energetics. *Biopolymers* **17**, 785-794 (1978).
18. L. W. Black, DNA packaging in dsDNA bacteriophages. *Annual review of microbiology* **43**, 267-292 (1989).
19. P. Serwer, Arrangement of double-stranded DNA packaged in bacteriophage capsids. An alternative model. *Journal of molecular biology* **190**, 509-512 (1986).
20. N. V. Hud, K. H. Downing, Cryoelectron microscopy of lambda phage DNA condensates in vitreous ice: the fine structure of DNA toroids. *Proceedings of the National Academy of Sciences of the United States of America* **98**, 14925-14930 (2001).
21. D. E. Smith *et al.*, The bacteriophage straight phi29 portal motor can package DNA against a large internal force. *Nature* **413**, 748-752 (2001).
22. P. K. Purohit *et al.*, Forces during bacteriophage DNA packaging and ejection. *Biophysical journal* **88**, 851-866 (2005).
23. Z. Zhang *et al.*, Visualization of the maturation transition in bacteriophage P22 by electron cryomicroscopy. *Journal of molecular biology* **297**, 615-626

(2000).

24. D. N. Fuller *et al.*, Measurements of single DNA molecule packaging dynamics in bacteriophage lambda reveal high forces, high motor processivity, and capsid transformations. *Journal of molecular biology* **373**, 1113-1122 (2007).
25. J. X. Cheng, S. Pautot, D. A. Weitz, X. S. Xie, Ordering of water molecules between phospholipid bilayers visualized by coherent anti-Stokes Raman scattering microscopy. *Proceedings of the National Academy of Sciences of the United States of America* **100**, 9826-9830 (2003).
26. S. Leikin, V. A. Parsegian, D. C. Rau, R. P. Rand, Hydration forces. *Annual review of physical chemistry* **44**, 369-395 (1993).
27. J. Faraudo, F. Bresme, Origin of the short-range, strong repulsive force between ionic surfactant layers. *Physical review letters* **94**, 077802 (2005).
28. E. Nurmemmedov, M. Castelnovo, C. E. Catalano, A. Evilevitch, Biophysics of viral infectivity: matching genome length with capsid size. *Quarterly reviews of biophysics* **40**, 327-356 (2007).
29. A. Evilevitch *et al.*, Effects of salt concentrations and bending energy on the extent of ejection of phage genomes. *Biophysical journal* **94**, 1110-1120 (2008).
30. J. Marek *et al.*, Interactive measurement and characterization of DNA molecules by analysis of AFM images. *Cytometry A* **63**, 87-93 (2005).
31. D. C. Rau, B. Lee, V. A. Parsegian, Measurement of the Repulsive Force between Poly-Electrolyte Molecules in Ionic Solution - Hydration Forces between Parallel DNA Double Helices. *P Natl Acad Sci-Biol* **81**, 2621-2625 (1984).
32. A. Evilevitch, L. Lavelle, C. M. Knobler, E. Raspaud, W. M. Gelbart, Osmotic pressure inhibition of DNA ejection from phage. *Proceedings of the National Academy of Sciences of the United States of America* **100**, 9292-9295 (2003).
33. C. Sao-Jose, M. de Frutos, E. Raspaud, M. A. Santos, P. Tavares, Pressure built by DNA packing inside virions: enough to drive DNA ejection in vitro, largely

insufficient for delivery into the bacterial cytoplasm. *Journal of molecular biology* **374**, 346-355 (2007).

34. A. Leforestier *et al.*, Bacteriophage T5 DNA ejection under pressure. *Journal of molecular biology* **384**, 730-739 (2008).
35. D. W. Bauer, J. B. Huffman, F. L. Homa, A. Evilevitch, Herpes virus genome, the pressure is on. *J Am Chem Soc* **135**, 11216-11221 (2013).
36. A. Evilevitch *et al.*, Effects of salts on internal DNA pressure and mechanical properties of phage capsids. *Journal of molecular biology* **405**, 18-23 (2011).
37. L. C. Gosule, J. A. Schellman, Compact form of DNA induced by spermidine. *Nature* **259**, 333-335 (1976).
38. M. Saminathan, T. Thomas, A. Shirahata, C. K. Pillai, T. J. Thomas, Polyamine structural effects on the induction and stabilization of liquid crystalline DNA: potential applications to DNA packaging, gene therapy and polyamine therapeutics. *Nucleic acids research* **30**, 3722-3731 (2002).
39. J. Pelta, Jr., D. Durand, J. Doucet, F. Livolant, DNA mesophases induced by spermidine: structural properties and biological implications. *Biophysical journal* **71**, 48-63 (1996).
40. D. Lof, K. Schillen, B. Jonsson, A. Evilevitch, Forces controlling the rate of DNA ejection from phage lambda. *Journal of molecular biology* **368**, 55-65 (2007).
41. T. Liu *et al.*, Solid-to-fluid-like DNA transition in viruses facilitates infection. *Proceedings of the National Academy of Sciences of the United States of America* **111**, 14675-14680 (2014).
42. I. S. Gabashvili, A. Grosberg, Dynamics of double stranded DNA reptation from bacteriophage. *Journal of biomolecular structure & dynamics* **9**, 911-920 (1992).
43. P. Grayson, L. Han, T. Winther, R. Phillips, Real-time observations of single bacteriophage lambda DNA ejections in vitro. *Proceedings of the National Academy of Sciences of the United States of America* **104**, 14652-14657 (2007).

44. D. Van Valen *et al.*, A single-molecule Hershey-Chase experiment. *Current biology : CB* **22**, 1339-1343 (2012).
45. A. Leforestier, F. Livolant, The bacteriophage genome undergoes a succession of intracapsid phase transitions upon DNA ejection. *Journal of molecular biology* **396**, 384-395 (2010).
46. W. M. Gelbart, C. M. Knobler, Pressurized Viruses. *Science* **323**, 1682-1683 (2009).
47. P. M. Ojala, B. Sodeik, M. W. Ebersold, U. Kutay, A. Helenius, Herpes simplex virus type 1 entry into host cells: reconstitution of capsid binding and uncoating at the nuclear pore complex in vitro. *Molecular and cellular biology* **20**, 4922-4931 (2000).
48. B. Sodeik, M. W. Ebersold, A. Helenius, Microtubule-mediated transport of incoming herpes simplex virus 1 capsids to the nucleus. *J Cell Biol* **136**, 1007-1021 (1997).
49. M. Tognon, D. Furlong, A. J. Conley, B. Roizman, Molecular genetics of herpes simplex virus. V. Characterization of a mutant defective in ability to form plaques at low temperatures and in a viral fraction which prevents accumulation of coreless capsids at nuclear pores late in infection. *Journal of virology* **40**, 870-880 (1981).
50. P. Malik *et al.*, Herpes simplex virus ICP27 protein directly interacts with the nuclear pore complex through Nup62, inhibiting host nucleocytoplasmic transport pathways. *The Journal of biological chemistry* **287**, 12277-12292 (2012).

CHAPTER 2 GENERAL EXPERIMENTAL DESIGN AND METHODS

2.1 Abstract

In this chapter, the general methodology and techniques applied in the thesis was introduced here. Isothermal titration calorimetry (ITC) was used to measure the energy contained in the encapsidated viral genome; solution small-angle x-ray scattering (SAXS) was used to investigate the ordered DNA structure inside viral capsid; confocal laser scanning microscopy (CLSM) was used to visualize bulk viral DNA ejection *in vitro*. A reconstituted system was applied to visualize and quantify HSV-1 DNA ejection into the nucleus. Quantitative PCR (q-PCR) assay was used to quantify the copy number of viral DNA ejected. Note that this is a general method section. More details of experimental design for different aims, reagents and samples, smaller assays used were later explained in each individual section.

2.2 Thermo-energy profile by microcalorimetry

To study the DNA state inside viral capsids, we first investigated the energy profile of en-capsidated viral genome. Isothermal titration calorimetry (ITC) was used to measure the ejection enthalpy and internal energy of λ genome. All ITC measurements in this study were performed using the MicroCal iTC200 system manufactured by GE Healthcare, Life Sciences. The principles of measuring DNA ejection enthalpy in phages λ were described in previous work published in the group (*1*). In ITC experiment, 2.69375 μL λ particles at 5 - 6×10^{12} pfu/mL (8 - 10nM) were titrated into 200 μL LamB solution in the sample cell (reference cell was always filled with MilliQ water) (Figure 2.1A). LamB was at a concentration of 0.2 - 0.5 mg/mL (1.4 - 3.5 μM). The molar ratio between LamB trimmers and λ particles in the sample cell was always kept above 104:1 (up to 3 titrations) to ensure the maximum ejection efficiency of λ with no delay time. Both LamB and λ particles were in the same dilution buffer containing TM (10 mM MgCl2 or MgSO4, as indicated, 50 mM Tris, pH7.4) and 1% oPOE. The dilution heat of phage particles,

LamB particles were measured separately and excluded from the final value of Figure 2.1B shows the ITC titration peaks from titrating phage solution into buffer and titrating phage solution into LamB solution. Integration of the area under the peak over time yields the reaction enthalpy, ΔH_{ej}.

Note that ΔH_{ej} measured in this method consists of other heat contributions such as pressure-volume work (pV-work), dilution heat of phage particles, dilution heat of LamB proteins. These additional heat sources that are not from the enthalpy of DNA translocation are measured separately by titrating phage into buffer, buffer into LamB solution, and buffer into buffer. Then being subtracted from the total enthalpy change using:

$$\Delta H_{ej} = \Delta H_{phage\ into\ LamB} - \Delta H_{phage\ into\ buffer} - \Delta H_{buffer\ into\ LamB} + \Delta H_{buffer\ into\ buffer}$$

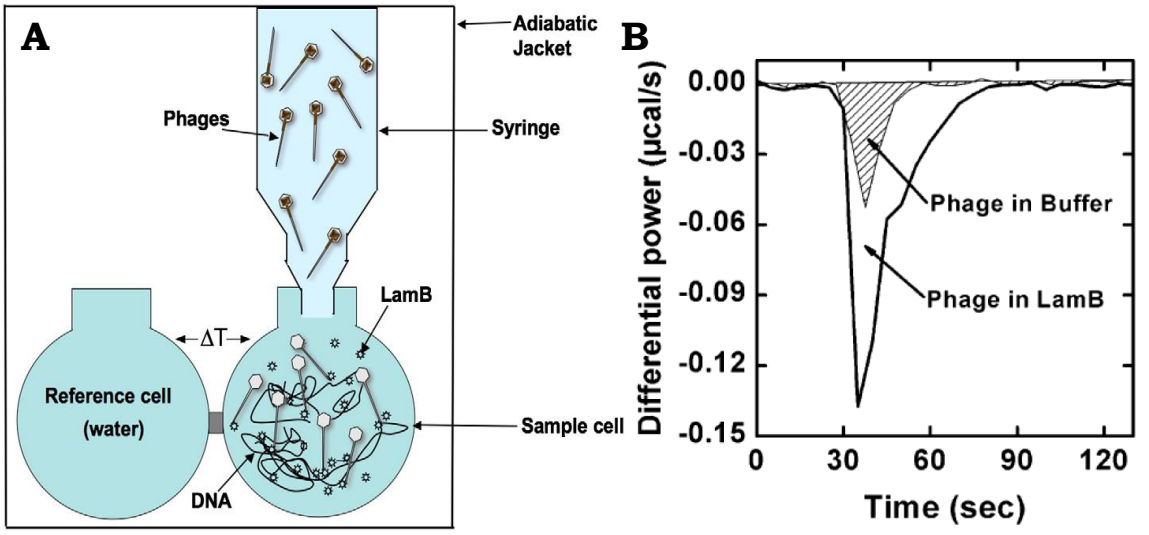

Figure 2.1 Measuring DNA ejection heat by isothermal titration calorimetry. (A) schematic illustration of the ITC setup. Purified λ particles were titrated into sample cell filled with receptor proteins. Upon binding to receptors, λ quickly releases its genome into the solution, and the heat associated with the process, known as the ejection entropy, was recorded. Figure re-produced from Jeembaeva M et al., JMB 2010 (*1*). (B) Isothermal titration calorimetry (ITC) titrations of phage λ to LamB and phage λ to buffer. Ionic conditions were 10 mM MgCl2, 50 mM Tris·HCl (pH 7.4) at 37°C. Differential power (µcal per second) is recorded versus ejection time.

(See Figure 2.1B for comparison between $\Delta H_{phage\ into\ LamB}$ and $\Delta H_{phage\ into\ buffer}$). Another heat source in the ITC sample cell during reaction is from biochemical interactions, which includes heat contributions from phage-LamB binding reaction, configurational change of the phage portal structure upon LamB binding, rearrangement of ejected phage DNA in solution (note that there is a significant increase in the occupying volume of the viral genomic DNA after it has been ejected into the solution) and heats accompanied with other proposed changes of the DNA states during the ejection, e.g. protonation of the DNA. While our method cannot differentiate these biochemical heats from the DNA ejection heat, we have verified that the ΔH_{ej} has a magnitude of 10^{-16} J/virion (10^4 kcal/mol) (*1*, *2*). However, most biochemical reaction heats (including binding heats and conformational change heats) are of the order of kcal/mol or tens of kcal/mol. For example, studies on phage T5 revealed a binding enthalpy between T5 and its receptor FhuA to be on the order of 10^{-19} J/virion (10 kcal/mol) (*3*); some additional studies on phage T5 using light scattering revealed an enthalpy required for the activation of DNA ejections (including configurational changes of both phage and receptor upon binding) to be also on the order of 10-19 J/virion (10 kcal/mol) (*4*). Also, a comparison between DNA genome of phage P22 in its packaged and unpackaged states has been studied using Raman spectroscopy and no significant deviations in terms of base pairing/stacking or electrostatic environment of DNA phosphate groups for packaged and unpackaged DNA states have been found (*5*).

On the other hand, the ejection enthalpy, ΔH_{ej} is a good estimate of the internal energy of λ genome, U_{encap_DNA}. In an ITC experiment, ΔH_{ej} is measured as an enthalpy change associated with the genome release process, $\Delta H = \Delta U + p\Delta V$, where ΔU is the change in internal energy of the system during DNA ejection ($\Delta U = U_{empty\_cap} - U_{filled_{cap}} = U_{encap\_DNA}$), p is the atmospheric pressure acting on the system and ΔV is the change in volume of the solution surrounding the phages

during DNA release. Since this volume change in solution, ΔV is negligible, ΔH ≈ ΔU. So through our carefully designed ITC experiment, we can get the internal energy of encapsidated λ genome, U_{encap_DNA}.

2.3 Intracapsid DNA structure by solution small-angle x-ray scattering

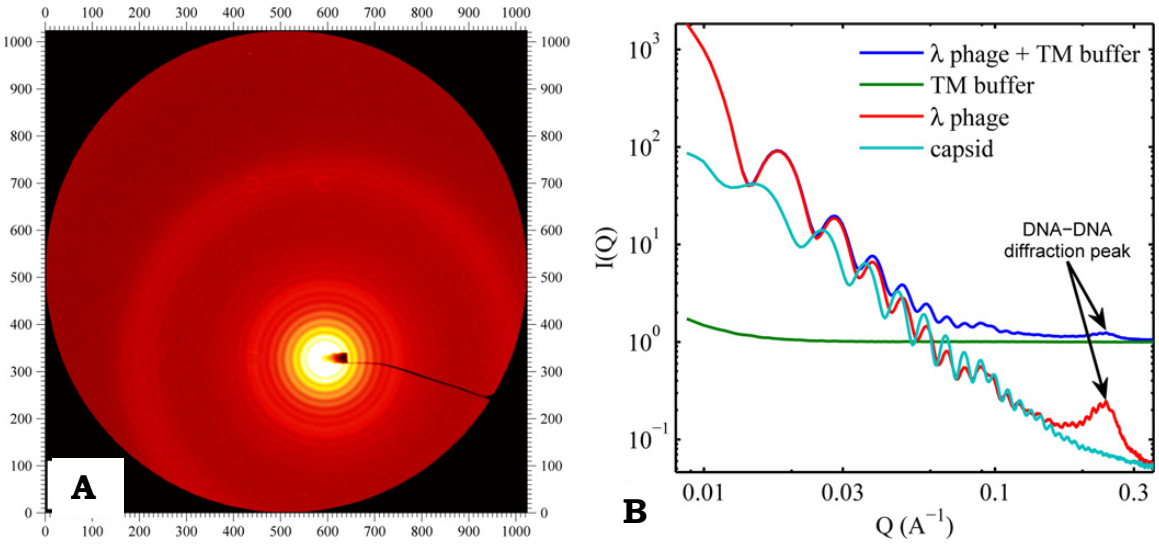

Figure 2.2 2D and 1D SAXS data. (A) Raw SAXS data in 2D form from scattering of λ particles, the off-center yellow core indicates position of beam-stop and the prominent ring features around the beam stop is due to diffraction from highly-ordered DNA structure inside. (B) Integration of density (*I*) along the ring gives the 1D diagram of scattering intensity versus scattering vector *Q* where $Q = 4\pi sin\theta / \lambda$ (θ: scattering angle; λ: wavelength of x-ray source. Each curve is labeled of the scattering material in the sample. We can see that the peak at Q = 0.26 only appears at DNA-filled viruses, this is scattering peak from hexagonal-packaged DNA structure. Figure reproduced from Qiu X et al., PRL 2011 (*6*).

Solution small-angle x-ray scattering (SAXS) was extensively applied in this thesis research. Solution SAXS is a powerful technique that provides structural information about the encapsidated genome (*6*, *7*). Scattering intensity (I) is recorded as a function of momentum transfer Q ($Q = 4\pi\sin\theta / \lambda$, where 2θ is the angle between the incident and scattered radiation) (*8*). Raw SAXS data was collected as 2D intensity information (Figure 2.2A), which shows a prominent

feature of concentric ring set around the beam stop (due to scattering of ordered structures). Integration of radial intensity along the ring give rise to 1D intensity versus scattering angle (2θ) or scattering vector (Q) profile (Figure 2.2B) (*6*). Protein capsids and DNA have different scattering profiles and are well-resolved (Figure 2.2B) (*2*, *6*, *7*, *9*). The short-range DNA interaxial spacings determine the position of the DNA diffraction peak in SAXS (Figure 2.2B), whereas the area of this peak provides information on the total number of ordered DNA base pairs of the encapsidated genome (*2*, *9*).

SAXS measurements were carried out at the 12-ID B station at the Advanced Photon Source (APS) at Argonne National Laboratory (ANL). A 12-KeV X-ray beam was used to illuminate the sample with an overall scattering vector q range from 0.006 to 0.850 $Å^{-1}$. A total of 120 μL of WT λ phage solution (~5 Å~ 1013 pfu/mL) was injected into a flow-through glass capillary, and the solution was oscillated during the SAXS measurement with a flow rate of 10 μL/s. Forty scans with 1s X-ray exposure time were collected and averaged for each sample (*2*, *9*).

The peak appeared at 0.2 $Å^{-1}$ in Figure 2.2B was due to scattering from ordered DNA structure inside λ phage. The width of DNA peak is closely related to long-range positional ordering. The intensity of radiation scattered from phage particle can be perceived as scattering from an unoriented structure, that it was averaged over all angular orientations (*10*). In this case the in-plane bond-orientational order will not contribute to the overall scattering pattern. The broadening the peak, the shorter of the positional correlation in these hexagonal packaged DNA segments and more liquid like the viral DNA is (this was later observed in Chapter 3 when λ phage incubation temperature rises). Interestingly, very similar phenomenon was observed in in vitro DNA sheets which exhibit in a line hexatic phase (*11*), those samples were prepared of similar DNA inter-axial spacing. It was found that the more condensed these DNAs are (shorter dint), the more liquid-like positional

correlation they have.

2.4 Visualizing bulk DNA ejection by confocal microscopy

Confocal laser scanning microscopy (CLSM) was used to visualize bulk DNA ejection process in real-time *in vitro*. In this set up, an Andor revolution XD imaging system with spinning disk was used for confocal imaging. EM gain of 300 was enabled. Exposure time was 100 ms and each frame was averaged of 4 times. A confocal 488 laser was used to excite the YOYO®-1 dye and lase intensity was set to 10%. Ejections were observed on an inverted micrcoscope using a 100x, 1.4 NA (or 60×, 1.45 NA) oil immersion objective at ambient temperature (≈28°C). In this set of data shown, a minimum of 5857 pixel intensities was set for all the images including controls and ejection sample images.

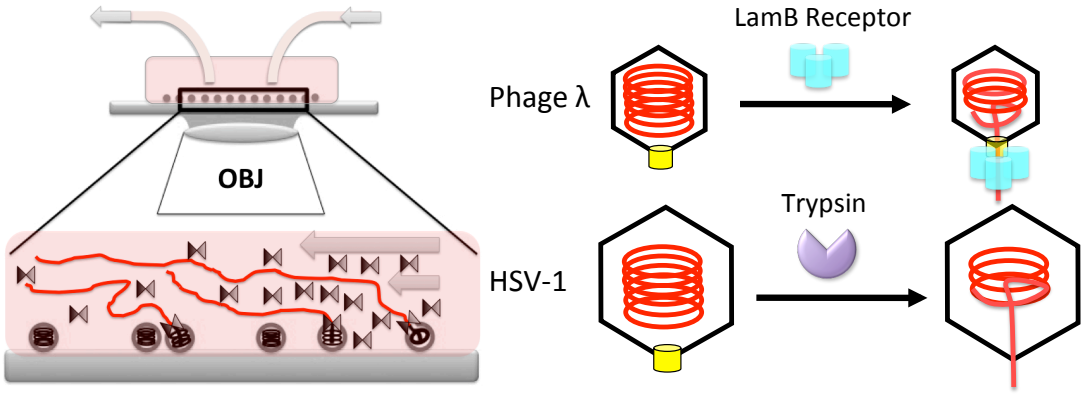

Figure 2.3 Real-time DNA ejection kinetics observed by FM. A flow cell was specifically built for this system where viral particles (λ or HSV-1) were pre-incubated and adsorbed onto glass surface, and their receptors or trypsin proteins flow to open or cut off the portal protein for DNA release. Ejected DNA molecules will be stained by non-capsid permeable DNA dyes in the flow chamber as soon as they leave the capsid, thus a real-time DNA translocation kinetics is recorded.

Samples (purified λ or HSV-1 capsids) were pre-bound to a HMDS (hexamethyldisilazane)-coated glass cover slip in a flow cell chamber (Figure 2.3). Then their receptors (LamB for λ) or trypsin proteins will be flown into the chamber

in presence with DNA staining dyes (i.e. 0.1 μM YOYO®-1, by life technologies). Studies have shown low-concentration trypsin proteins specifically target the portal structure (UL6 as the primary target) in HSV-1 (Figure 2.3) (*12*, *13*). The flow rate is normally set to be 0.15 mL/min rate. CLSM Images was taken at 1 minute interval for 30 minutes for real ejection kinetics measurements. Viral capsids (λ or HSV-1) has low permeability to YOYO®-1. Dye binding kinetics studies (by fluorescence spectrometer) show minimal fluorescence intensity increase within an hour when YOYO®-1 dye were incubated with intact viral capsids (data not shown). Upon addition of viral receptors or trypsin, the capsid portal was quickly opened and viral DNA was ejected into the surrounding solution, the viral heads remain attached onto the glass. Unexpectedly, experiments show that viral DNA remain associated with the viral heads when ejection was done under low flow rate (less than 0.15 mL/min). This was likely due to sticking of DNA ends to the capsid portals, this phenomenon was observed by others as well (*4*). In the preliminary investigation stage of this study, total internal reflection fluorescence (TIRF) and whole field illumination by a 100-W mercury lamp at full intensity were also tested for the purpose of observing viral DNA ejections. Compared to the other two methods, CLSM generate the most crisp and clear images on ejected DNA near glass surfaces with applied flow rate.

2.5 Reconstitution of HSV-1 DNA ejection into nucleus

An *in vitro* viral HSV-1 DNA ejection system was reconstituted in which HSV-1 genome was released into nucleoplasm in a homogenate solution mimicking cytoplasm environment. 8×10^5 counts of nuclei was incubated with approximately 10^9 counts of viruses on ice for 10min in a preferred capsid binding buffer (CBB: 20 mM HEPES-KOH with pH of 7.3, 80 mM K-acetate, 2 mM DTT, 1mM EGTA, 2mM Mg-acetate, 1mM PMSF, and 1X CLAP cocktail) as previously described (*14*) containing: (i) cytosol homogenate from BHK cell (final concentration reading about 2.5 mg/mL protein

contents) (ii) 1 mg/mL BSA (iii) ATP regenerating system composed of 5mM creatine phosphate (Sigma), 20 U of creatine phosphokinase (Sigma), 1mM ATP, 0.2 mM GTP. Then osmolytic solution of PEG 8k or Dextran 155k (or water in control sample) was added to make up a total of 500μL system. Final osmolytes in the solution reaches a concentration of 30% w/w. The system is incubated 37˚C for 30min then transferred on ice for a minimum of 10min. (See the first step: incubation in Figure 2.4).

After capsid-nuclei incubation, the system was centrifuged at 3k rpm to spin down the capsid-associated nuclei. Nuclei pellet was washed twice in CBB buffer at 4˚C to remove excessive osmolytes in the pellet (low temperature and placement of the sample on ice at all times were required to minimize DNA ejections after the incubation stage). The pellet was then resuspended and incubated for 20 min in 1x reticulocyte standard buffer (RSB: 10mM Tris of pH 7.5, 10mM KCl, 1.5mM MgCl2, 0.5% NP-40 substitute) for nuclear membrane lysis. The supernatant was collected separately (see step 2: separation of bound and unbound capsids in Figure 2.4).

Both extra-nuclear supernatant and lysed nuclear pellet were then incubated with 5□L anti-HSV1/2 ICP5/UL19 antibody (from Bernard Roizman lab) for overnight at 4˚C. 50□L 50% Protein A bead slurry (Sigma-Aldrich P1406) was added to each samples to capture viral capsid-antibody complex on the next day. Protein A bead complex was collected by low speed centrifugation (1500rpm, 5 minutes). The supernatant was collected as capsid-free part (sample b and d in Figure 2.4). In parallel, the pelleted beads parts were re-suspended in Proteinase K solution to digest the capsid and let viral DNA diffuse into the solution (sample a and c in Figure 2.4). Then all the sample solutions were phenol-chloroform treated and DNA was ethanol precipitated at re-suspended in clean water.

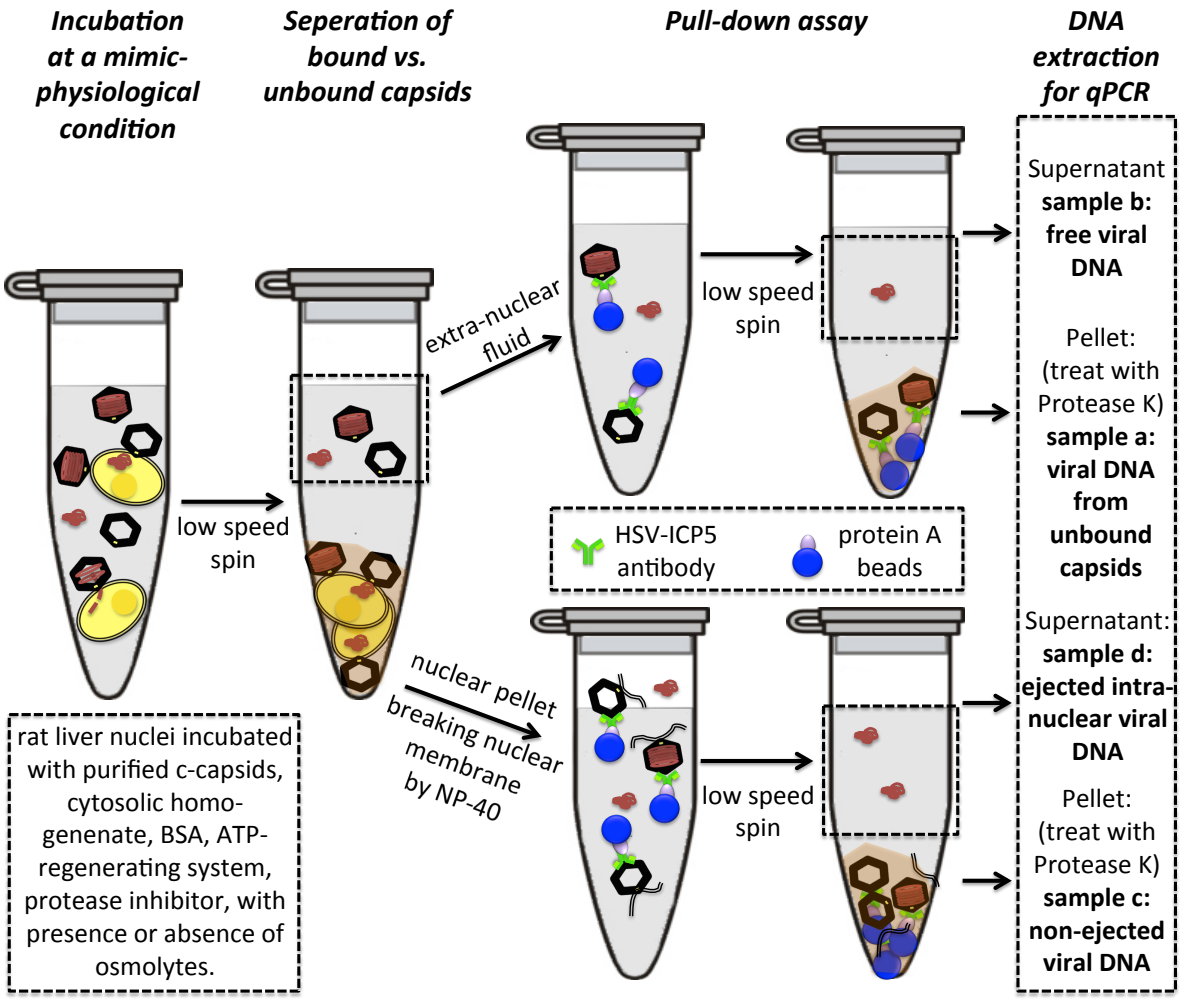

Figure 2.4 Schematic of nuclear viral DNA ejection assay. HSV c-capsids were incubated with purified rat liver cell nuclei, in the presence or absence of osmolytes Dextran 155k and PEG 8k (osmolytes not shown in the cartoon). An assay was developed to collect each portion of samples including (a) extra-nuclear fluid (b) free capsids in the extra-nuclear fluid (c) nuclear content including chromosomal DNA and ejected viral DNA (d) capsids associated with nuclear membrane. Note that HSV-1/2 ICP5 antibody has multiple binding sites on the capsids, only one is shown here for simplification. The host chromosomal DNA are in the sample (c) and not shown in any parts of the cartoon here. The final samples (a) to (d) collected were used to extract DNA by phenol-chloroform based purification.

This in vitro assay successfully parted HSV-1 DNA into four samples: (a)

HSV genome from those capsids unbound or failed to dock onto nuclear pore complex. (b) Free HSV DNA in the extra-nuclear solution due to contamination or broken capsids. (c) HSV genomes that are successfully ejected into nucleoplasm. (d) HSV DNAs still sustained inside the nuclear-associated capsids within the time frame of experimental incubation.

2.6 Quantification of DNA ejection from HSV-1

Quantification of each part of traces of viral genome in the *in vitro* translocation system was crucial to understand the efficiency of viral genome release in our reconstructed system. Extracted DNAs from sample a, b, c, d were quantified by real-time PCR analysis for DNA level by custom TaqMan assays as previously described (*15*): 2 μl of DNA, 1.6 μM concentrations of each primer (Table 2.1), and 2× Sybr green Mix (20 mM Tris (pH 8.3), 100 mM KCl, 6 mM MgCl2, 1.6% glycerol, 0.02% Tween 20, 4% dimethyl sulfoxide, 0.4 mM concentrations of deoxynucleoside triphosphates (*16*), 0.06 U of Platinum *Taq*/μl, 1× Sybr green). The specificity of each primer pair was analyzed by determining the melting curves for each PCR product. Samples were analyzed in duplicate, and relative copy numbers were determined by comparison with a standard curve generated by a 10-fold dilution series of pooled input samples.

Table 1 Quantitative PCR primers

Gene Region	Orientation	Primer Sequence
VP16 promoter	F	TCGGATTGGGAAACAAAGGCACGCAA
	R	TCCGTACCCAGACAATAAAGCACCAACAGG
ICP0 ORF	F	TTCGGTCTCCGCCTGAGAGT
	R	GACCCTCCAGCCGCATACGA

The assays were performed using a StepOnePlus sys system (Applied Biosystems) and were analyzed with software provided by the supplier. Viral

gene copies were calculated with comparison to amplification from wt HSV-1 DNA with known copy numbers.

References for Chapter 2

1. M. Jeembaeva, B. Jonsson, M. Castelnovo, A. Evilevitch, DNA heats up: energetics of genome ejection from phage revealed by isothermal titration calorimetry. *Journal of molecular biology* **395**, 1079-1087 (2010).
2. T. Liu *et al.*, Solid-to-fluid-like DNA transition in viruses facilitates infection. *Proceedings of the National Academy of Sciences of the United States of America* **111**, 14675-14680 (2014).
3. J. F. Conway *et al.*, A thermally induced phase transition in a viral capsid transforms the hexamers, leaving the pentamers unchanged. *J Struct Biol* **158**, 224-232 (2007).
4. P. Grayson, L. Han, T. Winther, R. Phillips, Real-time observations of single bacteriophage lambda DNA ejections in vitro. *Proceedings of the National Academy of Sciences of the United States of America* **104**, 14652-14657 (2007).
5. J. X. Cheng, S. Pautot, D. A. Weitz, X. S. Xie, Ordering of water molecules between phospholipid bilayers visualized by coherent anti-Stokes Raman scattering microscopy. *Proceedings of the National Academy of Sciences of the United States of America* **100**, 9826-9830 (2003).
6. X. Qiu *et al.*, Salt-dependent DNA-DNA spacings in intact bacteriophage lambda reflect relative importance of DNA self-repulsion and bending energies. *Physical review letters* **106**, 028102 (2011).
7. W. C. Earnshaw, S. R. Casjens, DNA packaging by the double-stranded DNA bacteriophages. *Cell* **21**, 319-331 (1980).
8. D. I. Svergun, M. H. J. Koch, Advances in structure analysis using small-angle scattering in solution. *Current Opinion in Structural Biology* **12**, 654-660 (2002).
9. D. Li *et al.*, Ionic switch controls the DNA state in phage lambda. *Nucleic acids research* **43**, 6348-6358 (2015).
10. W. Earnshaw, S. Casjens, S. C. Harrison, Assembly of the head of

bacteriophage P22: x-ray diffraction from heads, proheads and related structures. *Journal of molecular biology* **104**, 387-410 (1976).

11. H. H. Strey *et al.*, Refusing to twist: Demonstration of a line hexatic phase in DNA liquid crystals. *Physical review letters* **84**, 3105-3108 (2000).
12. D. W. Bauer, J. B. Huffman, F. L. Homa, A. Evilevitch, Herpes virus genome, the pressure is on. *J Am Chem Soc* **135**, 11216-11221 (2013).
13. W. W. Newcomb, F. P. Booy, J. C. Brown, Uncoating the herpes simplex virus genome. *Journal of molecular biology* **370**, 633-642 (2007).
14. P. M. Ojala, B. Sodeik, M. W. Ebersold, U. Kutay, A. Helenius, Herpes simplex virus type 1 entry into host cells: reconstitution of capsid binding and uncoating at the nuclear pore complex in vitro. *Molecular and cellular biology* **20**, 4922-4931 (2000).
15. M. H. Hancock, A. R. Cliffe, D. M. Knipe, J. R. Smiley, Herpes simplex virus VP16, but not ICP0, is required to reduce histone occupancy and enhance histone acetylation on viral genomes in U2OS osteosarcoma cells. *Journal of virology* **84**, 1366-1375 (2010).
16. F. P. Booy *et al.*, Finding a needle in a haystack: detection of a small protein (the 12-kDa VP26) in a large complex (the 200-MDa capsid of herpes simplex virus). *Proceedings of the National Academy of Sciences of the United States of America* **91**, 5652-5656 (1994).

CHAPTER 3 SOLID-TO-FLUID DNA TRANSITION IN BACTERIOPHAGE λ

3.1 Abstract

The efficiency of viral replication is limited by the rate of viral genome release into a cell. In many double-stranded DNA bacterial viruses and herpesviruses, the tightly packaged genome is hexagonally ordered and stressed in the protein shell called the capsid. It has remained unclear how this rigid crystalline structure can be rapidly ejected from a virus, reaching rates of 60,000 base pairs per second. Through a combination of single-molecule and bulk techniques, we mapped the delicate interplay between the energy, structure and fluidity of the encapsidated DNA in phage λ as a function of temperature. We discovered that DNA in the capsid is metastable and undergoes a solid- to-fluid phase transition which facilitates infection close to 37°C. This shows a remarkable physical adaptation of bacterial viruses to the environment of *E. coli* cells in a human host. At lower temperatures outside the host, DNA in the capsid is a rigid crystal, which prevents its spontaneous release. At the optimum temperature for infection, viral DNA gains the necessary fluidity for its efficient translocation into a cell.

3.2 Introduction

Nucleic acids constitute one of the main components of many viruses by weight. The viral genome is tightly packed into a small volume within a protein shell called the capsid. This is true for most prokaryotic viruses such as double-stranded (ds) DNA viruses (*1-6*), as well as many eukaryotic viruses (e.g. herpesviruses (*7*) and reoviruses (*8*)). The length of the ds-genome in these viruses is several hundred times longer than the diameter of the capsid. This tight packaging leads to genome bending stress and strong repulsive interactions resulting in internal capsid pressures reaching tens of atmospheres. The extreme efficiency of viral replication is associated with a rapid transfer of the genome from the capsid to the host cell. This pressure driven genome ejection occurs through a single portal opening in the

capsid with a cross-section of a few nanometers (9), allowing the passage of only one dsDNA strand. The energy and structure of the confined viral genome are closely related and determine the rate of major viral replication steps such as genome ejection and packaging (10-14). We have shown *in vivo* that the rate of ejection will affect the probability of infecting the cell (12), while the rate of packaging is the limiting step for viral assembly (15).

While DNA is always condensed inside the cell (16), it is not condensed to the same extent as inside a viral capsid. For example, in eukaryotic chromosomes, DNA forms aprecholesteric structure, while bacterial nucleoid DNA and sperm nuclei DNA have cholesteric structures. Packaging densities are ranging between 5 and 40% by volume (17, 18). It was suggested that the existence of a fluid cholesteric state was required for biological functions of these systems (19, 20). DNA confined in viral capsids, on the other hand, is at the extreme end of the packaging scale where it is confined to 55% by volume, forming a hexagonally ordered structure (2, 3, 11, 21). At only a few angstroms of DNA-DNA surface separation (e.g. 7 Å surface separation in the wild type (WT) DNA length of 48,500 bp packaged in phage λ) (11), hexagonally ordered DNA has been shown to have very restricted fluidity and behaves more like a rigid crystal (18). Despite decades of investigations of the encapsidated genome structure and its energetics (3, 22), it is not known what provides the required fluidity to the hexagonally ordered viral DNA during its ultra fast ejection reaching 60,000 bp/s (10). In this work we provide an answer to this fundamentally important question.
The well-known concept of viral metastability often refers to the viral capsid that needs to be sufficiently stable to protect the viral genome, and unstable enough to release its genome into the cell. In this work, using bacteriophage λ as a model system, we discovered a novel concept of viral metastability attributed to the viral genome. The energetics, structure and fluidity of the encapsidated DNA are studied as a function of temperature, a parameter that is rarely varied in biophysical

measurements on viruses but is pertinent to viral replication and survival. This revealed a remarkable phase transition of dsDNA in phage λ capsids, close to the ideal temperature for infection, i. e. 37°C. Since phage λ infects *E.coli* that originate in the human gut, the human body temperature makes phage DNA fluid and thus optimized for rapid release into bacterial cells. At the same time, at lower temperatures outside the host, DNA behaves more like a rigid crystal when the conditions are less favorable for infection, which prevents spontaneous genome release.

3.3 Materials and methods

3.3.1 Bacteriophage and LamB receptor

WT bacteriophage λ cI857, with a genome length of 48.5 kb was produced by thermal induction of lysogenic *E. coli* strain AE1 derived from S2773 strain. Phage purification details are described elsewhere (*1*). All phage samples were purified by CsCl equilibrium centrifugation and dialyzed from CsCl against $MgCl_2$ TM buffer (10 mM $MgCl_2$/50 mM Tris·HCl, pH 7.4) or $MgSO_4$ TM buffer (10 mM $MgSO_4$/50 mM Tris·HCl, pH 7.4). The final titer was ≈ 10^{12} virions/mL, which was determined by plaque assay. Empty phage particles were prepared by incubating WT phage with its extracted LamB receptor for 1h at 37°C. The details can be found elsewhere (*23*). The receptor was the LamB protein purified from pop 154, a strain of *E. coli* K12 in which the *LamB* gene has been transduced from *Shigella sonnei* 3070. The detailed preparation was previously described (*23*).

3.3.2 Isothermal titration calorimetry (ITC)

All calorimetric measurements were performed using the MicroCal iTC200 system manufactured by GE Healthcare, Life Sciences. The details of phage DNA ejection enthalpy measurements were previously described in ref (*24*). The ejection enthalpy at each given temperature, was measured by titrating 2.69 µL of λ particles at 5 - 6×10^{12} pfu/mL (8 - 10nM) concentration into 200 µL of LamB

solution in the sample cell (reference cell was always filled with MilliQ water). LamB was at a concentration of 0.2 - 0.5 mg/mL (1.4 - 3.5 μM). The molar ratio between LamB trimmers and phage λ particles in the sample cell was always kept above 104:1 (up to at least 3 titrations) to ensure that the maximum number of phage λ particles eject their genomes without delay (LamB concentration was tested for saturation). Both LamB and λ particles were in the same dilution buffer containing TM (10mM MgCl2 or MgSO4, as indicated, 50mM Tris, pH7.4) and 1% oPOE. Measurements were performed within the temperature range between 18°C - 42°C.

3.3.3 SAXS

Small angle X-ray scattering (SAXS) measurements were carried out at the 12-ID B station at the Advanced Photon Source (APS) at Argonne National Laboratory. A 12KeV X-ray beam was used to illuminate the sample with an overall q range from 0.006 to 0.850 $Å^{-1}$. Total of 120 μL of WT phage solution (~ 5×10^{13} pfu/mL) was injected into a flow-through glass capillary and the solution was oscillating during the SAXS measurement with a flow rate of 10 μL/s. 40 scans with 1 second X-ray exposure time were collected and averaged for each sample.

3.3.4 X-ray measurement of DNA-DNA forces in condensed arrays

The osmotic stress technique for measuring forces is described in ref (*25*). Force measurements were carried out at the Laboratory of Physical and Structural Biology, Program in Physical Biology, National Institutes of Health. Ni-filtered Cu-Ka radiation from an UltraBright microfocus x-ray source from Oxford Instruments equipped with polycapillary focusing x-ray optics was used for the small angle x-ray scattering (SAXS) experiments. The primary beam was also collimated by a set of slits. After equilibration, samples were sealed with ~ 100 ml equilibrating salt-PEG solution in a sample cell and mounted into a temperature-controlled holder. The flight path between the sample and detector, ~ 16 cm, was helium filled. Typical exposure times were ~ 30 min. Further details are described elsewhere (*26*).

3.3.5 Fluorescence Measurements

Purified phage λ at 1014 pfu/mL were dialyzed and diluted 5,000 times in buffer ($MgSO_4$–Tris buffer or $MgCl_2$–Tris buffer) for imaging purposes. Diluted phages were incubated on modified glass coverslips for at least 10 min before imaging and then washed with the same dilution buffer. After incubation, phages were exposed to YOYO-1 dye (Life Tech- nologies) at 100 nM for imaging. The diffusion of YOYO into the capsid interior is strongly kinetically limited (<1% of DNA- filled phage particles were stained within 10 minutes of in- cubation). LamB receptor solubilized in 1% oPOE was flown continuously into the chamber with YOYO dye. Phage particles then were imaged with a Nikon 2000E2 microscope with a spinning-disk confocal scan head (Yokagawa Industries). Images were collected by using a 488-nm laser at 60× 1.45 N.A. objective and an EM-CCD camera (Photometrics Cascade II) for a period of 10–15 min, until no further ejection events were observed. Fluorescence images were processed using ImageJ (public domain Java image-processing program, National Institutes of Health).

3.3.6 Plaque Assay Analysis

Purified phages were dialyzed in $MgCl_2$ – Tris buffer with 50 mM Tris and 10 mM $MgCl_2$ at pH 7.4 overnight, then diluted to 10^4 pfu/mL in the same buffer. E. coli C600 cells were grown to an OD600 of 0.5 in LB medium supplemented with 2 mg/mL thymine and 0.2% maltose. Cells then were spun down and re-suspended in $MgCl_2$ – Tris buffer. One hundred-microliter diluted phage samples were mixed with 200 μL prechilled resuspended C600 cells; this mixture then was spread on the LB agar plates. The plates were incubated at the desired temperatures for 12 h, and then plaque area was determined. At least 300 plaques were counted on each plate for the plaque area determination.

3.4 Energetics of intra-capsid DNA transitions

As mentioned above, the viral genome organization resulting from intra-capsid

confinement is closely associated to its energetic state (*13*, *27*). The effect of temperature on the energy state of the pressurized genome in the viral capsid has not been previously investigated. We designed a new micro-calorimetric assay that provides the most direct method to measure the internal energy of the confined viral genome. Using ITC, the enthalpy change ΔH_{ej}, associated with DNA ejection from phage λ is measured as heat released when concentrated phage particles are titrated into a LamB receptor solution, which triggers DNA ejection in vitro (*24*). Since the total volume of the system does not change during the DNA ejection, and the pressure is constant, the internal energy and the enthalpy are approximately equal (*24*). The temperature in the reference cell is continuously equilibrated to that of the sample cell after each titration of phage in LamB solution. The differential power between the reference cell and the sample cell is recorded in microcalories per second, as shown in Figure 3.1. Integration of the area under the heat change peak over time provides the reaction enthalpy, which includes DNA ejection from the phage, mixing of phage in LamB solution, dilution of LamB, and the pressure–volume work associated with titration of one volume into another. (Enthalpy contributions from binding of LamB to the phage tail and any subsequent protein conformational changes leading to initiation of DNA ejection are several orders of magnitude lower than the enthalpies listed above (*28*). These other contributions to the enthalpy change that are not arising from the enthalpy of DNA ejection (ΔH_{ej}), are measured separately by titrating phage into buffer, buffer into LamB solution, and buffer into buffer. These values are subtracted from the total enthalpy change, (all ΔH_{ej}, values are shown in Table 3.1). ΔH_{ej} was measured in the temperature range between 18°C and 42°C. Figure 3.2A reveals a discontinuity in the approximately linear dependence of ΔH_{ej} on temperature occurring at T^* ~33°C for WT DNA length (48.5 kbp) ejection from phage λ in 10 mM $MgCl_2$ Tris-buffer. The discontinuity demonstrates an abrupt phase transition that can be attributed to the DNA inside the capsid or the DNA that has been ejected. However, differential scanning calorimetry (DSC) analysis of free λ DNA in

solution confirmed that there is no phase transition in this temperature range, with double-to-single stranded DNA melting occurring at significantly higher temperatures (29). Therefore, it is the encapsidated DNA that undergoes the phase transition that has not been previously observed.

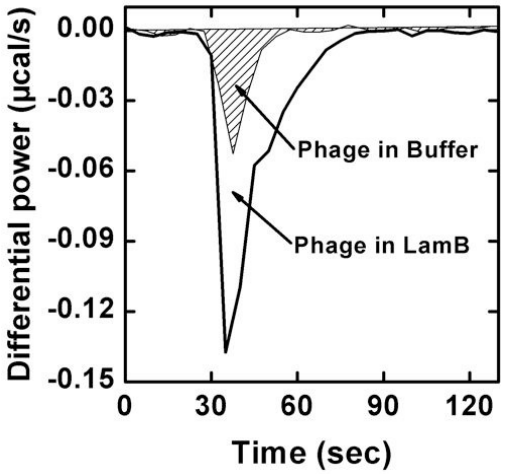

Figure 3.1 ITC titrations of phage λ to LamB and phage λ to buffer. Ionic conditions were 10 mM $MgCl_2$, 50 mM Tris-HCl (pH 7.4) at 37°C. Differential power (µcal/s) is recorded versus time in seconds.

Table 3.1 All measured DNA ejection enthalpies

Temperature (°C)	Ejection Enthalpies*, ΔH_{ej} ± SE (**×10^{-16} J/virion**)	
	10mM $MgCl_2$ **	10mM $MgSO_4$ **
18.0	--***	1.1067 ± 0.0554
22.0	0.9079 ± 0.1912	-0.7351 ± 0.1134
24.0	--	-0.9691 ± 0.2571
25.0	-0.9719 ± 0.1936	--
27.0	-1.8652 ± 0.1166	-1.9101 ± 0.3283
30.0	--	-0.3053 ± 0.1238
32.0	-3.2289 ± 0.4835	-0.1916 ± 0.1665
34.0	-2.4765 ± 0.2105	--
37.0	-1.6090 ± 0.0647	-0.5007 ± 0.0950
39.0	-1.3136 ± 0.0724	--
40.0	-1.4463 ± 0.2236	--
42.0	-1.2382 ± 0.1985	-0.0198 ± 0.1949

** All the ejection enthalpy values listed here were obtained as an average of 3-6 independent measurements. ** ΔH_{ej} values measured in TM buffer containing 10mM $MgCl_2$ (or 10mM $MgSO_4$). *** "--" means no measurement was done at this temperature for the given salt condition*

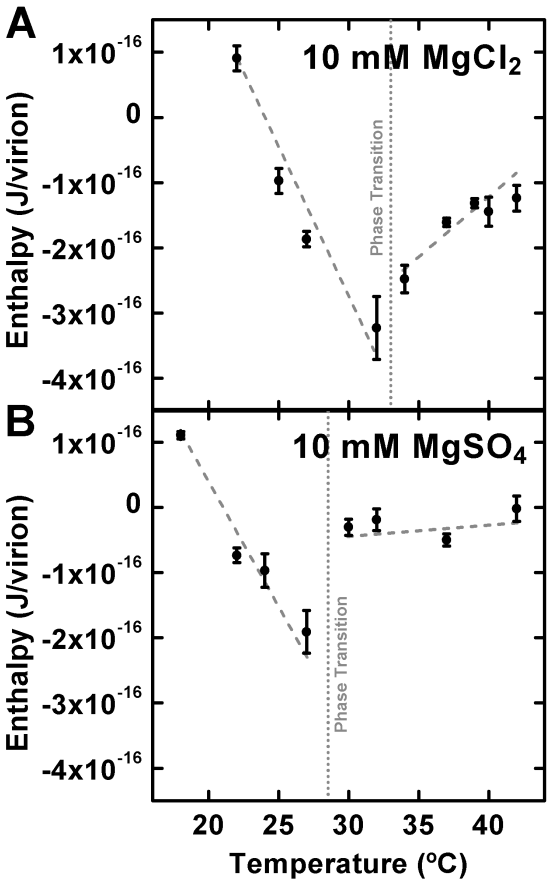

Figure 3.2 Enthalpy of DNA ejection per virion (J). All data from WT DNA phage λ versus temperature in (A) 10 mM $MgCl_2$ Tris-buffer and (B) in 10 mM $MgSO_4$ Tris-buffer. Dashed lines are drawn to guide the eye. ΔH_{ej} values were obtained as an average of 5-6 independent measurements for each sample. Vertical error bars are standard errors.

Prior to the transition, the absolute value of the ejection enthalpy change $|\Delta H_{ej}(T)|$ shows a strong linear increase with increasing temperature. $|\Delta H_{ej}(T)|$ increases nearly 4 times when the temperature is raised from 22ºC to 32ºC. This increase in the internal energy indicates an increase in the stress of the confined genome as temperature is being raised. At the transition temperature, T^*, the internal energy is reduced by almost half, suggesting partial relief of the stressed state. After the transition, $|\Delta H_{ej}(T)|$ shows only weak temperature dependence when the temperature is further increased to 42ºC. see Figure 3.2A. This observation demonstrates that the DNA inside λ capsid can exist in two energy states, which was later confirmed with atomic force microcopy (AFM) that the state prior to transition is more solid-like and of lower fluidity (Udom Sae-Ueng's work, (*30*, *31*)). It was also discovered that λ virions consists of two distinct populations, one with DNA in solid-like state and one with DNA in fluid-like state. λ population with solid-like genomes are trapped in an energy state unfavorable for DNA translocation, DNA transitions need to take place before this type of λ particles gain competency for genome release (for more details, see Chapter 5).

The critical genome stress is reached at temperature T^* and is required for the phase transition to occur. This suggests that varying the DNA stress inside the capsid should affect the temperature of phase transition, T^*. We test this hypothesis by repeating the ITC measurement of phage DNA ejection enthalpy under different ionic conditions, using Tris-buffer with 10 mM $MgSO_4$ instead of 10 mM $MgCl_2$. Since all viral capsids are permeable to smaller ions, ionic conditions of the host solution have a direct influence on the internal DNA stress by affecting the DNA-DNA repulsive interactions (*32*). Our previous studies have shown that DNA pressure inside λ capsids is larger in Tris- solution with 10 mM $MgSO_4$ than in 10 mM $MgCl_2$ (*32*). This is related to the difference in ion pairing energies of Mg^{2+} with Cl^- and SO_4^{2-}, leading to considerably fewer Mg^{2+} ions bound to DNA when the co-ion is SO_4^{2-}. This results in a weaker screening of the electrostatic repulsive forces between the DNA strands and therefore stronger repulsion. As a result, we found that the intracapsid DNA transition in 10 mM $MgSO_4$ Tris-buffer occurs at a lower temperature of T* ~28 °C, instead of 33 °C in10 mM $MgCl_2$ (Figure 3.2B). This finding confirms that there is a strong inter-dependence between the DNA structural transition temperature in λ and the internal genome stress. In the next section we investigate which structural changes of DNA in the capsid lead to the observed phase transition.

3.5 Ordering of encapsidated DNA

Solution SAXS provides direct structural information about the encapsidated genome (*3*, *33*). Protein capsids and DNA have different scattering profiles and are well-resolved, see Figure 3.3. We collected SAXS scattering data for WT DNA length phage λ in 10 mM $MgCl_2$ Tris-buffer in the temperature range between 22 and 40ºC. In the lower q region (0.007$Å^{-1}$ to 0.1$Å^{-1}$) (Figure 3.3), the scattering profile originates from the highly symmetrical icosahedral phage capsids. The single peak with the small oscillating ripples on its top at higher q (between 0.2 $Å^{-1}$ to 0.3 $Å^{-1}$) is due to the diffraction from the encapsidated DNA.

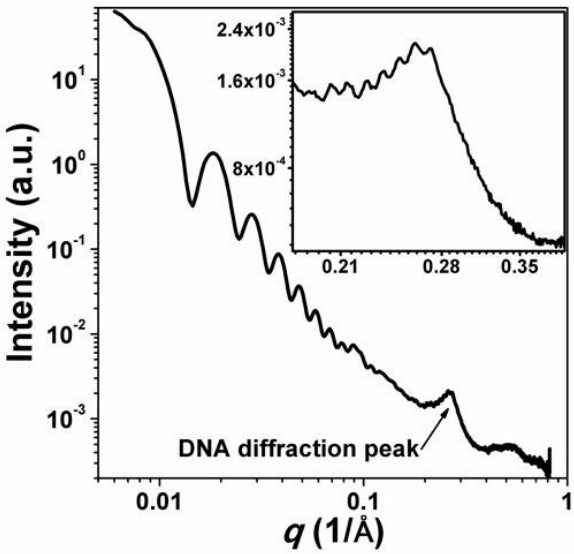

Figure 3.3 SAXS data for WT phage λ. Radially averaged scattered intensity versus the scattering vector *q* for WT phage λ in 10 mM $MgCl_2$ Tris-buffer, pH 7.4 at 27°C. Inset figure shows the DNA diffraction peak with the center at 0.263 $Å^{-1}$. The scattering profile at lower *q* is attributed to the protein capsid.

The short-range DNA interaxial spacings determine the position of the DNA diffraction peak, while the area of this peak provides information on the total number of ordered DNA base pairs of the encapsidated genome (*34*, *35*) (for more details on analyzing SAXS raw data, see Figure 2.2 in Chapter 2). When DNA inside the capsid becomes less ordered, the DNA peak area decreases as a result of less coherent diffraction. If the genome is completely disordered, the DNA diffraction peak disappears. Within the measured temperature range, the short-range DNA ordering appears to be unaffected with the diffraction peak position at scattering vector q ~0.26 Å−1. This corresponds to an average interlayer spacing of 23.8 ± 0.1 Å, which in turn is converted to a DNA interaxial spacing of 27.5 ± 0.1 Å, assuming hexagonal packing (Figure 3.4A). The area of the DNA scattering peak shows only a small decrease with the increasing temperature up to the DNA structural transition (Figure 3.4B). However, at ~33 °C, the DNA diffraction peak area undergoes a sudden drop. This area drop signifies a loss of the amount of ordered DNA inside the capsid. This observation supports the above ITC measured abrupt transition of the internal energy occurring at the same temperature *T**. As mentioned above, the decrease in genome ordering should provide a more fluid-like DNA state inside the capsid because of the locally reduced DNA packing density, resulting in weaker interstrand repulsion (*18*, *36*).

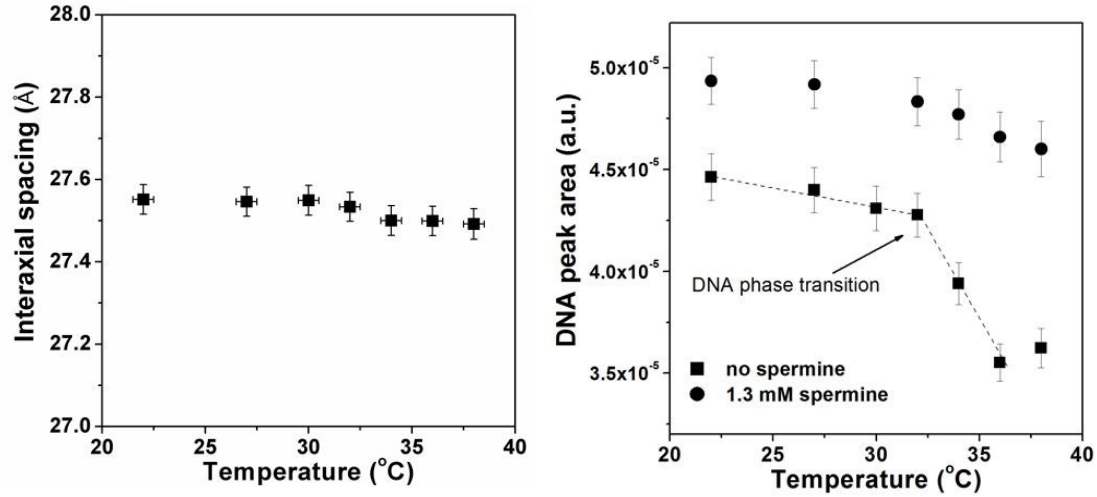

Figure 3.4 (A) DNA-DNA interaxial spacing *d* as a function of temperature. All data for WT DNA phage λ in 10 mM $MgCl_2$ Tris-buffer. Vertical error bars are from the non-linear fitting of the DNA diffraction peak with a Gaussian function with linear background subtraction. Horizontal error bars are from the instrument errors of the heating control unit. (B) DNA-DNA diffraction peak area as a function of temperature for WT DNA phage λ in 10 mM $MgCl_2$ Tris-buffer without (rectangles) and with 1.3 mM spermine (4^+) (circles). Peak area is obtained by fitting the scattering curve from 0.18 $Å^{-1}$ to 0.33 $Å^{-1}$ with a Gaussian function with linear background subtraction. The vertical error bars are from the non-linear fitting. The dashed line is drawn to guide the eye.

3.6 Structural changes of encapsidated DNA

The asymmetric cryo-EM single-particle reconstruction of WT DNA phage λ in **Figure 3.5 A** reveals that the entire capsid volume is filled with DNA, extending all the way to the center of the capsid. Starting from the capsid walls, there are well-ordered, multiple concentric DNA layers. The layers are spaced evenly, indicating that DNA has adapted an ordered repetitive structure characteristic of a liquid crystalline state. However, toward the center of the capsid, the ordered layers disappear, suggesting a less-ordered DNA structure with lower packing density than in the periphery of the capsid (*11*). Similar dsDNA distributions within the capsids also were observed for other viruses (*2*, *6*, *37-40*).

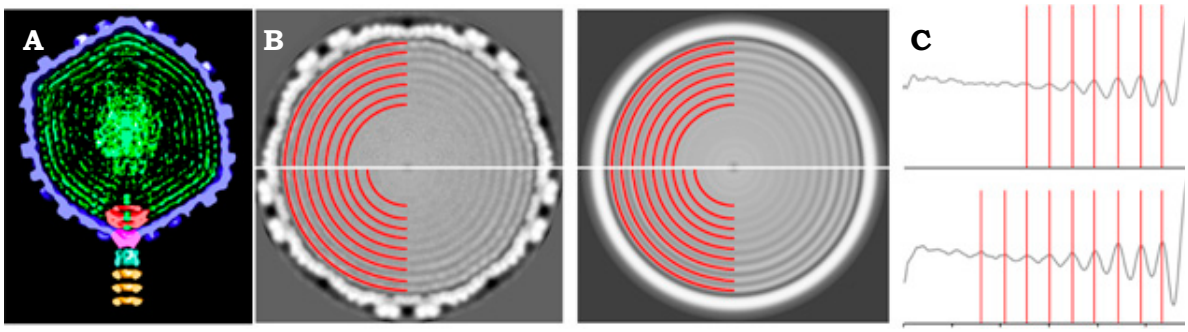

Figure 3.5 Ordering of λ DNA structure by EM. (**A**) Cutaway view of the asymmetric cryo-EM reconstruction of WT DNA phage λ, showing more ordered DNA (green) in the periphery of the capsid and less ordered DNA in the center. Density (green) in the center of the channel formed by the portal complex (red) likely is the end of the λ DNA that is being packaged last, and ejected first. (**B**) Central slices through the 3D cryo-EM icosahedral reconstructions of λ in the absence (**Upper**) and presence (**Lower**) of 1.3 mM spermine (4**+**). Radial averages of the 2D slices are shown to the right. The central slice of each reconstruction was extracted along the fivefold symmetric axis, providing a cross-section of density in which the capsid and packaged genome appear most circular. (**C**) One-dimensional plots of the radially averaged central slices of the phage symmetric reconstructions. DNA layers are marked with red vertical lines.

The DNA structure in viral capsids is determined by DNA–DNA interactions, bending stress and packing defects (*11*). With the help of osmotic stress measurements on bulk DNA arrays condensed in solution by an osmotic stress polymer (polyethylene glycol, PEG) (work by Donald Rau and Dong Li, data not shown in the thesis), we analyzed the effect of temperature on the DNA- DNA interaction energy alone without capsid induced bending (*25*, *32*, *33*). We found that the DNA-DNA repulsive interactions for linearly packaged DNA, at the same interaxial distances as in the capsid, are not significantly affected by the temperature increase from 5 to 50 °C and no phase transition occurs (work by Donald Rau, data not shown). This is explained by the strong repulsion between tightly confined DNA helices so that the DNA fluctuations are suppressed, which limits the effect of temperature on the interaction energy.

At the same time, intra-capsid confinement requires DNA to bend along radii

that are energetically unfavorable given the internal λ-capsid radius of ~30 nm (*41*) and 50 nm dsDNA persistence length (*42*), which creates bending stress on the packaged genome. (Persistence length defines the stiffness of a polymer, describing the minimum radius of curvature it can adopt by the available thermal energy. Bending it to a smaller radius requires additional work). To relieve the bending stress, helices are packed closer to the capsid wall, decreasing the bending radius and also decreasing the spacing, therefore increasing the interaction energy. At the same time the repulsive DNA-DNA interactions will push DNA strands as far from each other as possible, filling the entire capsid volume and maximizing the interstrand separations. There is a trade-off between bending and interaction energies. Furthermore, when DNA is bending inside the capsid, the initial correlation between two helices that have slightly different radii of curvature is lost, and the mutual orientation between helices must be re-established. This leads to the packing defects that are absent for linear packaging of DNA in solution. Packing defects are required in order to re-establish a favorable phosphate-phosphate 'phasing' of helices, reducing the repulsive interactions due to bending (*43*). The higher temperature is likely to hinder finding this optimum correlation between the helices. The spacing remains the same since DNA is simply filling a volume (as shown by SAXS in Figure 3.4A), but the inter-helical repulsion will increase. This is confirmed by an increase in the internal energy (measured by ITC, Figure 3.2) and an increase in the stiffness of DNA in the capsid (measured by AFM, work by Udom Sae-Ueng, data not shown) when the temperature is increased prior to the phase transition.

3.7 Bending stress induced DNA transition

In parallel with the increasing inter-strand repulsions, the increase in temperature will decrease the DNA persistence length (*44*), leading to less bending stress. If the bending stress decreases and if there is room to expand in the capsid, then spacings would increase and interaction energy decrease. However,

the spacing remains constant (Figure 3.4A), suggesting that there is no room for DNA to expand in the λ-capsid. Instead, as a result of increasing repulsive interactions (due to packing defects) and decreasing bending stress with increasing temperature, the disordering phase transition occurs, as confirmed by SAXS. We propose that this transition takes place closer to the center of the capsid, where DNA bending stress is stronger and packing defects are larger than for DNA closer to the capsid wall, making the DNA in the center more destabilized and therefore more sensitive to the increasing temperature. At the phase transition temperature, the DNA bending stress becomes sufficiently small, allowing a fraction of the ordered DNA layers closest to the capsid's center to undergo a disordering transition. The disordered phase will have a lower packing density than the ordered phase, which maximizes DNA-DNA spacings and simultaneously reduces the repulsive interactions. This yields an overall lower energy state of the encapsidated genome. Also, as earlier shown by cryo-EM (*11*), the DNA in the center is already less ordered than in the periphery of the capsid, providing larger available volume for the disordering phase transition.

We test this assumption and reconcile SAXS and cryo-EM observations by adding spermine (4^+) ions to the WT λ-DNA phage. Spermine introduces attractive interactions between the DNA strands and strongly reduces the interstrand repulsions (*11*, *45*). This allows re-establishing of inter-strand packing defects (that were hindered by the increased temperature), and therefore increases ordering of the DNA in the capsid. Cryo-EM reconstruction cross-sections in Figure 3.5 demonstrate that addition of 1 mM spermine induces an increased ordering of the DNA in the center of the capsid, while it does not affect the ordered DNA in the periphery of the capsid. We observed that the concentric DNA layers now extend further towards the center of the capsid and their number is increased from 7 to 9 layers. However, the DNA ordering and the inter-axial distance for the first 7 DNA layers in the periphery of the capsid remains unaffected. This is explained by the

dominant short-range DNA-DNA hydration repulsion over the electrostatic repulsion interaction at interaxial spacings of a_h = 27.5Å in WT DNA phage λ. SAXS measurements on WT DNA phage λ in 1 mM spermine confirm the increased amount of ordered encapsidated DNA with an increased DNA diffraction peak area compared to the case without spermine (shown in Figure 3.4B). Furthermore, with spermine, the DNA diffraction peak area varies only slightly in the entire temperature range (20-40ºC) and no phase transition is observed. This is due to the fact that the increasing DNA repulsive interactions with increasing temperature (resulting from hindering of the packing defects) are now offset by the spermine induced attractive interactions. As a result, the inter-strand repulsive interactions in the center of the capsid are not large enough to induce the phase transition. These observations support the validity of our assumption that the structural phase transition is occurring closer to the capsid core.

3.8 Effect of DNA transition on the Kinetics of Initiation of DNA Ejection

Additional AFM data (work by Udom Sae-Ueng, data not shown) suggested that repulsive interstrand interactions restrict the mobility of the intracapsid genome, which may lead to an energy barrier for the initiation of genome ejection from the capsid at temperatures below that of the structural DNA transition. To test this hypothesis, we triggered DNA ejection from phage λ in vitro by adding purified LamB receptor. Using single-molecule fluorescence, we measured the average ensemble kinetics of the number of phages that ejected their DNA versus time once LamB was added (Figure 3.6). It is important to emphasize that the ejection time for individual phage particles is significantly shorter than the time frame for our measurements, which we confirmed with single-molecule FM measurements and which also was verified in refs. (*10*) and (*46*). The LamB was used in excess (1:10,000 phage-to-LamB ratio) so that the initiation of DNA ejection was not limited by the LamB diffusion (which was confirmed experimentally).

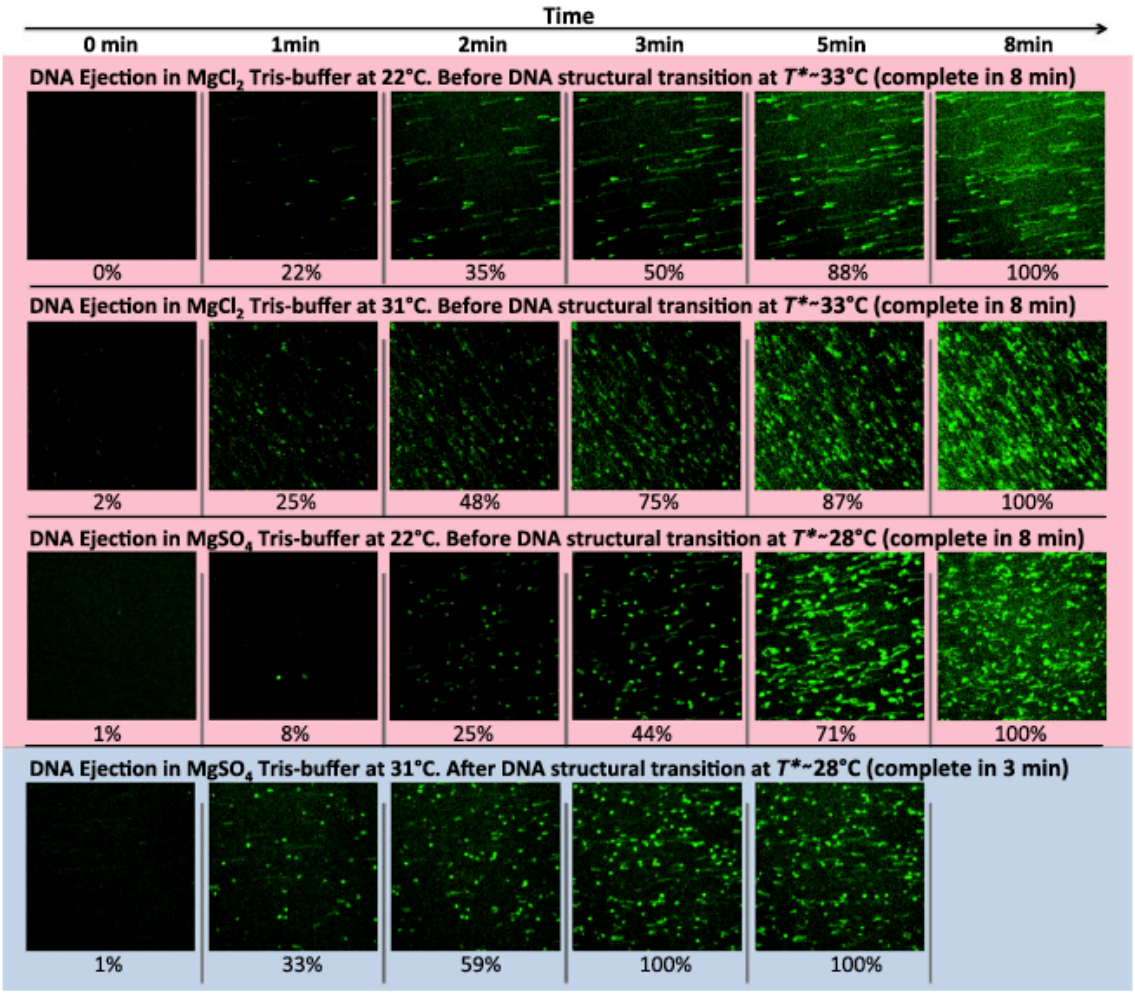

Figure 3.6 Single-molecule fluorescence measurements of the ensemble kinetics for DNA ejection. Data from phage λ over time in $MgCl_2$ and $MgSO_4$ Tris-buffers at 22 °C and 31 °C. Green YOYO dye shows particles with ejected DNA stretched in the flow. The ejection is triggered by LamB receptor addition at time 0 and flown continuously with YOYO in the flow chamber.

We performed fluorescence measurements of DNA ejection using a spinning-disk confocal microscope. Phage λ particles were adsorbed to a hydrophobically modified glass surface in a flow cell chamber. Fluorescent dye (YOYO-1) was flown in together with LamB at time 0. The diffusion of YOYO into the capsid interior was strongly kinetically limited. Once the DNA was ejected, YOYO instantly bound to it and indicated the number of phage particles that ejected genome, appearing as

fluorescent spots over time (Figure 3.6). The ejected DNA remained attached to the capsid, which also was observed in ref. (*10*). Furthermore, the ejected DNA immediately adhered to the modified glass surface and appeared partially stretched in the flow, helping us visualize phages that had ejected their genomes. Figure 3.6 demonstrates that ejection from all phage particles does not start simultaneously.

We measured population ejection kinetics in $MgSO_4$ Tris-buffer below and above the DNA transition temperature (T^* ~28 °C), at 22 °C and 31 °C. The data show that before the transition at T = 22 °C, all phages have ejected their DNA after ~8 min. At the same time, at T = 31 °C after the DNA transition has occurred, all phage particles have ejected their DNA after only ~3 min. To confirm that this significant rate increase in the observed ensemble kinetics is associated with the structural transition and increased mobility of the encapsidated DNA, rather than the temperature effect on the portal-complex opening kinetics, we repeated those measurements at the same temperatures (22 °C and 31 °C) but in $MgCl_2$ Tris-buffer (Figure 3.6). Both these temperatures now were below the DNA transition temperature of T^* ~33 °C. Figure 3.6 shows that this time, temperature had essentially no effect on the ensemble ejection kinetics. At both 22 °C and 31 °C, it took ~8 min for all phage particles to eject their genomes. These kinetics data suggest that the intracapsid DNA mobility, regulated by the temperature and ionic conditions, strongly affects the ability of the virus to initiate its genome release, which likely affects the rate of viral replication in vivo.

These observations provide new insight into the physical conditions in vivo required for successful delivery of the phage genome into the cell. Our data suggest that variations in temperature and ionic conditions in the cellular cytoplasm might affect viral infectivity and the rate of infection spread. Interestingly, using plaque assays, we found that the average area of phage λ plaques formed on a fixed layer of *E. coli* cells during the same incubation time of 12 h has strong temperature

dependence at temperatures above the intracapsid DNA transition temperature (T^* ~33 °C in $MgCl_2$ Tris-buffer; Figure 3.8). Both phages and cells were resuspended in $MgCl_2$ Tris-buffer (also used for the in vitro measurements above). Remarkably, the plaque area essentially was unchanged between 30 °C and 35 °C; however, it increased rapidly once the favorable temperature of infection was reached at $T \geq 37$ °C and almost doubled when the temperature increased from 37 °C to 42 °C. Likewise, many factors might contribute to this behavior (*47*), although the temperature-sensitive variation in intracapsid DNA mobility also might play a role.

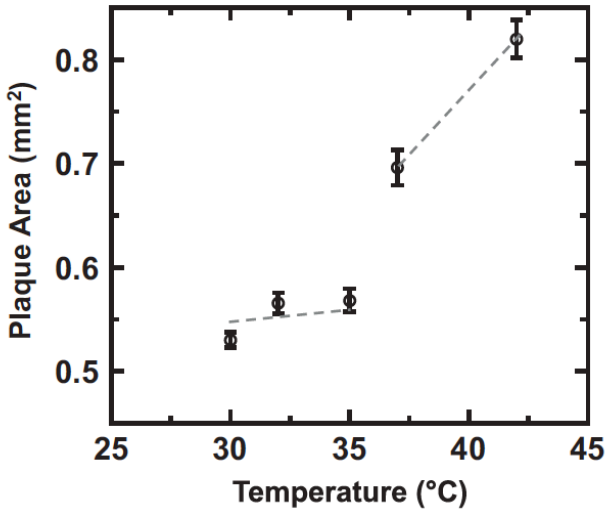

Figure 3.8 Averaged plaque area plotted as a function of incubation temperature. At least 300 plaques were analyzed for each sample. Error bars show the SD. Plaques were measured after 12 h for all samples. The plaque area is associated with the rate of infection spread of phage λ at each temperature.

3.9 Conclusions

We discovered that dsDNA in phage λ capsids undergoes a solid-to-fluid phase transition as a result of decreased genome ordering occurring close to the optimum temperature for infection in the environment of the human host (i.e. 37 °C). This finding explains how an otherwise rigid and crystalline encapsidated viral genome can be rapidly and readily ejected into the cell. This is the first demonstration of viral metastability attributed to the genome rather than the capsid. Since phage infectivity in vivo is significantly affected by the efficiency of viral DNA translocation into the cell (*12*, *15*), the metastable state of the tightly packaged DNA is likely to be rate limiting for the viral replication cycle. Thus, at lower temperatures outside the host, the DNA in the capsid is rigid which prevents its spontaneous release. Once

inside the host, the increased temperature induces the necessary fluidity of the viral genome facilitating its infection of bacterial cells. This demonstrates an evolutionary physical adaptation of viruses to their host environment. Similar work was done by others in our group on human Herpes Simplex virus (HSV-1) that its intra-capsid stressed DNA state leads to the pressure driven DNA ejection analogous to that of phage λ (*31*). This suggests that this unique metastable state of DNA in viral capsids can be universal for many pressurized viruses and can serve as a new target for drugs interfering with viral replication.

References for Chapter 3

1. A. Evilevitch, L. Lavelle, C. M. Knobler, E. Raspaud, W. M. Gelbart, Osmotic pressure inhibition of DNA ejection from phage. *Proceedings of the National Academy of Sciences of the United States of America* **100**, 9292-9295 (2003).
2. M. E. Cerritelli *et al.*, Encapsidated conformation of bacteriophage T7 DNA. *Cell* **91**, 271-280 (1997).
3. W. C. Earnshaw, S. C. Harrison, DNA arrangement in isometric phage heads. *Nature* **268**, 598-602 (1977).
4. W. C. Earnshaw, J. King, S. C. Harrison, F. A. Eiserling, The structural organization of DNA packaged within the heads of T4 wild-type, isometric and giant bacteriophages. *Cell* **14**, 559-568 (1978).
5. W. C. Earnshaw, S. R. Casjens, DNA packaging by the double-stranded DNA bacteriophages. *Cell* **21**, 319-331 (1980).
6. G. C. Lander *et al.*, The structure of an infectious P22 virion shows the signal for headful DNA packaging. *Science* **312**, 1791-1795 (2006).
7. D. W. Bauer, J. B. Huffman, F. L. Homa, A. Evilevitch, Herpes virus genome, the pressure is on. *J Am Chem Soc* **135**, 11216-11221 (2013).
8. B. V. Prasad *et al.*, Visualization of ordered genomic RNA and localization of transcriptional complexes in rotavirus. *Nature* **382**, 471-473 (1996).
9. C. Bazinet, J. King, The DNA translocating vertex of dsDNA bacteriophage. *Annual review of microbiology* **39**, 109-129 (1985).
10. P. Grayson, L. Han, T. Winther, R. Phillips, Real-time observations of single bacteriophage lambda DNA ejections in vitro. *Proceedings of the National Academy of Sciences of the United States of America* **104**, 14652-14657 (2007).
11. G. C. Lander *et al.*, DNA bending-induced phase transition of encapsidated genome in phage lambda. *Nucleic acids research* **41**, 4518-4524 (2013).
12. S. Koster, A. Evilevitch, M. Jeembaeva, D. A. Weitz, Influence of internal capsid pressure on viral infection by phage lambda. *Biophysical journal* **97**, 1525-

1529 (2009).

13. S. Tzlil, J. T. Kindt, W. M. Gelbart, A. Ben-Shaul, Forces and pressures in DNA packaging and release from viral capsids. *Biophysical journal* **84**, 1616-1627 (2003).
14. D. E. Smith *et al.*, The bacteriophage straight phi29 portal motor can package DNA against a large internal force. *Nature* **413**, 748-752 (2001).
15. E. Nurmemmedov, M. Castelnovo, E. Medina, C. E. Catalano, A. Evilevitch, Challenging packaging limits and infectivity of phage lambda. *Journal of molecular biology* **415**, 263-273 (2012).
16. S. B. Zimmerman, L. D. Murphy, Macromolecular crowding and the mandatory condensation of DNA in bacteria. *FEBS Lett* **390**, 245-248 (1996).
17. F. Livolant, Ordered Phases of DNA Invivo and Invitro. *Physica A* **176**, 117-137 (1991).
18. F. Livolant, A. Leforestier, Condensed phases of DNA: Structures and phase transitions. *Prog Polym Sci* **21**, 1115-1164 (1996).
19. J. Pelta, Jr., D. Durand, J. Doucet, F. Livolant, DNA mesophases induced by spermidine: structural properties and biological implications. *Biophysical journal* **71**, 48-63 (1996).
20. B. A. Todd, D. C. Rau, Interplay of ion binding and attraction in DNA condensed by multivalent cations. *Nucleic acids research* **36**, 501-510 (2008).
21. J. Lepault, J. Dubochet, W. Baschong, E. Kellenberger, Organization of double-stranded DNA in bacteriophages: a study by cryo-electron microscopy of vitrified samples. *The EMBO journal* **6**, 1507-1512 (1987).
22. S. C. Riemer, V. A. Bloomfield, Packaging of DNA in bacteriophage heads: some considerations on energetics. *Biopolymers* **17**, 785-794 (1978).
23. I. Ivanovska, G. Wuite, B. Jonsson, A. Evilevitch, Internal DNA pressure modifies stability of WT phage. *Proceedings of the National Academy of Sciences of the United States of America* **104**, 9603-9608 (2007).
24. M. Jeembaeva, B. Jonsson, M. Castelnovo, A. Evilevitch, DNA heats up:

energetics of genome ejection from phage revealed by isothermal titration calorimetry. *Journal of molecular biology* **395**, 1079-1087 (2010).

25. V. A. Parsegian, R. P. Rand, N. L. Fuller, D. C. Rau, Osmotic stress for the direct measurement of intermolecular forces. *Methods Enzymol* **127**, 400-416 (1986).
26. J. DeRouchey, B. Hoover, D. C. Rau, A comparison of DNA compaction by arginine and lysine peptides: a physical basis for arginine rich protamines. *Biochemistry* **52**, 3000-3009 (2013).
27. P. K. Purohit, J. Kondev, R. Phillips, Mechanics of DNA packaging in viruses. *Proceedings of the National Academy of Sciences of the United States of America* **100**, 3173-3178 (2003).
28. D. Lof, K. Schillen, B. Jonsson, A. Evilevitch, Forces controlling the rate of DNA ejection from phage lambda. *Journal of molecular biology* **368**, 55-65 (2007).
29. S. Chakraborty *et al.*, Mechanistic Insight into the Structure and Dynamics of Entangled and Hydrated lambda-Phage DNA. *J Phys Chem A* **116**, 4274-4284 (2012).
30. T. Liu *et al.*, Solid-to-fluid-like DNA transition in viruses facilitates infection. *Proceedings of the National Academy of Sciences of the United States of America* **111**, 14675-14680 (2014).
31. U. Sae-Ueng *et al.*, Solid-to-fluid DNA transition inside HSV-1 capsid close to the temperature of infection. *Nature chemical biology* **10**, 861-867 (2014).
32. A. Evilevitch *et al.*, Effects of salt concentrations and bending energy on the extent of ejection of phage genomes. *Biophysical journal* **94**, 1110-1120 (2008).
33. X. Qiu *et al.*, Salt-dependent DNA-DNA spacings in intact bacteriophage lambda reflect relative importance of DNA self-repulsion and bending energies. *Physical review letters* **106**, 028102 (2011).
34. W. C. Earnshaw, S. C. Harrison, DNA arrangement in isometric phage heads. *Nature* **268**, 598-602 (1977).

35. T. Liu *et al.*, Solid-to-fluid-like DNA transition in viruses facilitates infection. *Proc Natl Acad Sci U S A*, (2014).
36. I. S. Gabashvili, A. Grosberg, Dynamics of double stranded DNA reptation from bacteriophage. *Journal of biomolecular structure & dynamics* **9**, 911-920 (1992).
37. F. P. Booy *et al.*, Liquid-crystalline, phage-like packing of encapsidated DNA in herpes simplex virus. *Cell* **64**, 1007-1015 (1991).
38. W. Jiang *et al.*, Structure of epsilon15 bacteriophage reveals genome organization and DNA packaging/injection apparatus. *Nature* **439**, 612-616 (2006).
39. A. Huet, J. F. Conway, L. Letellier, P. Boulanger, In vitro assembly of the T=13 procapsid of bacteriophage T5 with its scaffolding domain. *Journal of virology* **84**, 9350-9358 (2010).
40. L. R. Comolli *et al.*, Three-dimensional architecture of the bacteriophage phi29 packaged genome and elucidation of its packaging process. *Virology* **371**, 267-277 (2008).
41. G. C. Lander *et al.*, Bacteriophage lambda stabilization by auxiliary protein gpD: timing, location, and mechanism of attachment determined by cryo-EM. *Structure* **16**, 1399-1406 (2008).
42. J. Kindt, S. Tzlil, A. Ben-Shaul, W. M. Gelbart, DNA packaging and ejection forces in bacteriophage. *Proceedings of the National Academy of Sciences of the United States of America* **98**, 13671-13674 (2001).
43. S. Y. Park, D. Harries, W. M. Gelbart, Topological defects and the optimum size of DNA condensates. *Biophysical journal* **75**, 714-720 (1998).
44. S. Geggier, A. Kotlyar, A. Vologodskii, Temperature dependence of DNA persistence length. *Nucleic acids research* **39**, 1419-1426 (2011).
45. D. C. Rau, V. A. Parsegian, Direct Measurement of Temperature-Dependent Solvation Forces between DNA Double Helices. *Biophysical journal* **61**, 260-271 (1992).

46. N. Chiaruttini *et al.*, Is the in vitro ejection of bacteriophage DNA quasistatic? A bulk to single virus study. *Biophysical journal* **99**, 447-455 (2010).
47. V. Doceul, M. Hollinshead, L. van der Linden, G. L. Smith, Repulsion of superinfecting virions: a mechanism for rapid virus spread. *Science* **327**, 873-876 (2010).

CHAPTER 4 AN IONIC SWITCH IN BACTERIOPHAGE λ CONTROLS VIRAL REPLICATION

4.1 Abstract

Following our discovery in Chapter 3 that DNA packaged in phage λ undergoes a disordering transition triggered by temperature, which results in increased genome mobility. This solid-to-fluid like DNA transition markedly increases the number of infectious λ particles facilitating infection. However, the structural transition strongly depends on temperature and ionic conditions in the surrounding medium. Using titration microcalorimetry combined with solution X-ray scattering, we mapped both energetic and structural changes associated with transition of the encapsidated λ-DNA. Packaged DNA needs to reach a critical stress level in order for transition to occur. We varied the stress on DNA in the capsid by changing the temperature, packaged DNA length, and ionic conditions. We found striking evidence that the intracapsid DNA transition is "switched on" at the ionic conditions mimicking those in vivo and also at the physiologic temperature of infection at 37 °C. These results suggest a remarkable adaptation of phage λ to the environment of its host bacteria in the human gut. This metastable DNA state in the capsid provides a new paradigm for the *physical evolution* of viruses. Similar to a "genetic switch", this temperature and ion regulated on-off switch of packaged DNA mobility can either inhibit or facilitate infection. Linking viral infectivity with the energetics and structure of encapsidated DNA creates novel prospects for control of viral replication.

4.2 Introduction

The idea that genes could be switched on and off has revolutionized molecular biology (*1*, *2*). It originates from studies on bacteriophage λ, which allowed establishment of the temperature induced mechanism of lysogeny-lysis transition, called "A Genetic Switch" (*1*). In this work, we discovered for the first time, that the

temperature and ionic composition in the surrounding medium of bacterial cells not only switch phage λ genes on and off (*1*, *3*), but also serve as an on-off switch for DNA structural transition in l-capsid. This transition increases DNA mobility, which facilitates the initiation of genome ejection from phage into a cell, and thus leads to infection (*4*). Virion metastability is one of the central concepts in virology (*5*). It implies that the virus, in order to successfully replicate, must be sufficiently stable to prevent spontaneous release of its genome outside the cell between infection events, and at the same time be unstable enough to release its genome during infection (*5*). Viral particles are therefore not inert structures and have not attained the minimum free energy conformation, separated by an energetic or kinetic barrier, prior to cell attachment and entry. Thus, viral structure plays an active role in genome delivery to the host cell. Viral metastability is mostly associated with structural transformations in the nucleocapsid and/or surrounding lipid envelop in response to changes in the virion's environment (*5*). However, this does not apply to motor-packaged double-stranded (ds) DNA viruses (e.g. dsDNA phages and Herpesviruses) whose capsid remains intact after the genome is released into a cell through a portal opening in the capsid structure (*6-9*). We recently found that it is the encapsidated DNA rather than the capsid itself in these viruses that is metastable (Chapter 3) (*10*, *11*). Specifically, we have shown that dsDNA packaged in phage λ and in human Herpes Simplex virus 1 (HSV-1) (*11*) undergoes a solid-to-fluid like structural transition facilitating initiation of viral genome ejection from the capsid during infection.

Ds-DNA packaged in both HSV-1 and phage λ is two orders of magnitude longer than the diameter of the capsid. This tight genome confinement leads to strong DNA-DNA repulsions and bending stress on the genome generating pressure of tens of atmospheres on the capsid walls (*7*, *8*). The encapsidated DNA is at the extreme end of the packing limit (reaching packing fraction of 55% by volume) (*12-15*), with only ~7-12 Å of interhelical surface separation (*15*). DNA at this packing density

assumes a hexagonally ordered structure with very restricted mobility (16, 17). This is caused by interhelical electrostatic sliding friction (Coulomb friction) (18-20), occurring from dragging closely packed negatively charged DNA helices past other helices.

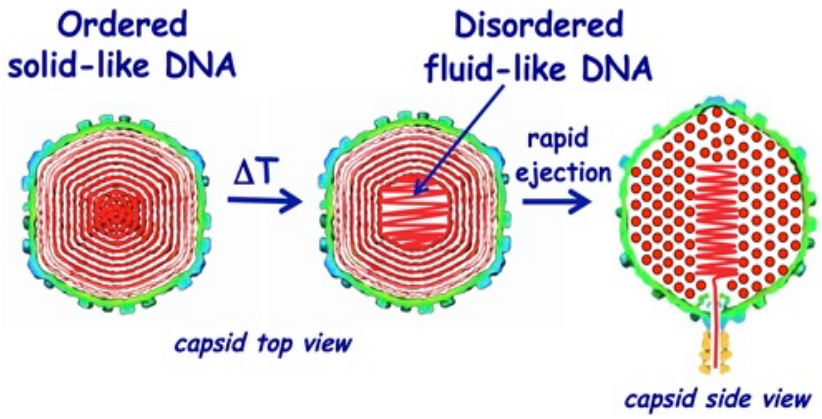

Figure 4.1 DNA disordering illustration. The DNA transition occurs when the temperature is increased. As a result, the increased mobility of the encapsidated viral DNA provides faster genome release in the cell, facilitating the infection process. Two schematic images on the left show the cross-sections of the top view of the capsid. DNA closer to the center of the capsid is likely to be ejected first since it is the last DNA portion to be packaged in the capsid during the phage assembly, due to the dsDNA bending stress constraints. This is illustrated with the side view cross-section of the capsid (right image). The schematic illustration of DNA inside the capsid shows the ordering of an averaged DNA structure and not the arrangement of individual DNA strands.

We have demonstrated for phage λ that DNA layers closest to the capsid's center undergo a disordering transition induced by an increase in temperature in Chapter 3. This occurs from an increase in interstrand repulsions leading to stronger genome stress. DNA disordering at the transition temperature leads to a locally lower packing density in the center of the capsid, maximizing DNA-DNA spacings which reduces interstrand repulsions. This, in turn, leads to a more mobile, or fluid, DNA state, which can be readily ejected, from the capsid. This observation is schematically illustrated in Figure 4.1. Thus, below the transition temperature, viral DNA is trapped in a solid-like metastable state inside the capsid, which prevents

spontaneous deactivation of the virion. An increase in temperature induces the necessary mobility of the packaged genome, facilitating its release and infection of the bacterial cell. Indeed, using a plaque assay we confirmed a marked increase in the rate of infection spread at temperatures above that of DNA transition.However, it is important to emphasize that we also found that the transition temperature is directly coupled to the critical DNA stress value in the capsid. The encapsidated genome stress is, in turn, regulated by DNA counterions and packaged DNA density, both affecting the repulsive interactions between DNA helices (*21*, *22*). This raises a fundamentally important question, whether the packaged DNA density in phage λ and the ionic conditions in vivo lead to an intracapsid DNA transition occurring at the physiological temperature of infection, i.e. 37 °C? Only then can the observed DNA transition phenomenon in phage have physiological relevance and impact on the efficiency of viral replication.

With this aim, we investigate DNA transition in phage λ as a function of packaged DNA density and at varying ionic conditions mimicking those in vivo. We mapped both energy (using Isothermal Titration Calorimetry, ITC) and structure (using solution Small Angle X-ray Scattering, SAXS) of the packaged λ-genome and found a remarkable paradigm of physical adaptation of viruses to their host. Our data show that mobility of the packaged DNA in λ-capsid is "switched on" for release from the capsid at the most favorable ionic and temperature (37 °C) conditions for E. coli infection. Furthermore, the transition occurs only at the wild-type (WT) λ-DNA length (48,500 kbp) density packaged in the capsid, as opposed to the shorter DNA length phage l mutants. This suggests that similar to a "genetic switch", this ion-regulated DNA mobility transition mechanism is likely to be a part of the phage λ replication decision.

4.3 Materials and methods

4.3.1 Phage l and LamB purification

WT bacteriophage λ cI857, with a genome length of 48.5 kb was produced by thermal induction of lysogenic E. coli strain AE1 derived from the S2773 strain. Two phage λ mutants with shorter genome lengths (78% and 94% of the WT DNA length) were produced using a similar procedure. The receptor was the LamB protein purified from pop 154, a strain of E. coli K12 in which the LamB gene has been transduced from Shigella sonnei 3070. Phage and LamB purification details are described in previous work and previous chapters (*8*, *23*).

4.3.2 Isothermal titration calorimetry (ITC)

All calorimetric measurements were performed using the MicroCal iTC200 system manufactured by GE Healthcare, Life Sciences. The details of phage DNA ejection enthalpy measurements are described in Chapter 3 (*10*, *24*).

4.3.3 SAXS

Small angle X-ray scattering (SAXS) measurements were carried out at the 12-ID B station at the Advanced Photon Source (APS) at Argonne National Laboratory. A detailed description is provided in Chapter 3.

4.3.4 Analysis of SAXS measured DNA diffraction peak position and area

Small angle X-ray scattering (SAXS) measurements were carried out at the 12-ID B station at the Advanced Photon Source at Argonne National Laboratory. A 12-KeV X-ray beam was used to illuminate the sample with an overall scattering vector q range from 0.006 to 0.850 Å−1. A total of 120 μl of phage solution (~5 × 1013 pfu/ml) was injected into a flow-through glass capillary and the solution was oscillated during the SAXS measurement with a flow rate of 10 μl/s. Forty scans with 1 s X-ray exposure time were collected and averaged for each sample. A buffer solution of the dialysis buffer for phage samples was measured using the same SAXS setup, which was further subtracted as the background. After the background subtraction, the scattered intensity I versus q was plotted and the DNA peak region

was truncated from 0.18 Å−1 to 0.33 Å−1. This DNA diffraction peak was fitted with a Gaussian curve plus a linear background using function-1, where q_0 is the peak center, w is the peak width, A_0 is the peak area, k is the slope of the linear background and c is the offset.

$$I = \left(\frac{A_0}{w \times \sqrt{\pi/2}}\right) e^{-2\left(\frac{q-q_0}{w}\right)^2} + kq + c \qquad \text{(Function-1)}$$

The DNA peak area A_0 was chosen as the most convenient measure of the ordered DNA strands, because it includes a temperature factor or the displacement parameter, which signifies the drop in the diffraction peak intensity due to the thermally induced vibration or displacement of the scattering centers.

4.4 Effect of packaged genome density on intracapsid DNA transition

Temperature is a parameter that is rarely varied in biophysical measurements on viruses. Yet, temperature is directly pertinent to the ability of viruses to survive outside of their hosts and multiply within them. As mentioned above, we found that WT DNA length packaged in phage λ undergoes a disordering transition in response to a temperature increase. This structural change leads to a more mobile DNA state inside the capsid, which facilitates the initiation of its rapid release into a cell during infection. In this section we investigate how the packaged genome length in λ affects the structural transition behavior. Using ITC and SAXS we are analyzing changes in the energy and structure of the encapsidated DNA with 78%, 94% and 100% of the WT λ-DNA length between 10 and 40 °C. The ionic conditions in these measurements are set by 10 mM $MgCl_2$ Tris-buffer, chosen to mimic the free Mg-concentration in the *E. coli* (*25-27*). This Mg-concentration was also shown to provide the most efficient phage λ adsorption to bacterial cells, maximizing the subsequent infection (*28*, *29*).

We designed a new micro-calorimetric assay that allows direct measurements of the internal energy of the confined viral genome . Using micro-ITC, the enthalpy change *(ΔH)* associated with DNA ejection from phage λ is measured as heat

released when concentrated phage particles are titrated into a LamB receptor solution, which triggers DNA ejection in vitro. Since the total volume of the system does not change during the DNA ejection, and the pressure is constant, the internal energy and the enthalpy are approximately equal (*10*, *24*). $\Delta H_{ej}(T)$ was measured in the temperature range between 18°C and 42°C. Our data show that the critical genome stress is reached at temperature T^* and is required for the structural transition to occur. This suggests that varying the initial DNA stress inside the capsid should determine whether the transition will occur within the studied temperature range. We test this hypothesis by repeating the ITC measurements above for shorter packaged genome length λ-mutants, 78% and 94% of the WT λ-DNA length, while keeping the buffer conditions the same. DNA pressure inside λ capsids is significantly reduced when shorter DNA length is packaged (15 atm in 78% λ-DNA versus 35 atm in WT λ-DNA phage mutants) (*21*). Lower DNA density in the capsid has larger spacings between packaged DNA helices, resulting in weaker repulsive interactions and lower genome stress (*21*). Indeed, we found that no DNA transition occurred inside the capsid for these l-mutants with shorter packaged DNA length than WT λ-DNA (within the investigated temperature range), see Figure 4.2A. This demonstrates that there is a strong dependence between the internal genome stress and the structural DNA transition in phage λ. Next, we investigate how the structural changes of DNA in the capsid are associated with the observed energy transition using SAXS.

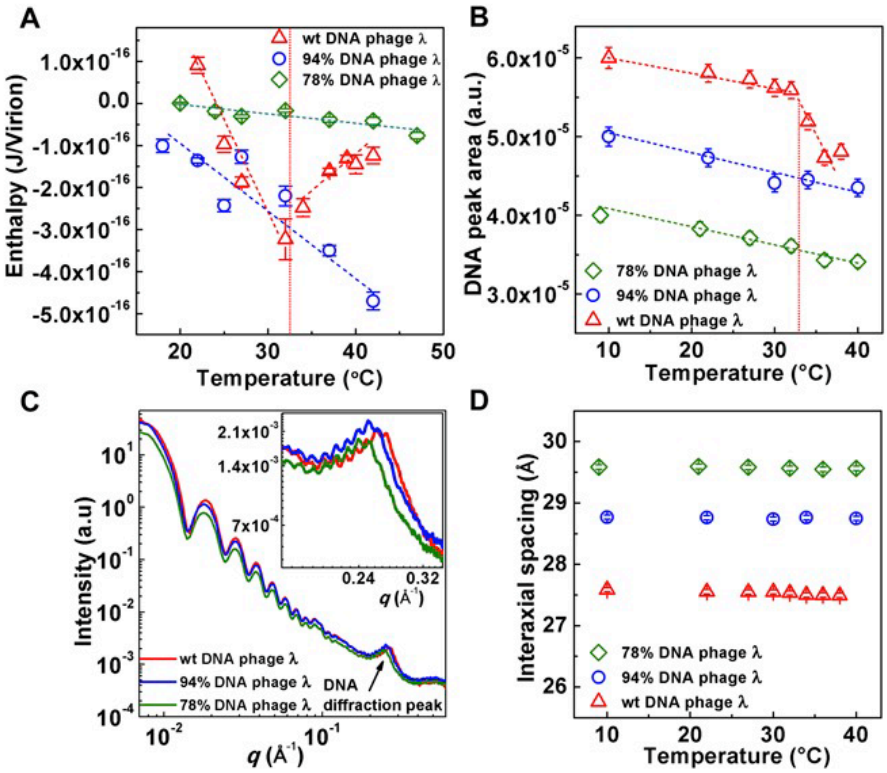

Figure 4.2 ITC and SAXS data of different λ mutants. data collected in 10 mM $MgCl_2$ Tris-buffer. (A) Enthalpy of DNA ejection per virion (J) versus temperature for phage λ with 100, 94 and 78% of WT packaged λ-DNA length. Dashed lines are drawn to guide the eye. ΔH_{ej} values were obtained as an average of five to six independent measurements for each sample. Vertical error bars are SEs. (B) DNA–DNA diffraction peak area as a function of temperature for 100, 94 and 78% of WT DNA length packaged in phage λ. The peak area is obtained by fitting the scattering curve with a Gaussian function with linear background subtraction. The vertical error bars are from the nonlinear fitting. A constant has been added to each set of area values corresponding to one DNA length phage mutant in order to vertically separate the data for visual comparison. The dashed line is drawn to guide the eye. (C) Radially averaged scattered intensity versus the scattering vector q for 100, 94 and 78% of WT DNA length phage λ mutants at 22°C. Inset figure shows the zoom-in of the DNA diffraction peak for three DNA length l-phages. The scattering profile at lower q is attributed to the protein capsid. (D) DNA–DNA interaxial spacing d as a function of temperature for 100, 94 and 78% of WT λ-DNA length packaged in phage λ. Vertical error bars are from the non-linear fitting of the DNA diffraction peak with a Gaussian function with linear background subtraction.

Solution SAXS provides direct structural information about the encapsidated genome([10](), [12](), [30]()). Figure 4.2B shows integrated scattering intensity, I, versus scattering vector q for all three packaged genome length λ particles (78%, 94%, and 100% of WT DNA length). In the lower q region (0.007Å^{-1} to 0.1Å^{-1}), the scattering

profile originates from the highly symmetrical icosahedral phage capsids. The single peak with the small oscillating ripples on its top at higher q (between 0.2 $Å^{-1}$ to 0.3 $Å^{-1}$) is due to the diffraction from the encapsidated DNA. The short-range DNA interaxial spacings determine the position of the DNA diffraction peak, while the area of this peak provides information on the total number of ordered DNA base pairs of the encapsidated genome (*10*, *12*). When DNA inside the capsid becomes less ordered, the DNA peak area decreases as a result of less coherent diffraction. The average DNA-DNA interaxial spacing, d, is calculated using $d = \frac{4\pi}{\sqrt{3}q}$, assuming the hexagonal packing structure of DNA (*12*). The position of the DNA diffraction peak gradually shifts to lower q values as the packaged DNA length decreases from 100% to 78% of WT l-DNA length (see the inset in Figure 4.2B), indicating that the interaxial distance between packaged DNA strands increases, shown in Figure 4.2C. The DNA interaxial distance was nearly constant between 10 and 40 °C for each DNA length λ-mutant.

The encapsidated DNA structure and interaxial distance between ordered DNA strands are determined by DNA–DNA electrostatic and hydration repulsive interactions (*31-34*), as well as the genome bending stress (*15*, *30*). Intracapsid confinement requires DNA to bend along radii that are energetically unfavorable given the stiffness of dsDNA (*35*, *36*). To relieve the bending stress, helices are packed closer to the capsid wall, increasing the bending radius and also decreasing the DNA-DNA spacing. At the same time, the repulsive DNA-DNA interactions attempt to push DNA strands as far from each other as possible, maximizing the interstrand separations (*15*) and filling the entire capsid volume. With shorter λ-DNA length packaged in the capsid, the DNA-DNA distance is increased in order to minimize the interstrand repulsions.

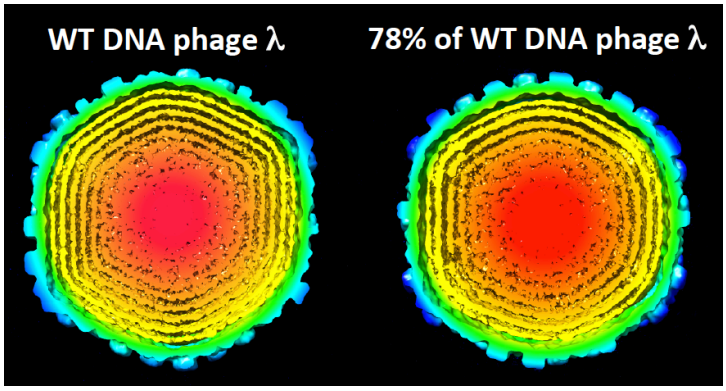

Figure 4.3 Cutaway views of cryo-EM reconstructions of phage λ containing different amounts of DNA (100% and 78% of the WT λ-DNA length). Spacing between the outermost layers of the DNA can be observed, while the DNA becomes more disordered closer to the center of the capsid. Owing to the icosahedral symmetry imposed during the reconstruction, concentrically packed DNA within the capsid becomes shells of density. The density maps are from our ref. (*15*).

Figure 4.3 shows cryo electron microscopy (cryo-EM) single particle reconstructions of λ-capsids filled with 78% and 100% of WT DNA length. The image cross-sections show that the entire capsid volume for both types of capsids is filled with DNA extending all the way to the center of the capsid (*15*). Starting from the capsid walls, there are well ordered, multiple concentric DNA layers. The layers are evenly spaced indicating that DNA has adapted an ordered repetitive structure characteristic of a liquid crystalline state. However, toward the center of the capsid, the ordered layers disappear suggesting a less ordered DNA structure than in the periphery of the capsid (*7*). We have previously discussed that with increasing temperature, DNA-DNA repulsive interactions are not significantly affected. However, an increase in temperature will decrease the DNA persistence length (*37*), leading to less bending stress. If the bending stress decreases due to repulsive interactions, the DNA will expand towards the center of the capsid, increasing interstrand separations. However, Figure 4.2C shows that the spacing remains essentially constant for all three λ-DNA length mutants in 10 mM $MgCl_2$ Tris-buffer, suggesting that the temperature induced decrease in the bending stress is insufficient to affect the balance between the repulsive forces and the bending stress on the encapsidated genome. (The effect of increased interaxial spacing with

increasing temperature due to a decrease in the bending stress will be demonstrated below under different ionic conditions than those above.)

Besides repulsions and bending stress, when DNA is bending inside the capsid, the initial correlation between two helices that have slightly different radii of curvature is lost, and the mutual orientation between helices must be re-established. This leads to the packing defects that are absent for linear packaging of DNA in solution. Packing defects are required in order to re-establish a favorable phosphate-phosphate 'phasing' of helices, reducing the repulsive interactions due to bending (*15*, *38*, *39*). Indeed, ITC data in Figure 4.2A show a progressive increase in the packaged DNA energy with increasing temperature prior to DNA transition. To relieve this increasing DNA stress in the capsid, the genome undergoes a disordering transition when the maximum stress value is reached at temperature T*. Figure 2D shows the area of DNA scattering peak versus temperature, reflecting the overall ordering of the packaged genome for all three DNA length λ-mutants. For WT λ-DNA length phage at T*~33 °C, the DNA diffraction peak area undergoes a sudden drop. This area drop signifies a loss of the amount of ordered DNA inside the capsid and occurs precisely at the transition temperature observed with ITC in Figure 2A. We have shown that a disordering transition takes place closer to the center of the capsid, where packing defects are larger than for DNA closer to the capsid wall, as illustrated in Figure 4.1. Since with increasing temperature the DNA bending stress becomes smaller. This allows a fraction of the ordered DNA layers closest to the capsid's center (where DNA bending stress is stronger) to undergo a disordering transition. The disordered DNA will have a locally lower packing density in the center, which maximizes DNA-DNA spacings and simultaneously reduces the repulsive interactions. This yields an overall lower energy state of the encapsidated genome and increases its mobility, which in turn facilitates DNA release during infection.

At the same time, in agreement with ITC results, SAXS data in Figure 2D show that shorter λ-DNA length mutants (78% and 94% of WT DNA length phages), do not undergo a disordering transition within the investigated temperature range of 10 - 40 °C. The DNA peak area shows only a weak linear decrease with increasing temperature for these shorter DNA λ-mutants without an abrupt drop. This result confirms that in order for DNA transition to occur, the encapsidated genome has to reach the critical stress value first, which is not achieved if the DNA packing density is lower than in the WT phage λ. It is remarkable that intracapsid genome transition occurs within the physiologic temperature range only when packaged DNA in the λ-capsid has a length corresponding to that of the WT λ-genome. While shorter genome length λ-mutants will also experience reduced electrostatic sliding friction and therefore result in a more mobile DNA state in the capsid, those λ-mutants will have reduced capsid pressure (*21*). We have shown that the reduced DNA pressure in these phage λ DNA mutants leads to a markedly reduced probability of infection due to the lack of driving force for DNA ejection (e.g. infectivity is reduced by ~30% for 78% DNA length λ compared to the WT DNA phage λ)(*40*). The specific WT DNA length (48.5 kbp) in phage λ appears to provide the unique genome structure with a stress value capable of both driving DNA release from the capsid and creating a metastable DNA state required for solid-to-fluid like DNA transition to occur. These physical parameters are required for efficient DNA release from phage λ during infection.

Thus, we have shown that intracapsid DNA transition is strongly correlated with the internal DNA stress. However, the DNA stress in the capsid is regulated by both packaged DNA length and by the concentration and nature of the DNA counterions freely diffusing through the capsid wall of most viruses (22). This fact leads us to the next important question which is whether extra- and intra-cellular ionic conditions in the bacterial host are favorable for DNA to undergo a transition in the phage

λ capsid close to the physiologic temperature of infection? The effect of ionic conditions on the DNA transition temperature is investigated in the next section.

4.5 Effect of ionic conditions on DNA transition temperature

While variation in the monovalent ion concentration has a small influence on intra-capsid DNA stress(*22*), polyvalent cations present in the bacterial cytoplasm, such as polyamines and Mg2+, have been shown to have a strong effect on the repulsive interactions between packaged DNA helices(*22*, *30*). Since the free polyamine concentration in cells is very low as most polyamines are bound to cellular DNA and RNA(*41-43*), we are specifically interested in the effect of the Mg-ion concentration on the DNA transition temperature in phage l at concentrations similar to those of free Mg^{2}+ in vivo.

Mg-ions are essential for both cellular metabolism (e.g. enzyme activity, protein synthesis, preservation of ribosome and nucleic acid structures)(*25*, *44-46*), as well as the phage λ infectious cycle (*28*, *29*). It has been shown that a concentration of 10-20 mM of Mg^{2+} ions in the extracellular solution is critically important for optimum adsorption and infection of E. coli by phage λ(*28*). Mg-concentrations below or above 10-20 mM had a strong negative effect on the number of bacterial cells that could be infected. Interestingly, a similar Mg-concentration (~10 mM Mg^{2+}) has also been shown to provide optimum conditions for DNA packaging in phage λ (*29*, *47*) and also corresponds to the free Mg-concentration in E. coli cytoplasm (*25-27*). As mentioned above, since the Mg-concentration affects DNA stress in the capsid, it also strongly influences the transition temperature of the encapsidated genome. Therefore, we investigate whether the physiologic Mg-concentrations described above provide optimum conditions for phage λ infectivity in vivo by facilitating DNA transition in the λ capsid close to the temperature of infection (37 °C). Such a unique correlation between the Mg-concentration and DNA

transition temperature would suggest that the intracapsid DNA transition is an important regulatory mechanism for viral replication.

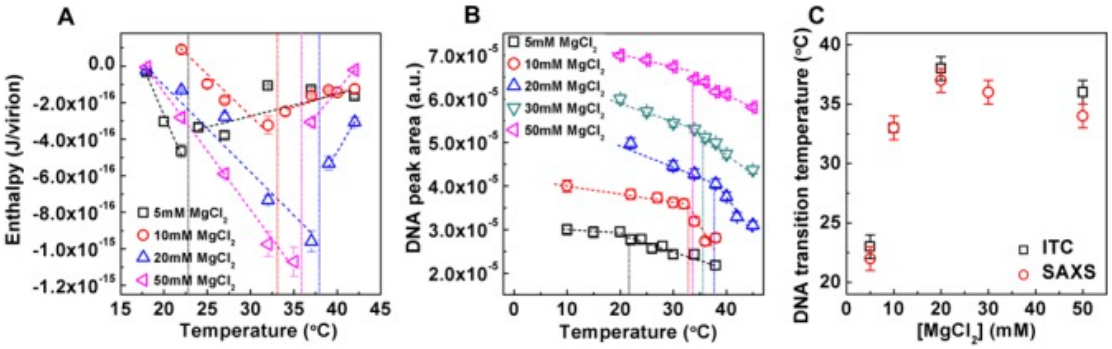

Figure 4.4 (A) Enthalpy of DNA ejection with different $MgCl_2$ concentrations. Data from WT DNA phage λ. (A) ΔH_{ej}, in $MgCl_2$ – Tris buffers. (B) Area of the fitted DNA diffr-action peak for WT phages in $MgCl_2$ – Tris buffers with different $MgCl_2$ concentrations as a function of temperature. For each Mg concentration, a constant was added to the DNA areas in order to separate them from other series. The area values were calculated by fitting the DNA diffraction peak with a Gaussian curve plus a linear background. (C) Comparison of the DNA transition temperature determined by ITC and SAXS as a function of $MgCl_2$ concentration.

We are using ITC and SAXS assays described above to determine DNA transition temperatures for WT λ-DNA length phage in $MgCl_2$ Tris-buffer with $MgCl_2$ concentrations varied between 5 and 50 mM, see Figure 4.4. The intracapsid DNA transition occurs at temperature *T*,* corresponding to either a discontinuity in the linear dependence of ΔH_{ej} on temperature (Figure 4.4A) or to an abrupt change in the linear decay of the DNA diffraction peak area versus temperature measured by SAXS (Figure 4.4B). DNA transition temperatures as a function of Mg-concentration determined by both techniques are in good agreement with each other and are summarized in Figure 4.4C. Increasing the Mg-concentration will initially significantly reduce the strength of the interstrand repulsive interactions in the capsid due to the counterion screening of the negative charges between packaged DNA helices (*15*, *22*). However, we have previously shown that at DNA packing densities in phage l, the screening effect of Mg-ions will become progressively

smaller due to the counter-ion saturation (*22*). Furthermore, if the Mg-ion concentration continues to increase, the counterions are forced into regions on the helices that begin to increase the effective repulsions between packaged DNA strands. Thus, there is a minimum in interstrand repulsive interaction versus Mg-concentration (*22*, *48*).

Figure 4.4C shows that the DNA transition temperature T^* is at first significantly increased with increasing Mg-concentration, from T^*~22 °C at 5 mM $MgCl_2$ Tris-buffer to T^*~37 °C at 20 mM $MgCl_2$ Tris-buffer. However, increasing the Mg-concentration further has an opposite effect on the DNA transition temperature, showing a weak decrease in T^* between 20 and 50 mM $MgCl_2$. T^* reaches ~35 °C at 50 mM $MgCl_2$, see Figure 4.4C. This variation in the transition temperature correlates well with previously observed nonmonotonic variation in the DNA stress in the capsid with increasing Mg-concentration (*22*), as described above. Initially, as the Mg-concentration is increased between 5 and 20 mM, the internal DNA stress is reduced leading to a higher transition temperature. That is, a higher temperature is required to reach the critical DNA stress limit in order to overcome the energetic barrier triggering the structural genome transition. Once the Mg^{2+}-ion saturation yielding maximum counterion screening between the packaged DNA helices occurs at ~20 mM (*22*), the interstrand repulsive interactions start to increase again with increasing Mg-concentration. This results in a decrease of T^*, since the critical intracapsid DNA stress level required for transition is now achieved at a lower temperature. Thus, while T^* varies significantly with Mg^{2+} concentration, the most favorable Mg-concentration for phage λ infection of *E. coli* (~10-20 mM) (*28*) triggers DNA transition in the capsid precisely at the physiologic temperature of infection (~37 °C). This striking correlation confirms our assumption. Namely, that the intracapsid DNA transition mechanism in λ is evolutionarily adapted to both the ionic environment and temperature of its host, suggesting its significance for viral replication.

In the next Section we investigate how polyvalent ions in the host solution can switch the DNA transition in phage λ on and off by directly affecting the interstrand repulsions, and consequently, the stress level of the encapsidated genome. Since DNA transition markedly affects the ability of the virion to eject its DNA into a cell, these results demonstrate how variations in the host's ionic environment can lead to favorable as well as inhibiting conditions for infectivity.

4.6 Switching intracapsid DNA transition on and off

As discussed above, intracapsid DNA transition is triggered by a temperature increase. However, DNA in the capsid has to reach the critical stress value at T^* before the transition can occur. The overall DNA stress can in turn be varied by packaged DNA length (*21*) or by polyvalent cations (*22*) diffusing into the capsid and affecting the interstrand repulsive interactions. We observed that by varying either of these two parameters leads to variation in the internal DNA stress and transition temperature. This suggests that the intracapsid DNA transition can be switched on and off for the same viral particle within the physiologically relevant temperature range studied here (10-45 °C). To demonstrate this assumption, we selected 78% and 100% WT DNA length phage λ in 10 mM $MgCl_2$ Tris-buffer as our reference systems. The 78% WT DNA length λ does not display an intracapsid DNA transition (Figure 4.2A and D), while 100% WT DNA length phage λ undergoes a DNA transition at ~33 °C (Figure 4.2A and D).

In the first set of measurements, we added spermine($^{4+}$) ions to the WT DNA length phage λ to introduce attractive interactions between packaged DNA strands (*15*, *22*, *31*). This allows re-establishing of inter-strand packing defects (that were hindered by the increased temperature) and reduces the overall DNA stress. The DNA diffraction peak area now shows only slight variation in the entire temperature range (20-40 °C), and no abrupt DNA transition is observed, in contrast to WT DNA phage λ without added sperimine($^{4+}$), see Figure 4.5A. Thus, the DNA transition in

the capsid has been switched off with spermine($^{4+}$) ions, where the increasing DNA repulsive interactions with increasing temperature (resulting from hindering of the packing defects) are now offset by the spermine($^{4+}$) induced attractive interactions. The DNA stress in the capsid is therefore insufficient for DNA transition to occur.

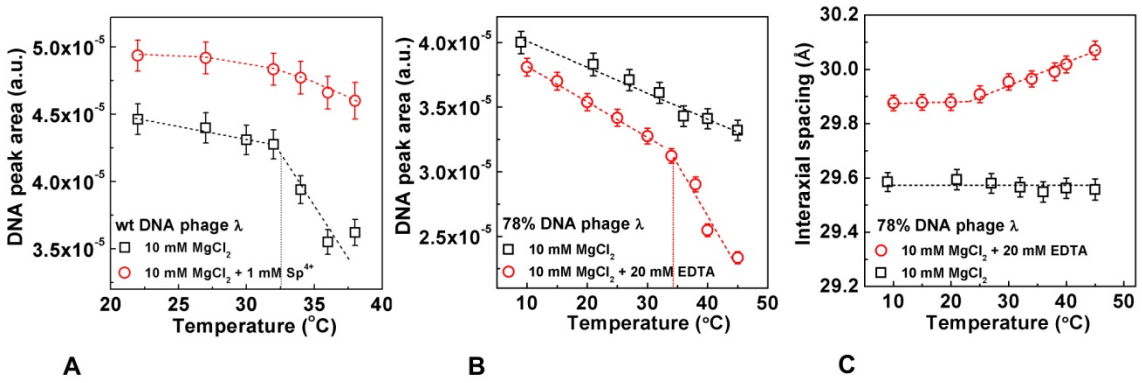

Figure 4.5 An ionic switch of DNA transition. (A) DNA-DNA diffraction peak area as a function of temperature for WT DNA phage λ in 10 mM $MgCl_2$ Tris-buffer without (squares) and with 1 mM spermine (circles). (B) Area of the fitted DNA diffraction peak as a function of temperature for 78% DNA phage λ in 10 mM $MgCl_2$ Tris-buffer (black squares) and in 10 mM $MgCl_2$ Tris-buffer plus 20 mM EDTA (red circles). (C) DNA-DNA interaxial spacing *d* of 78% DNA phage λ in 10 mM $MgCl_2$ Tris-buffer and in 10 mM $MgCl_2$ Tris-buffer plus 20 mM EDTA as a function of temperature.

Next, we investigate if DNA transition can instead be switched on in the 78% WT DNA length phage λ. As shown above, 78% WT DNA length λ in 10 mM $MgCl_2$ Tris-buffer does not display a DNA transition between 10 and 40 °C due to insufficient DNA stress in the capsid, see Figure 4.2A and 4.2D. Through addition of excess EDTA, we chelate Mg-ions (20 mM EDTA added to 10 mM $MgCl_2$ Tris-buffer solution), which increases repulsion between packaged DNA strands and leads to a higher DNA stress in the capsid. This increase in DNA stress in the 78% WT DNA length phage λ appears to be sufficient to trigger DNA transition at T^* ~36 °C. Figure 4.5B shows the DNA diffraction peak area versus temperature for 78% WT DNA length phage λ with and without EDTA. There is an abrupt drop in the DNA peak

area when EDTA is added, demonstrating a DNA disordering transition. We conclude that DNA transition in a viral capsid can be switched on and off by varying the polyvalent counterion concentration, which affects the repulsive interactions between packaged genome strands.

Figure 4.5C shows variation in the interaxial DNA-DNA distance in the capsid as a function of temperature for 78% WT DNA length λ in 10 mM $MgCl_2$ Tris-buffer with and without EDTA addition. As expected the interaxial distance is increased when EDTA is added. This is caused by increased repulsive interactions between packaged DNA strands when Mg-ions are chelated by EDTA. However, it is interesting to note that with EDTA added, the DNA interaxial distance is increasing with temperature, while it remains essentially constant with increasing temperature without EDTA addition, see Figure 4.5C. As described above, the balance between the bending stress and the interstrand interactions determines the interaxial distance between the ordered DNA strands (*15*, *30*). As discussed before, with temperature increasing from 10 to 45 °C, interstrand interactions remain essentially unchanged, but DNA persistence length is decreased by almost 30% (*37*), making DNA more flexible, which leads to smaller bending stress. Reduced bending stress should in turn cause DNA-DNA spacings to increase due to repulsive interactions striving to push the DNA closer to the center of the capsid (where the bending stress is higher than in the periphery due to the higher curvature). However, if the temperature induced change in the bending stress is insufficient to affect the force balance between interaction and bending forces, DNA spacing will remain unchanged. This is indeed the case for 78% WT DNA length phage l without EDTA added in 10 mM $MgCl_2$ Tris-buffer. The DNA interaxial distance remains at ~29.6 Å between 10 and 45 °C, see Figures 4.2C and 4.5C. Interestingly, when EDTA is added to the same phage solution, the stronger DNA-DNA repulsive forces (due to chelated Mg^{2+}) start to dominate over the opposing forces on the DNA due to the bending stress, resulting in an increase in DNA interaxial spacing with increasing

temperature. At first there is almost no change in DNA spacing between 10 and 20 °C, but later, as bending stress becomes smaller, we observe a progressive increase in interaxial spacing from 29.6 Å at 20ºC to 30.1 Å at 45 °C, see Figure 4.5C. These data illustrate a delicate interplay between bending and interaction forces on the packaged genome, which determine its structure and the overall stress level.

4.7 Conclusions

Various aspects of genetic evolution have been investigated in the field of virology (*5*). The physical aspects of viral evolution, however, are less understood. Recently, an intimate relationship was found between the physical and genetic evolution of dsDNA viruses (*49*). Specifically, it was shown that the physical limit of DNA length imposed by the capsid volume has led to gene overlap evolving as a mechanism for producing more proteins from the same genome length (*49*). This demonstrates how a genetic mechanism has evolved from a physical constraint by the capsid on the packaged genome density. Similarly with this finding, our data suggest that the genome packing density in phage λ is unique and highly conserved. This precise packing density not only determines the number of genes required for replication, but also creates an internal stress in the capsid required for the solid-to-fluid like DNA transition to occur at the temperature of infection. Such intracapsid DNA transition in λ facilitates initiation of DNA delivery from phage into a cell, and was shown to markedly increase the number of infectious viral particles once the transition temperature was reached (*10*).

We found striking evidence that the packaged genome density in phage λ, corresponding to WT λ-DNA length (as opposed to the shorter λ-DNA length mutants), presents the most energetically and structurally optimized balance between genome mobility and its internal stress, both of which are required for efficient DNA ejection from the capsid. We show that DNA transition occurs once the critical DNA stress level in the capsid is reached. The genome stress is generated by

interstrand repulsive interactions, packing defects and DNA bending stress, which is in turn controlled by the temperature and the ionic conditions of the surrounding solution. We discovered that at the most favorable external Mg^{2+}-concentration for phage λ adsorption to E. coli and subsequent replication (~10-20 mM Mg^{2+}) (*28*), the DNA transition in the capsid occurs precisely at the physiologic temperature of infection (37 °C). This suggests a remarkable evolutionary adaptation of the DNA transition mechanism in phage λ to the temperature and ionic environment of its host (λ replicates in E. coli in the human gut at 37 °C). Thus, DNA transition in the capsid is physiologically relevant, which suggests its importance for viral replication.

Similar to a genetic switch in phage λ (*1*), both temperature and the surrounding conditions facilitate viral replication by "switching on" the mobility of the encapsidated genome, which initiates its rapid release into the cell. We also demonstrate that the DNA transition can be "switched off" by varying the ionic conditions. Restricting intracapsid DNA mobility can have a virucidal effect (*10*, *11*), which is less prone to genetic mutations in the viral genome that can lead to development of drug resistance. We recently found that an analogous metastable DNA state inside the viral capsid is also present in HSV-1, with solid-to-fluid like DNA transition occurring close to 37 °C (*7*, *11*). This suggests that the DNA transition mechanism regulating infectivity may be universal for many pressurized DNA viruses. In conclusion, correlating structure and energetics of the encapsidated genome with the efficiency of viral replication provides a unique approach to explore the connection between physical and genetic aspects of viral evolution, and creates novel opportunities for control of viral infections.

References for Chapter 4

1. M. Ptashne, *A genetic switch : phage lambda revisited*. (Cold Spring Harbor Laboratory Press ; [Oxford : Lavis Marketing, distributor], New York, ed. 3rd ed., 2004).
2. B. Alberts, J. H. Wilson, T. Hunt, *Molecular biology of the cell*. (Garland Science, New York, N.Y. ; Abingdon, ed. 5th ed., Reference ed., 2008).
3. P. Shkilnyj, G. B. Koudelka, Effect of salt shock on stability of lambdaimm434 lysogens. *J Bacteriol* **189**, 3115-3123 (2007).
4. T. Liu *et al.*, Solid-to-fluid-like DNA transition in viruses facilitates infection. *Proceedings of the National Academy of Sciences of the United States of America* **111**, 14675-14680 (2014).
5. S. J. Flint, L. W. Enquist, V. R. Racaniello, A. M. Skalka, *Principles of Virology: Pathogenesis and Control*. (ASM Press, ed. 3rd, 2009), pp. 1028.
6. R. W. Hendrix, Ed., *Lambda II*, (Cold Spring Harbor, N.Y. : Cold Spring Harbor Laboratory, 1983).
7. D. W. Bauer, J. B. Huffman, F. L. Homa, A. Evilevitch, Herpes virus genome, the pressure is on. *J Am Chem Soc* **135**, 11216-11221 (2013).
8. A. Evilevitch, L. Lavelle, C. M. Knobler, E. Raspaud, W. M. Gelbart, Osmotic pressure inhibition of DNA ejection from phage. *Proceedings of the National Academy of Sciences of the United States of America* **100**, 9292-9295 (2003).
9. P. M. Ojala, B. Sodeik, M. W. Ebersold, U. Kutay, A. Helenius, Herpes simplex virus type 1 entry into host cells: reconstitution of capsid binding and uncoating at the nuclear pore complex in vitro. *Molecular and cellular biology* **20**, 4922-4931 (2000).
10. T. Liu *et al.*, Solid-to-fluid-like DNA transition in viruses facilitates infection. *Proc Natl Acad Sci U S A*, (2014).
11. U. Sae-Ueng *et al.*, Solid-to-fluid DNA transition inside HSV-1 capsid close to the temperature of infection. *Nature chemical biology* **10**, 861-867 (2014).

12. W. C. Earnshaw, S. C. Harrison, DNA arrangement in isometric phage heads. *Nature* **268**, 598-602 (1977).
13. M. E. Cerritelli *et al.*, Encapsidated conformation of bacteriophage T7 DNA. *Cell* **91**, 271-280 (1997).
14. J. Lepault, J. Dubochet, W. Baschong, E. Kellenberger, Organization of double-stranded DNA in bacteriophages: a study by cryo-electron microscopy of vitrified samples. *The EMBO journal* **6**, 1507-1512 (1987).
15. G. C. Lander *et al.*, DNA bending-induced phase transition of encapsidated genome in phage lambda. *Nucleic acids research* **41**, 4518-4524 (2013).
16. F. Livolant, A. Leforestier, Condensed phases of DNA: Structures and phase transitions. *Prog Polym Sci* **21**, 1115-1164 (1996).
17. A. Leforestier, F. Livolant, The bacteriophage genome undergoes a succession of intracapsid phase transitions upon DNA ejection. *Journal of molecular biology* **396**, 384-395 (2010).
18. T. Odijk, Statics and dynamics of condensed DNA within phages and globules. *Philos Trans A Math Phys Eng Sci* **362**, 1497-1517 (2004).
19. I. S. Gabashvili, A. Grosberg, Dynamics of double stranded DNA reptation from bacteriophage. *Journal of biomolecular structure & dynamics* **9**, 911-920 (1992).
20. Z. T. Berndsen, N. Keller, S. Grimes, P. J. Jardine, D. E. Smith, Nonequilibrium dynamics and ultraslow relaxation of confined DNA during viral packaging. *Proceedings of the National Academy of Sciences of the United States of America* **111**, 8345-8350 (2014).
21. P. Grayson *et al.*, The effect of genome length on ejection forces in bacteriophage lambda. *Virology* **348**, 430-436 (2006).
22. A. Evilevitch *et al.*, Effects of salt concentrations and bending energy on the extent of ejection of phage genomes. *Biophysical journal* **94**, 1110-1120 (2008).
23. I. Ivanovska, G. Wuite, B. Jonsson, A. Evilevitch, Internal DNA pressure

modifies stability of WT phage. *Proceedings of the National Academy of Sciences of the United States of America* **104**, 9603-9608 (2007).

24. M. Jeembaeva, B. Jonsson, M. Castelnovo, A. Evilevitch, DNA heats up: energetics of genome ejection from phage revealed by isothermal titration calorimetry. *Journal of molecular biology* **395**, 1079-1087 (2010).
25. J. E. Lusk, R. J. Williams, E. P. Kennedy, Magnesium and the growth of Escherichia coli. *J Biol Chem* **243**, 2618-2624 (1968).
26. F. C. Kung, J. Raymond, D. A. Glaser, Metal ion content of Escherichia coli versus cell age. *J Bacteriol* **126**, 1089-1095 (1976).
27. C. Hurwitz, C. L. Rosano, The intracellular concentration of bound and unbound magnesium ions in Escherichia coli. *J Biol Chem* **242**, 3719-3722 (1967).
28. B. A. Fry, Conditions for the infection of Escherichia coli with lambda phage and for the establishment of lysogeny. *J Gen Microbiol* **21**, 676-684 (1959).
29. H. Gaussier, Q. Yang, C. E. Catalano, Building a virus from scratch: assembly of an infectious virus using purified components in a rigorously defined biochemical assay system. *J Mol Biol* **357**, 1154-1166 (2006).
30. X. Qiu *et al.*, Salt-dependent DNA-DNA spacings in intact bacteriophage lambda reflect relative importance of DNA self-repulsion and bending energies. *Physical review letters* **106**, 028102 (2011).
31. D. C. Rau, V. A. Parsegian, Direct Measurement of Temperature-Dependent Solvation Forces between DNA Double Helices. *Biophysical journal* **61**, 260-271 (1992).
32. M. Rodriguez *et al.*, Genetic structure and linkage disequilibrium in landrace populations of barley in Sardinia. *TAG. Theoretical and applied genetics. Theoretische und angewandte Genetik* **125**, 171-184 (2012).
33. H. H. Strey, R. Podgornik, D. C. Rau, V. A. Parsegian, DNA--DNA interactions. *Curr Opin Struct Biol* **8**, 309-313 (1998).
34. S. Leikin, V. A. Parsegian, D. C. Rau, R. P. Rand, Hydration forces. *Annual*

review of physical chemistry **44**, 369-395 (1993).

35. S. Tzlil, J. T. Kindt, W. M. Gelbart, A. Ben-Shaul, Forces and pressures in DNA packaging and release from viral capsids. *Biophys. J.* **84**, 1616-1627 (2003).
36. J. Kindt, S. Tzlil, A. Ben-Shaul, W. M. Gelbart, DNA packaging and ejection forces in bacteriophage. *P Natl Acad Sci USA* **98**, 13671-13674 (2001).
37. S. Geggier, A. Kotlyar, A. Vologodskii, Temperature dependence of DNA persistence length. *Nucleic acids research* **39**, 1419-1426 (2011).
38. S. Y. Park, D. Harries, W. M. Gelbart, Topological defects and the optimum size of DNA condensates. *Biophysical journal* **75**, 714-720 (1998).
39. A. A. Kornyshev, D. J. Lee, S. Leikin, A. Wynveen, Structure and interactions of biological helices. . *Rev. Mod. Phys.* **79**, 943-996 (2007).
40. S. Koster, A. Evilevitch, M. Jeembaeva, D. A. Weitz, Influence of internal capsid pressure on viral infection by phage lambda. *Biophysical journal* **97**, 1525-1529 (2009).
41. R. H. Davis, D. R. Morris, P. Coffino, Sequestered end products and enzyme regulation: the case of ornithine decarboxylase. *Microbiological reviews* **56**, 280-290 (1992).
42. W. Gibson, B. Roizman, Compartmentalization of spermine and spermidine in the herpes simplex virion. *Proc Natl Acad Sci U S A* **68**, 2818-2821 (1971).
43. K. Igarashi, K. Kashiwagi, Polyamines: mysterious modulators of cellular functions. *Biochemical and biophysical research communications* **271**, 559-564 (2000).
44. P. M. Coates, *Encyclopedia of dietary supplements*. (Informa Healthcare, New York, ed. 2nd ed., 2010).
45. A. Rodgers, The exchange properties of magnesium in Escherichia coli ribosomes. *Biochem J* **90**, 548-555 (1964).
46. C. Morgan, H. S. Rosenkranz, B. Chan, H. M. Rose, Electron microscopy of magnesium-depleted bacteria. *J Bacteriol* **91**, 891-895 (1966).
47. E. Nurmemmedov, M. Castelnovo, E. Medina, C. E. Catalano, A. Evilevitch,

Challenging packaging limits and infectivity of phage lambda. *Journal of molecular biology* **415**, 263-273 (2012).

48. J. Yang, D. C. Rau, Incomplete ion dissociation underlies the weakened attraction between DNA helices at high spermidine concentrations. *Biophys J* **89**, 1932-1940 (2005).

49. N. Chirico, A. Vianelli, R. Belshaw, Why genes overlap in viruses. *Proceedings. Biological sciences / The Royal Society* **277**, 3809-3817 (2010).

CHAPTER 5 HETEROGENEITY OF DNA EJECTION DYNAMICS FROM BACTERIOPHAGE λ

5.1 Abstract

During viral infection, high DNA mobility is required to enable fast genome translocation. A DNA transition is required to facilitate fast genome ejection in bacteriophages and a tailless virus, the herpes simplex virus. This DNA transition enabled flow of λ genome when ejection starts. Studies using optical tweezers to investigate DNA packaging revealed a long relaxation time of packaged volume of DNA; This non-equilibrium packaging dynamics would likely result in intrinsic heterogeneity of fully-packed DNA states. In this work we reported viral DNA ejection kinetics by using isothermal titration calorimetry (ITC) and solution x-ray scattering techniques. Bulk-solution calorimetric measurements enabled us to observe a distinguishable population behavior which only exists in full length λ genome ejection: a fast-ejecting population that DNA ejection takes place within 20 seconds and a slow-ejecting population which takes anywhere from 10 seconds to several minutes to translocate all of its genome. We found that this population behavior is dependent on genome stress inside the capsid and can be altered by changing the ionic strength in the buffer. We suggest that genome packaging in phages is not quasi-static: full-length phage genomes can be packaged into different equilibrated states. Some states are of lower energy and no phase transition is needed for phage genome release; others are packaged to more solid-like crystal structure and a phase transition is required for initial DNA translocation. The fast-ejecting population we observed in the experiment are phages whose DNA are at more fluid state already thus genome release starts spontaneously upon receptor binding; the slow-ejecting population are phages whose genome are at a higher-energy state and needs to transform into the liquid state to allow unceasing DNA ejection.

5.2 Introduction

Analysis of virus-host interaction and resulting virus population dynamics has been instrumental for understanding of infectious cycle, viral diversity and fitness as well as the environmental factors that inhibit viral spread (*1-4*). These studies monitor the growth and evolution of viruses providing insights into the evolutionary dynamics of virus populations as they mutate to evade antiviral drugs or the immune system. These measurements were pioneered by "one-step growth cycle" method developed for phage growth in *E. coli* by Ellis and Delbruck (*5*). The method determines the rate of one cycle of phage replication in a synchronized bacterial infection. They demonstrated that phage growth curve could be divided into two main periods starting with a latent period. The latent period initiated by infection includes adsorption of phage to the bacterial cell, genome ejection into a cell, replication, synthesis, assembly and maturation of first phage particles within the cell. No extracellular phages are detected during the latent period. The latent period is followed by the rise period during which cell lysis occurs and extracellular phages are detected. Each of these periods can take between a few minutes to tens of minutes depending on the phage type and the external conditions (*4*, *6-8*).

The dynamics of phage adsorption and cell lysis have been extensively investigated (*9-12*), the dynamics of viral genome ejection into a cell is less understood. Genome ejections in bacteriophages are stochastic events with a signature exponential decay time and activation energy (*13-17*). This activation energy is generally perceived as the energy barrier for opening of the head-tail-connector structure (known as the portal vertex) (*13*, *16*, *17*), linked to the helical tail tube as DNA release channel. After the reversible adsorption of phage to its receptor (*18*), the binding triggers conformational changes in the phage tail that are transmitted to the portal, allowing its opening (*14*). Opening of portal vertex can be purely thermo-activated and independent of receptor binding (*19*), studies

confirmed receptor binding significantly lowers the threshold for critical portal destabilization prior to DNA ejection (*16*). The DNA ejection process is generally assumed to occur spontaneously after portal opening, with various thermodynamic driving forces, cellular viral-DNA binding factors and diffusion models proposed to describe the overall translocation process (*20*, *21*).

The lab has previously analyzed non-synchronized dynamics of DNA ejection events related to the portal stability (*16*, *22*). Here we investigate the effect of DNA fluidity on initiation and duration of DNA translocation once the portal is opened. ITC allows measurement of energy released only in a synchronized DNA ejection event where large portion of particles simultaneously needs to contribute to the heat released in ejection. For this purpose, We designed a new microcalorimetric assay, using ultra-sensitive isothermal titration calorimetry (ITC), to measure time-resolved energy release associated with DNA ejection dynamics from phage λ triggered by isolated λ-receptor, LamB. The data shows time-resolved energy distributions resulting from phage populations with distinctly different DNA ejection dynamics. Furthermore, using time-resolved solution small angle X-ray scattering (SAXS), we quantified the energy of activation required for DNA ejection by monitoring specifically the DNA area from these phage populations. We found that activation energy for DNA ejection (not the portal opening) is close to zero for phages with DNA in a fluid-like state.

In this work we discovered a striking bimodality in the virus population dynamics associated with kinectis of DNA ejection from phage λ. We found that upon phage λ adsorption to its receptor (LamB), viral particles consisted of two populations. First phage population had fast dynamics of DNA ejection occurring in only ~10 s immediately after receptor addition. Second population had 10-25 times slower DNA ejection dynamics (depending on the experimental conditions) occurring on the time-scale of several minutes. Furthermore, the entire phage

population had either prevalently fast or slow dynamics of DNA release which could be controlled by the external ionic conditions. Such heterogeneous genome ejection dynamics leads to variable initiation times for viral replication, with delays on the time scale comparable to other steps in the infectious cycle, as described above. This in turn contributes to heterogeneity in the viral population dynamics influencing mutation rates and viral fitness (*9*, *23*). The experimental data presented in this work explain the mechanism regulating dynamics of DNA ejection from phage. We show, for the first time, that bimodal phage population dynamics is directly correlated with the two distinct structural DNA states in the phage capsid: solid-like and fluid-like states (*24*, *25*). The fluid-like DNA state yields fast DNA ejection dynamics, while the solid-like DNA state both delays the initiation of genome ejection process and reduces the rate of DNA translocation from phage. This occurs due to higher sliding friction between tightly packaged DNA strands (*22*, *24-26*). Structural disordering transition in the capsid is induced by the temperature or ionic conditions and results in reduced interstrand friction which can be characterized as transition from solid to fluid-like DNA states. We show that this transition occurs at physiologic external conditions optimum for infection, i.e. 37 °C and ionic conditions mimicking those of extra- and intracellular environment (*25*, *27*). We demonstrate that deviation from physiologic conditions leads to a significant increase in phage population with DNA in a solid-like state significantly slows down DNA ejection dynamics. This suggests non-synchronized /heterogeneous dynamics of genome ejection (initiation and translocation) into cells, despite synchronized phage-to-cell adsorption required for one-step growth rate studies. These findings are therefore essential for understanding of infectivity and viral growth.

5.3 Materials and methods

5.3.1 Bacteriophage λ and LamB receptor

Following previous protocols (*28*), phage λ strain cI867 with a wild type (wt-)

genome length of 48.5 kbp were produced by thermal induction of lysogenic Escherichia coli (E.coli) strain AE1 derived from S2773 strain. After cell harvest, phage particles were precipitated in 10% polyethylene-glycol (PEG) 8000 and purified by CsCl equilibrium centrifugation. Later on phages were dialyzed against TM-$MgSO_4$ buffer (10mM $MgSO_4$, 50mM Tris□HCl, pH7.4) or TM-$MgCl_2$ (10mM $MgCl_2$, 50mM Tris-HCl, pH7.4) for overnight at 4°C. The shorter genome λ-mutants with 45.7 kbp DNA (corresponding to 94% of the wt- DNA length) and 37.7kbp DNA (corresponding to 78% of the wt- DNA length) were produced by thermal induction of E.coli strain S2739 and S2775 separately. They were purified in the same way as cI867 strain. The receptor protein LamB was expressed and purified from pop-154, an *E. Coli* K12 strain in which the LamB gene was transduced from *Shigella sonnei* 3070. The detailed preparation method was described earlier (*29*).

5.3.2 Isothermal titration calorimetry (ITC)

Isothermal titration calorimetry (ITC) was used to measure the ejection enthalpy of λ genome, ΔH_{ej}. All ITC measurements in this study were performed using the MicroCal iTC200 system manufactured by GE Healthcare, Life Sciences. The principles of measuring DNA ejection enthalpy in phages λ were described before (*30*). In ITC experiment, 2.69375 μL λ particles at 5 - 6×10^{12} pfu/mL (8 - 10nM) were titrated into 200 μL LamB solution in the sample cell (reference cell was always filled with MilliQ water). LamB is at a concentration of 0.2 - 0.5 mg/mL (1.4 - 3.5 μM). The molar ratio between LamB trimmers and λ particles in the sample cell is always kept above 10^4:1 (up to 3 titrations) to ensure the maximum ejection efficiency of λ with no delay time. Both LamB and λ particles were in the same dilution buffer containing TM (10mM $MgCl_2$ or $MgSO_4$, as indicated, 50mM Tris, pH7.4) and 1% oPOE. The dilution heat of phage particles, LamB particles were measured separately and excluded from the final value of ΔH_{ej} (*30*).

5.3.3 Internal energy of λ genome and ejection enthalpy

The ejection enthalpy, ΔH_{ej} is a good estimate of the internal energy of λ genome, U_{encap_DNA}. In an ITC experiment, ΔH_{ej} is measured as an enthalpy change associated with the genome release process, $\Delta H = \Delta U + p\Delta V$, where ΔU is the change in internal energy of the system during DNA ejection ($\Delta U = U_{empty\_cap} - U_{filled_{cap}} = U_{encap\_DNA}$), p is the atmospheric pressure acting on the system and ΔV is the change in volume of the solution surrounding the phages during DNA release. Since this volume change in solution, ΔV is negligible, $\Delta H \approx \Delta U$. So through our carefully designed ITC experiment, we can get the internal energy of encapsidated λ genome, U_{encap_DNA}.

5.3.4 Small-angle X-ray scattering study of viral genome ejection

Small angle X-ray scattering (SAXS) measurements were carried out at the 12-ID B station at the Advanced Photon Source (APS) at Argonne National Laboratory. A 12KeV X-ray beam was used to illuminate the sample with an overall q range from 0.006 to 0.850 $Å^{-1}$. Total of 120 μL of WT phage solution (~ 5Å~1013 pfu/mL) was injected into a flow-through glass capillary and the solution was oscillating during the SAXS measurement with a flow rate of 10 μL/s. 40 scans with 1 second X-ray exposure time were collected and averaged for each sample.

5.4 Measuring λ DNA ejection dynamics by ITC

Light scattering (LS) (*14*, *16*, *17*, *22*, *31*, *32*) and solution small angle x-ray scattering (SAXS) (*16*) have been applied widely in bulk measurements of viral ejection kinetics. The bulk method allows large-scale analysis of phage DNA ejection dynamics, providing significantly more robust statistics compared to the single molecule fluorescence techniques (*13*, *15*). In LS and SAXS measurements, phage particles are mixed with their receptors at time t_0 and a continuous change in scattering intensity was recorded. Upon binding to their receptors, phage quickly ejects their DNA into the surrounding solution and the extreme ordering of encapsidated DNA molecule is lost, resulting in a rapid loss of scattering intensity

(Figure 5.1A).

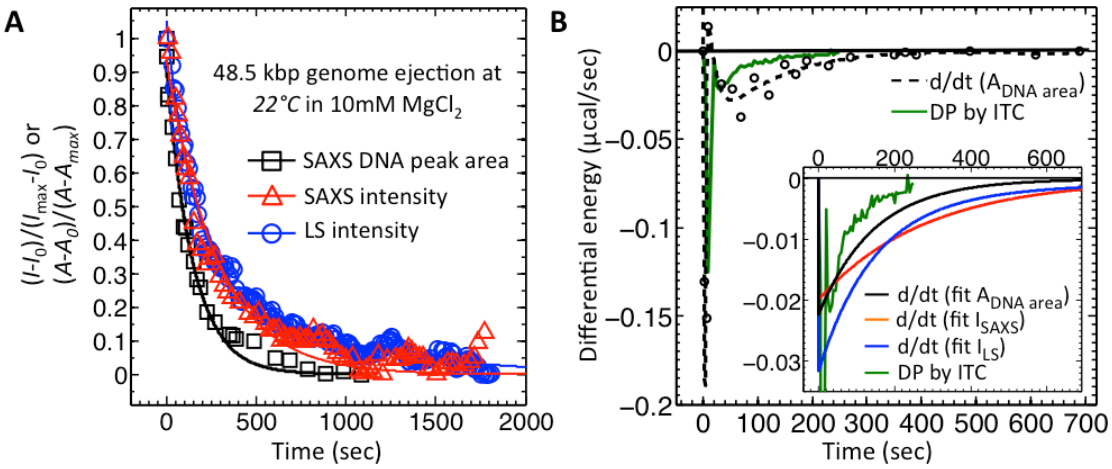

Figure 5.1 Comparison of ejection dynamics measured by LS, SAXS and ITC. (A) DNA ejection process with time monitored by, black: area of DNA scattering peak in SAXS; red: initial scattering intensity I_0 in SAXS; blue: scattering intensity I in LS at a given angle. The lines connecting the data are exponential fit of each set of data. (B) Raw ITC data (green solid), measured as heat released per time unit (DP), is compared to: derivative of DNA peak area. Figure inset is the time-scale comparison between ITC data and derivative of the exponential fit from DNA peak area (black solid), derivative of the exponential fit from SXAS intensity (red solid), LS (blue solid) time profile. All the non-ITC data were scaled to theoretical DP value for comparison by multiplying amount of effective scattering particles and heat released per particle.

Figure 5.1A shows the measured DNA ejection process from wild-type DNA length phage λ at 22 °C in TM Tris-buffer (10mM $MgCl_2$, 50mM Tris, pH7.5). The blue curve in the figure shows the normalized decay in LS intensity versus time, $\Delta I = \frac{I(t)-I(final)}{I(initial)-I(final)}$. This normalized intensity is well described by an exponential fit (solid blue line), $\Delta I = Ae^{-t/\tau o}$, with the characteristic time constant τo, defining the mean lifetime of this exponential process and can be considered as the average lab time between receptor binding a DNA ejection event (*16*). The red curve is the normalized SAXS intensity I_0 at scattering vector q≈0 plotted versus time. I_0 is proportional to Mw of the scattering particle (scattering most from high mass-

density of encapsidated DNA). I_0 decreases as the DNA ejects from the phage and λ DNA coil relaxation-diffusion processes proceed. I_0 versus time can also be described by an exponential decay fit (solid red line) and have similar characteristic time constant as determined from LS data (Figure 5.1A). Both LS and SAXS time-resolved intensity data are affected by the diffusion of ejected λ DNA coil into the surrounding solution (*16*, *22*), especially in the tail part. Another method to describe the ejection kinetics is by monitoring the DNA peak area from SAXS over time (black curve, Figure 5.1A). In this way we look only at mass changes (or considered as changes in ordered DNA layers) in encapsidated part of λ DNA and is not affected by ejected portion of DNA molecule. Thus the kinetics described by DNA peak area is most accurate and has the shortest time constant.

We designed a micro-ITC assay that allows direct measurements of time-resolved internal energy released during DNA ejection from phage. The primary signal of ITC is a heat power in Joules per seconds (in Watts) (*33*). ITC has been shown to be a powerful tool in measuring kinetics of not only simple reactions like $A + B \rightleftharpoons C$ but also could be extended to two or multiple kinetics steps (*33*, *34*). In our application, we correlated the kinetic time-scale information of heat change measured by ITC with the energy state of the packaged genome. The enthalpy change (ΔH) is measured as heat released when concentrated phage λ particles are titrated into a LamB receptor solution, which triggers DNA ejection in vitro. The temperature in the reference cell is continuously equilibrated to that of the sample cell after each titration of phage in LamB solution. The differential power (DP) between the reference cell and the sample cell is recorded in microcalories per second (Figure 5.1B). The raw DP data from ITC is shown in green curve. The response time of the ITC instrument is only ~3.5 s (*33*), while the measured heat released during the DNA ejection process occurs on the time-scale of ~250 s. Thus, by evaluating the time scale and distribution of the exothermic peaks on the ITC titration curve, we can analyze the dynamics of DNA ejection process from phage

([34](#)). High sensitivity ITC has been previously successfully used to study reaction kinetics ([33](#), [34](#)). Other exothermic enthalpy contributions are subtracted from the raw DP signal for the total enthalpy change occur on a shorter time scale of <10 s ([24](#), [30](#)). Since DP is the differential change of enthalpy during ejection by time. We calculated the differential curve for kinetics data from the other two methods (LS, SAXS), $\frac{dI}{dt}$ (I: intensity measured by LS or SAXS, t: time). We know that this is an indication and proportional to the change in number of un-ejected particles (effective scattering particles) over time, $\frac{dN}{dt} = N_{estimate\ effective\ scattering\ particles} \cdot \frac{dI}{dt}$. We scaled $\frac{dI}{dt}$ value by multiplying this number with enthalpy change per phage particle during ejection, ΔH_{ej} per phage and estimated number of scattering particles, to give an estimate of change in enthalpy:

$$DP_{estimate} = \frac{dH_{ej}}{dt} = N_{estimate\ effective\ scattering\ particles} \cdot \frac{dI}{dt} \cdot \Delta H_{ej\ per\ phage}.$$

Figure 5.1B shows the comparison between measured ITC DP and differential curve of measured DNA peak area data by SAXS. The inset box of Figure 5.1B shows the differential curve comparison between the fit of LS intentisy, SAXS intensity, SAXS DNA peak area data and measured ITC DP with time. As mentioned above, the DNA peak area data by SAXS is the most reliable in describing the ejection kinetics. And its differential curve correlates well with the ITC DP curve, confirming the accuracy of using ITC to measure phage λ ejection kinetics.

The ITC data can be nicely fit into an asymmetric Gaussian. The DP curve is the derivative of the energy profile as we discussed and DP value is a convoluted signal of (1) Number of ejecting phage particles versus time and (2) Change in energy of en-capsidated DNA per phage particle versus time. We know the first term is Gaussian based on dynamics experiments studying phage particle ejection events using fluorescence microscopy techniques ([13](#)). While the second term, change in en-capsidated energy per particle over time can be calculated using convolution of

change in ejection length (ejection speed, dL/dt versus ejection time) and energy profile at each packaged length (reserved energy versus ejection time). Both theoretical and experimental work has shown that ejection speed increase at the beginning due to decrease of frictional force as more DNAs come out, and decrease towards the end of ejection due to decrease of intra-capsid pressure (*13*, *20*, *26*, *35-37*). This gives the second term a peak shape as well. Thus the overall DP curve is a convolution of 2 peak-shaped signals and can be perfectly fit by Gaussian curve. The asymmetry, especially we can see that the skewness of the second peak is large, comes most likely from the combination of delayed particle ejection modes and non-uniform motion of ejecting for the slower population.

5.5 Solid-to-fluid like DNA transition controls genome ejection dynamics

We have shown for phage λ that DNA layers packaged closest to the capsid's center undergo a disordering transition induced by an increase in temperature (*38*). This occurs due to temperature sensitive DNA bending stress and packing defects (*38*) resulting in an increase in interstrand repulsions and in overall genome stress. At the transition temperature (T^*), packaged DNA becomes more locally disordered leading to a lower packing density in the center of the capsid. This increases locally DNA-DNA spacings which in turn reduces interstrand repulsions and partially relives packaged genome stress. With help of nanoindentation atomic force microscopy we have shown that DNA disordering transition leads to a more mobile, or fluid, DNA state in the capsid (*25*, *27*, *38*). Below the transition temperature, the encapsidated DNA is trapped in a solid-like metastable state. These observations have lead us to realize that dynamics of DNA ejection from the capsid can be significantly influenced by the packaged DNA state. In ITC, ΔH_{ej} was measured in the temperature range between 18 °C and 42 °C, Figure 5.2D shows a discontinuity in the approximately linear dependence of ΔH_{ej} on temperature occurring at T* ~33 °C for WT λ-DNA length ejection from phage λ in 10 mM $MgCl_2$ Tris-buffer. As we have

previously shown, the discontinuity is attributed to DNA disordering transition inside the capsid leading to a transition from a solid-like to a fluid-like state (*24*).

Figure 5.2A shows ITC titration curves (DP versus time) recorded for WT DNA ejection from phage λ in TM-buffer at different temepratures, below and above the DNA transition temperature. However, the DP curve is not symmetrical and shows a right shoulder suggesting an unresolved second peak. Indeed, when the temperature was decreased below the transition temperature, the DP curve splits into two modes corresponding to two heat release dynamics populations. The first peak is equilibrated at ~20 s after phage is titrated into LamB, corresponding to fast population dynamics. Close to this time, the second peak appears and lasts up to 200 s, corresponding to slow population dynamics. Since two heat change peaks are not completely resolved, using previously described high-precision deconvolution method (*39*), we have deconvoluted the experimental DP curves into two asymmetric Gaussian functions with an exponential damping term $\frac{a}{2b} \cdot \exp\left(\frac{c^2}{2b^2} + \frac{d-t}{b}\right) \cdot (\mathrm{erf}\left(\frac{t-d}{c\sqrt{2}} - \frac{c}{\sqrt{2}b}\right) + 1)$ (equation-1) (*40*). In equation (1), parameter a denotes the peak area from the deconvoluted Gaussian peak, b denotes the exponential damping term (exponent relaxation time), with b=0 for perfect symmetric Gaussian curve. c indicates the width of the Gaussian, which was used to calculate the median time of population DNA ejection (see Table 5.1, 5.2, 5.3). d is the position of the individual Gaussian peak. The estimated population mean of EMG shifted slightly from the peak position, it is the peak position plus the exponential relaxation time $\mu = d + b$, the population standard derivation, $s^2 = c^2 + b^2$ (*40*). Skewness of the distribution can be defined as $\gamma = \frac{2b^3}{(c^2+b^2)^{3/2}}$, with the positive γ values indicating right-tailed distribution (as shown in Tables) with perfectly symmetric Gaussian having γ=0 (population mean equals to population median). The median of the distribution equals to $\mu - (1/3)s\gamma$ (according to Pearson's second skewness law).

This deconvolution fitting was also applied to the heat change peaks above the DNA transition temperature (Figure 5.2A), even if they appear almost as a single peak, for the sake of consistent comparison of DNA ejection dynamics under different conditions. However, above the DNA transition temperature, two deconvoluted peaks derived from fitting would essentially converge into a single Gaussian function, suggesting that there is mainly only one population of phage λ particles contributing fast heat release dynamics (e.g. Figure 5.2B shows DNA ejection dynamics at 37 °C). Since the Gaussian functions in our data analysis are right skewed, we use the median value (instead of mode value) to estimate the central tendency corresponding to the average time for DNA ejection from a population of phage particles. Figure 5.2C shows the median values of DNA ejection for "fast" and "slow" phage populations at temperatures 22 - 42 °C. The error bars are obtained from the width of the Gaussian curves. Figure 5.2C (shows median values) demonstrates that phage population with fast ejection dynamics (corresponding to the first exothermic peak) has an average ejection time of ~10 s at all temperatures. This corresponds well to the time for DNA translocation from a phage λ capsid under similar buffer conditions previously measured by single molecule fluorescence (*13*). This suggests that majority of phage particles in the fast population eject their genomes immediately after receptor addition in a synchronized manner. The average ejection time for the slow phage population at 22 - 32 °C, below DNA transition temperature is 30 - 40 s (corresponding to the second exothermic peak) (Table 5.1A). Since previous single molecule fluorescence analysis of DNA translocation times indicates that DNA ejection completes within tens but not hundreds of seconds, the fact that second exothermic peak does not equilibrate for ~200 s suggests that there are also delays in the initiation of DNA ejection events. Furthermore, wide distribution of the second population peak shows that ejection events occur in a desynchronized manner. Both slower DNA translocation dynamics and delayed initiation of DNA ejection occur due to higher interstrand sliding friction in the solid-like DNA state. It can be argued that

temperature variation can affect phage-to-LamB adsorption dynamics which in turn can affect DNA ejection dynamics. However, by studying DNA ejection dynamics for a shorter packaged DNA length phage λ mutant (with 78% of WT l-DNA length) (Figure 5.2E), we confirmed in the next section that phage-to-LamB adsorption dynamics is not influenced by the temperature, with LamB present in a strong excess in all of our measurements (phage:LamB ratio is 1:1000).

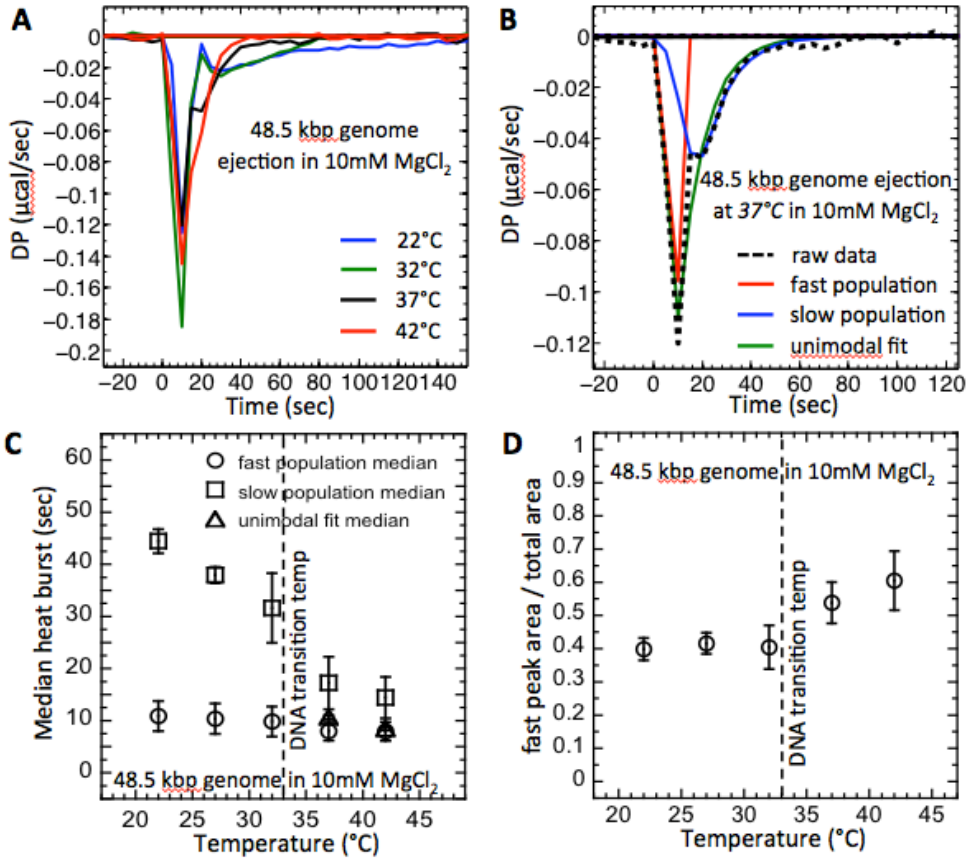

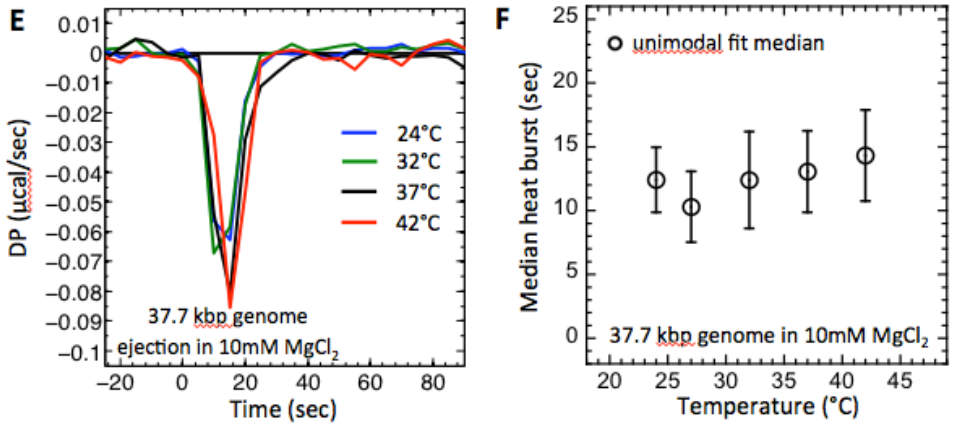

Figure 5.2 ITC data of genome ejection enthalpy for phages λ at different temperatures. (A) λ virions with full length genome were titrated into LamB solution in TM buffer containing 10mM Mg^{2+}. Two temperature known before DNA transition (22 and 32°C) and two temperature after DNA transition (37 and 42°C) were selected to be shown here. (B) Ejection curve at 37°C, the de-convoluted peak 1 and 2 majorly overlap with each, and the raw data can be fit better with one single assymetric Gaussian. (C) Peak position for fast and slow peaks at 5 different temperatures were analyzed and median values were calculated and plotted. Errors shown are the width of Gaussian distribution. Before the DNA transition temperature (32°C), peak 1 resolves from peak 2 very well and after 32°C, the peak positions overlap and peaks start to merge. Ejection curves at 37 and 42°C can be fit with one single Gaussian, as shown in (B). (D) The ratio of fast peak area divided by the total enthalpy were calculated for ejection curves at different temperatures. Experiments were repeated 3 times and standard errors of the mean were plotted. (E) Titration peaks for λ virions with 37.7kbp genome. (F) Median ejection time of 37.7kbp λ mutant at different temperatures. Errors shown are the width of Gaussian distribution.

In Figure 5.2D we plot the ratio between the fast population peak area and the total area of the exothermic peaks. This area ratio reflects the approximate fraction of the phage population with fast DNA ejection dynamics compared to the total phage population. Figures 5.2C and 5.2F summarize the observations above. They demonstrate that below the DNA transition temperature at ~33 °C, phage DNA ejection dynamics is divided into two main populations. Fast dynamics phage population ejects the genomes synchronously and immediately after receptor addition on the time-scale of seconds. Slow dynamics population displays reduced

DNA translocation rate (compared to the fast population) and heterogeneous delays in initiation of DNA ejection process with completion within minutes. When temperature is increased, the fraction of fast phage population is progressively increased (Figure 5.2D). After DNA transition at T > 33 °C, both phage populations merge into one fast dynamics population. These observations show that temperature induced solid-to-fluid like DNA transition in the capsid is directly correlated and strongly affects the dynamics of genome ejection from phage. Above the DNA transition temperature, the fluid-like DNA state in the capsids results in fast ejection dynamics where genome can be immediately released once phage adsorbs to receptor. However, below the transition temperature, there is co-existence between phage populations with DNA in solid-like and fluid-like states in the capsid. The solid-like DNA state yields an order of magnitude slower ejection dynamics and heterogeneity in genome translocation and initiation of ejection events. DNA transition is a gradual process, with fraction of the fluid-like DNA state particles gradually increasing with increasing temperature and completely dominating above the transition temperature.

These data suggests that by reducing DNA-DNA sliding friction in the capsid, by packaging less DNA, the encapsidated genome would be prevalently in a fluid-like state even at lower temperatures and the solid-to-fluid like DNA transition would be lost. This should in turn lead to fast DNA ejection dynamics in a broad temperature range. Such experimental demonstration would be the stringent test of the conclusions drawn in this section. With this motivation, we investigate below the dependence of DNA ejection dynamics on temperature for phage λ with only 78% of the WT λ-DNA length packaged in the capsid.

Table 5.1 Peak parameters (including total peak area (enthalpy) from each titration) based on the curve deconvolution for 48.5 kbp (wt) phages at different temperatures, all in TM (10mM Mg^{2+} buffer).

Temper-ature (°C)		Position d (sec)	Area A (µcal)	Width C (sec)	Exponential decay time b (sec)	Mean μ (sec)	S.D. S (sec)	Skewness (γ)	Median (sec)	Total enthalpy (µcal)
22	Fast Peak	10.3849	-0.9664	2.9052	0.4999	10.8848	2.9479	0.0098	10.8752	-2.4249
	Slow Peak	22.2082	-1.5410	2.3005	66.5621	88.7703	66.6018	1.9964	44.4485	
27	Fast Peak	9.9021	-0.9479	2.9258	0.4806	10.3826	2.9650	0.0085	10.3742	-2.2780
	Slow Peak	19.8582	-1.2568	1.5389	54.2030	74.0612	54.2248	1.9976	37.9550	
32	Fast Peak	9.4119	-0.9576	2.8738	0.4202	9.8321	2.9044	0.0061	9.8262	-2.3681
	Slow Peak	22.8002	-1.3370	6.7024	22.8139	45.6141	23.7781	1.7664	31.6132	
37	Fast Peak	7.6667	-1.0910	1.8144	0.3139	7.9816	1.8414	0.0099	7.9755	-2.0265
	Slow Peak	12.2756	-0.8093	5.0193	11.0877	23.3633	12.1709	1.5121	17.2287	
42	Fast Peak	7.6313	-0.7727	1.8129	0.3078	7.9391	1.8388	0.0094	7.9334	-2.2220
	Slow Peak	11.0547	-1.3440	3.9484	6.7049	17.7596	7.7811	1.2796	14.4406	

Table 5.2 Peak parameters based on the curve deconvolution for 48.5 kbp (wt) phages in different salt conditions all at 37°C.

$\lvert Mg^{2+} \rvert$ (M)		Position d (sec)	Area A (µcal)	Width C (sec)	Exponential decay time b (sec)	Mean μ (sec)	S.D. S (sec)	Skewness (γ)	Median (sec)	Total enthalpy (µcal)
5	Fast Peak	7.6477	-0.6584	1.8342	0.3103	7.9580	1.8603	0.0093	7.9522	-1.0363
	Slow Peak	7.5261	-0.4316	4.6184	7.6731	15.1992	8.9558	1.2579	11.4442	
10	Fast Peak	7.6677	-1.0910	1.8144	0.3139	7.9816	1.8414	0.0099	7.9755	-2.0265
	Slow Peak	12.2756	-0.8093	5.0193	11.0877	23.3633	12.1709	1.5121	17.2287	
20	Fast Peak	10.3014	-0.7284	0.8207	7.4313	17.7327	7.4765	1.9640	12.8382	-5.5995
	Slow Peak	41.0977	-5.4603	10.6048	34.7425	75.8402	36.3250	1.7498	54.6526	
50	Fast Peak	10.3019	-0.6115	0.4572	3.6832	13.9851	3.7115	1.9546	11.5669	-2.5795
	Slow Peak	44.1380	-1.7638	11.5565	65.7180	109.8560	66.7264	1.9107	67.3582	

Table 5.3 Peak parameters based on the curve deconvolution for phages of different genome length in 10mM Mg^{2+} at 32°C.

Genome length (bp)		Position ***d*** (sec)	Area ***A*** (µcal)	Width ***C*** (sec)	Exponential decay time ***b*** (sec)	Mean ***μ*** (sec)	S.D. ***S*** (sec)	Skewness (γ)	Median (sec)	Total enthalpy (µcal)
37,769	Fast Peak	11.5549	-0.7466	3.7064	0.8527	12.4076	3.8032	0.0225	12.3790	-0.7310
	Slow Peak	10.7512	-0.0037	8.0116	0.9675	11.7187	8.0698	0.0034	11.7094	
45,592	Fast Peak	9.7649	-1.4355	2.8480	0.4268	10.1917	2.8798	0.0065	10.1855	-3.0077
	Slow Peak	20.6055	-1.3002	7.2966	1.2534	21.8589	7.4035	0.0097	21.8349	
48,502	Fast Peak	9.4119	-0.9576	2.8738	0.4202	9.8321	2.9044	0.0061	9.8262	-2.3681
	Slow Peak	22.8002	-1.3370	6.7024	22.8139	45.6141	23.7781	1.7664	31.6132	

Table 5.4 Peak parameters based on the curve deconvolution for 37.8 kbp (wt) phages at different temperatures, all in TM (10mM Mg^{2+} buffer)

Temperature (°C)	Position ***d*** (sec)	Area ***A*** (µcal)	Width ***C*** (sec)	Exponential decay time ***b*** (sec)	Mean ***μ*** (sec)	S.D. ***S*** (sec)	Skewness (γ)	Median (sec)
24	10.4932	-0.7155	2.5428	3.3228	13.8160	4.1841	1.0017	12.4189
27	5.0479	-0.9195	2.7795	4.1828	9.2307	5.0221	1.1555	10.2963
32	11.6355	-0.7515	3.7899	0.7809	12.4164	3.8695	0.0164	12.3952
37	10.4085	-0.9570	3.1909	5.0954	15.5039	6.0121	1.2176	13.0639
42	11.9977	-0.9511	3.5704	3.4030	15.4007	4.9324	0.6568	14.3208

5.6 Effect of packaged DNA density on phage ejection dynamics

In this section we investigate how the packaged genome length in phage λ affects the dynamics of DNA ejection from the capsid. Using ITC and SAXS we are analyzing changes in the packaged DNA energy, ejection population dynamics and activation energy required to initiate ejection of the phage encapsidated genome with 78%, 94% and 100% of the WT λ-DNA length. The ionic conditions in these measurements are set by 10 mM $MgCl_2$ Tris-buffer as in the experiments above. This Mg-concentration mimics the extracellular Mg-concentration which was shown to provide the most efficient phage λ adsorption to bacterial cells, maximizing the

subsequent infection(*41*, *42*). (Similar free Mg-concentration was found in the *E. coli* cytoplasm (*43-45*))

In the first set of measurements we repeat the ITC measurements above for shorter packaged genome length λ-mutants, 78% and 94% of the WT λ-DNA length, while keeping the buffer conditions the same. The solid-to-fluid like DNA transition in the capsid observed for the WT λ-DNA length phage occurs when the critical genome stress is reached at temperature T^*. This is evident from the continuously increasing internal energy of the packaged genome with increasing temperature until an abrupt energy and structural transition occurs at T^* ~33ºC (Figure 5.3D). Lower DNA density in the capsid has larger spacings between packaged DNA helices, resulting in weaker repulsive interactions and lower genome stress (*26*). The resulting DNA pressure in the capsid is also significantly reduced when shorter DNA length is packaged (15 atm in 78% λ-DNA versus 35 atm in WT λ-DNA phage mutants)(*26*). Indeed, we found that no DNA transition occurred inside the capsid for these λ-mutants with shorter packaged DNA length than WT λ-DNA (within the investigated temperature range), see Figure 5.3D. This observation further demonstrates strong dependence between the internal genome stress and the structural DNA transition in phage λ. Lower DNA stress resulting from larger DNA-DNA spacing should in turn lead to reduced interstrand DNA sliding friction and more mobile DNA state in the capsid. The test of this hypothesis is shown in Figure 5. 3B, where we investigated using time-resolved ITC, the dynamics of energy release during DNA ejection events from these variable DNA-length phage λ mutants at 32 °C. As we discussed above, Figure 5.2A shows that WT λ-DNA length phage below the transition temperature displays well-resolved two population ejection dynamics. This corresponds to fast population with almost instantaneous DNA ejections (for phages with DNA in a fluid-like state) and slow population with strongly delayed DNA ejections (for phages with DNA in a solid-like state). However, when the packaged DNA length is reduced to 94% of the WT λ-DNA length, the slow

phage population becomes smaller with faster DNA ejection dynamics. Both fast and slow population peaks are merging into one mode and are no longer resolved. The shortest DNA length mutant (78% of the WT λ-DNA length) clearly shows that there is only one fast ejection dynamics population present. In Figure 5.3C we plot the average time for ejection events for all three DNA length phage mutants at 32 °C. The average time for population ejection events is estimated by taking the median value Gaussian fit to each time resolved DP curve in Figure 5.3B. As discussed above, the median value of the right skewed Gaussian fit of the slow population peak corresponds to the central tendency. However, since Gaussian fit to the fast population peaks is approximately symmetric, the median value is approaching the mean value of the distribution. Figure 5.3B shows that average time for DNA ejection events for fast population in all packaged DNA length phage λ mutants studied is ~10 s (Table 5.3). This time corresponds nicely to the time for DNA translocation from a single phage λ particle (Grayson). Thus, once LamB receptor is added, DNA ejection occurs instantaneously and simultaneously for all λ particles in this population. In case of 78% DNA length phage mutant, with most mobile DNA state, this applies to 100% of phage particles. For 94% and 100% of WT λ-DNA length phages, the average ejection time for the slow population is ~25-30 s, showing a delay in the ejection initiation dynamics.

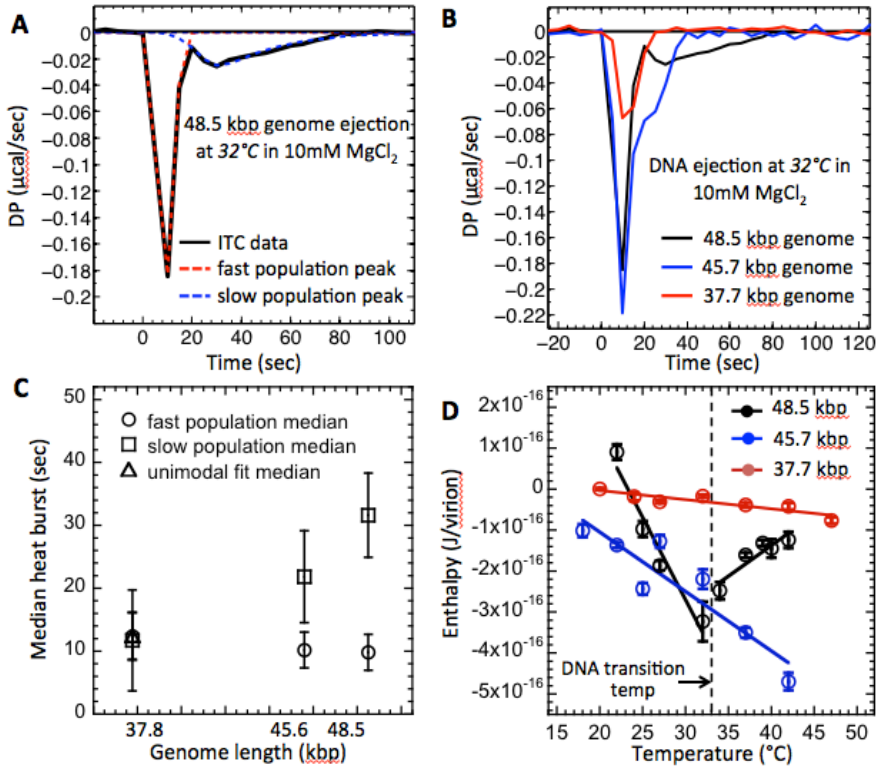

Figure 5.3 ITC data of genome ejection enthalpy for phages λ. (A) ITC titration curve of DNA ejection enthalpy from wild type (wt, full-length genome) phages λ. The control curve (grey) is the enthalpy coming from phage titration into buffer. The ejection curve (black) can be deconvoluted into two asymmetric Gaussian functions with an exponential damping term, $\frac{a}{2b} \cdot \exp\left(\frac{c^2}{2b^2} + \frac{d-t}{b}\right) \cdot (\mathrm{erf}\left(\frac{t-d}{c\sqrt{2}} - \frac{c}{\sqrt{2}b}\right) + 1)$using a pre-described deconvolution method with high-precision. Addition of two fit peaks is shown in dotted line. (B) λ virions with different genome length was titrated into LamB solution at T = 32°C in TM buffer containing 10mM Mg^{2+}. (C) Each deconvoluted peak corresponds to a Gaussian distribution of heat release events. Each Gaussian has a unique population median, which estimates the average ejection time in a given Gaussian distribution. The same deconvolution method were done for ejection curve from phages λ with full-length, 45.7 and 37.7 kbp genome and the peak ejection time were plotted. For 37.7 kbp genome the peak positions from the fast (circle) and slow (square) peaks overlap, and a single Gaussian (triangle) is more appropriate to fit the original data. Errors shown are the width of Gaussian distribution. (D) Phase diagram for λ with different genome length.

In previous section, Figures 5.2E and F, we analyzed the effect of temperature on DNA ejection dynamics for 78% DNA length phage. ITC data shows that time-resolved DP curves are essentially not affected by the temperature within the

investigated range of 22 - 42 °C. This behavior is strikingly different from ejection dynamics for the WT λ-DNA length phage, where the size of the slow population has strong temperature dependence correlated with the solid-to-fluid like DNA transition temperature. Figure 5.2F shows that average ejection time remains at ~10 s and only one fast population is observed in the whole temperature range. These findings provide a demonstration of the direct link between the packaged DNA structure in the capsid and dynamics of DNA ejection. For the first time we explain the mechanism behind the non-synchronized DNA ejection events from phage despite the excess addition of its receptor. Our data show that high DNA-DNA sliding friction, arising from densely packaged negative charges on the DNA backbone, is responsible for the solid-like DNA state. This in turn leads a significant delay in the initiation of DNA ejection, on the time scale comparable to that of the key steps for the one–step viral growth cycle. Furthermore, we show that when DNA is packaged to extreme densities in phage capsid (e.g. WT λ -DNA length phage λ with 60% DNA filling volume fraction), leading to co-existence between phage populations with DNA in a solid-like and a fluid-like states, the solid-to-fluid like DNA transition is a requirement in order to have synchronized and instantaneous DNA ejection from all phage particles adsorbed to a LamB receptor. This suggests that solid-to-fluid intra-capsid transition is one of the key steps to be taken into consideration when investigating viral population dynamics and its effects on viral fitness, due to the physiologically relevant time scale comparable to other main viral growth periods.

In order to confirm the relationship between ejection dynamics and packaged DNA state, suggested by the data above, it is critically important to demonstrate the existence of a true fluid-like DNA state in the capsid. This implies that there should be no activation energy barrier for initiation of DNA release, which should result in instantaneous DNA ejection upon phage-receptor adsorption. On the contrary, overcoming such activation energy barrier in the solid-like DNA state, due to the

interstrand frictional forces, leads to a time delay in ejection. With this motivation, we designed a time-resolved solution small angle X-ray scattering (SAXS) method, allowing us to determine the activation energy for DNA ejection events from WT and 78% packaged DNA length in phage λ.

5.7 Activation energy of solid and fluid like DNA states in the capsid

Solution SAXS provides direct structural information about the encapsidated genome(*38*, *46*, *47*). Capsid proteins and packaged DNA have well-resolved scattering profiles(*25*, *38*). Figure 5.4A shows integrated scattering intensity, *I*, versus scattering vector *q* full-length λ particles. In the lower *q* region (0.007$Å^{-1}$ to 0.1$Å^{-1}$), the scattering profile originates from the highly symmetrical icosahedral phage capsids. The single peak with the small oscillating ripples on its top at higher *q* (between 0.2 $Å^{-1}$ to 0.3 $Å^{-1}$) is due to the diffraction from the encapsidated ordered DNA strands. The short-range DNA-DNA interaxial spacings determine the position of the DNA diffraction peak (*46*). Most relevant for this work, the area of this peak indicates how well the DNA strands are aligned relative each other, i.e., it provides information on the total number of ordered DNA base pairs of the encapsidated genome(*38*, *46*). When DNA inside the capsid becomes less ordered, due to its ejection from the capsid, the DNA peak area decreases as a result of less coherent diffraction. When the genome is completely disordered, the DNA diffraction peak disappears. Using time-resolved SAXS, we were recoding the area of the DNA diffraction peak over a period of ~600 s after instantaneously mixing phage with LamB solution using a static mixing tee with the LamB : phage ratio of 200:1 (LamB is added in excess and has been confirmed not to influence DNA ejection kinetics. The mixed sample was then injected into a flow cell, which is perpendicular to the incident X-ray beam.

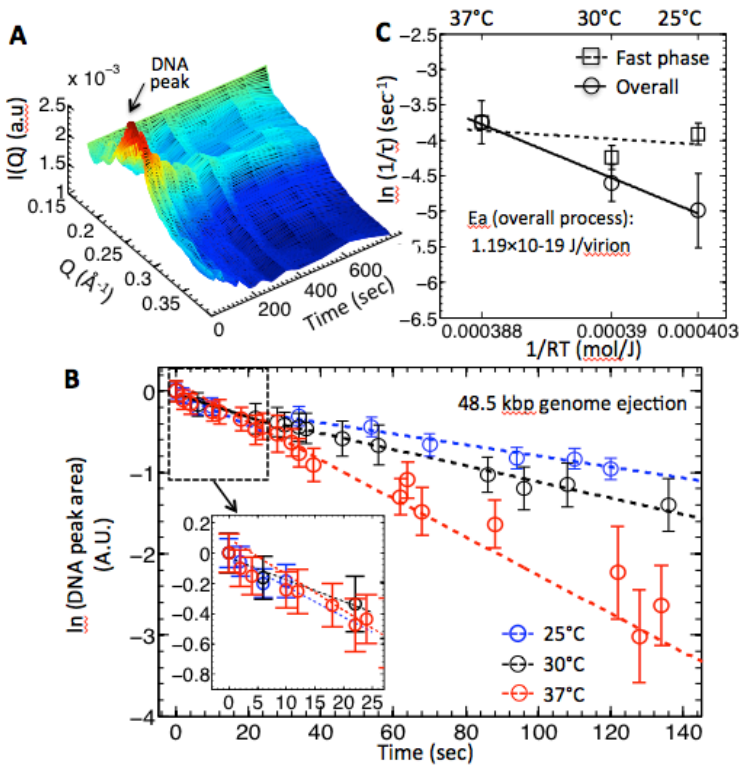

Figure 5.4 DNA ejection kinetics by SAXS (A) 3D representation of the change in DNA diffraction peak with time for wt phage lambda in in 10 mM MgCl2 Tris buffer at 25°C. The raw SAXS data were passed through a 0.2 span Lowess (based on local regression) filter in both x (Q) and y (time) direction. The data were colored based on their relative hight to x-y plane. (B) DNA ejection kinetics of 48.5 kbp phage lambda in 10 mM MgCl2 Tris buffer at different temperatures monitored by SAXS. DNA peak area was calculated and plotted. The inset figure shows in the initial 0s -25s the drop of DNA area, which is not temperature dependent, and correlates to the fast ejection peak observed in our ITC measurements. (C) Activation energy Ea of the DNA ejection process (circular) calculated from SAXS data in 48.5 kbp phage compared to $\ln(1/\tau)$ calculated from the fast phase (first 25 sec) (square) using Arrhenius equation. We can see that for the overall process, points $\ln(1/\tau)$ vs. 1/RT fall nicely into a linear trend and an activation energy can be calculated. For the three points in fast phase, they do not fit into a line very well. But the overall changes of $\ln(1/\tau)$ vs. 1/RT at three different temperatures for fast phase is very small. Error bars for each $\ln(1/\tau)$ plotted are the progressed S.E. values of the τ, S.E. are calculated from 95% interval lower and upper limit from the fit.

The area of this DNA peak (indicates retained DNA volumes inside the capsid) was then plotted versus ejection time (Figure 5.4A). DNA release from the viral particles was well-described in previous literature as a first order reaction with a single rate-limiting step (*13*, *17*). In this experiment, the natural logarithm of DNA peak area is recorded for λ at three different temperatures (Figure 5.4B). The exponential decay corresponds to a straight line of slope equal to $1/\tau$ and τ is the rate constant of DNA translocation in vitro. For wt full DNA length λ particles, it was

found that at temperatures lower than T^* (25°C and 30°C), there is a change in the rate constant of DNA release. We hypothesized that the ln (DNA peak area) curve is an addition of curves from two populations each with a distinct rate constant. Plotting ln(1/τ) versus 1/RT (Figure 5.4C) gives us the activation energy, based on Arrhenius law $\frac{1}{\tau} = Ae^{-\Delta E/RT}$. In this case, ΔE was found to be 1.19×10^{-19} J/virion for the overall process of wt full length DNA λ. As a comparison, the activation energy was calculated to be close to 0 for just the initiation stage (the fast phase). We concluded that for full length DNA λ, an activation energy in genome (note that this is different than activation energy for biochemical reactions such as portal opening upon receptor binding) is required for DNA release. This activation energy is likely related to the energy barrier between solid and fluid DNA states and absent in viral genomes that significantly shorter and occupy less capsid volume.

Thus, the energy of activation which needs to be overcome in order to facilitate genome ejection from phage with the solid-like structural DNA state is relatively high (~20 times higher than molecular thermal energy). It is of the same order of magnitude as the activation energy required for phage adsorption to receptor (*16*, *17*, *19*). It is therefore feasible, that solid-like DNA state can significantly delay or even completely arrest the DNA ejection process from phage, in agreement with our observations. This energy of activation can be attributed to the solid-to-fluid like DNA transition in the capsid which would facilitate DNA ejection process. However, it can also be simply related to a significant DNA-DNA sliding friction occurring in the initial stage of DNA ejection process. The fact that activation energy behavior for the overall process of the ejection versus just the starting phase is different, demonstrates that measured energy of activation is mainly related to the packaged DNA state rather than to phage-receptor interaction.

In summary, besides temperture induced structural DNA transition, the interstrand friction can also be reduced by reduced DNA packing density, which

results in a more fluid-like DNA state in the capsid with increased DNA mobility and similarly synchronized, rapid DNA ejection events. These data demonstrates for the first time a direct correlation between virally encapsidated DNA structure and its ejection dynamics. As we have previously shown, the DNA transition in the capsid is in turn strongly correlated with the internal DNA stress (*27*). However, besides from packaged DNA length, the DNA stress in the capsid is also regulated by the concentration and nature of the DNA counterions freely diffusing through the capsid wall of most viruses(*48*). This fact leads us to the next important question which is whether extra- and intra-cellular ionic conditions in the bacterial host are favorable for synchronized rapid DNA ejections from phage facilitating the rate of viral growth. In the next section we investigate how deviation from the ionic conditions mimicking those for optimum phage infectivity in vivo, influence DNA ejection dynamics at physiologic temperature of infection (37 °C).

5.8. Ion regulated on-off switch between fast and slow DNA ejection dynamics.

While variation in the monovalent ion concentration has a small influence on intra-capsid DNA stress (*48*), polyvalent cations present in the bacterial cytoplasm, such as polyamines and Mg2+, have been shown to have a strong effect on the repulsive interactions between packaged DNA helices (*47*, *48*). Since the free polyamine concentration in cells is very low as most polyamines are bound to cellular DNA and RNA (*49-51*), we are specifically interested in the effect of the Mg-ion concentration on the dynamics of DNA ejection from phage λ at concentrations similar to those of extra- and intracellular Mg^{2+} in vivo.

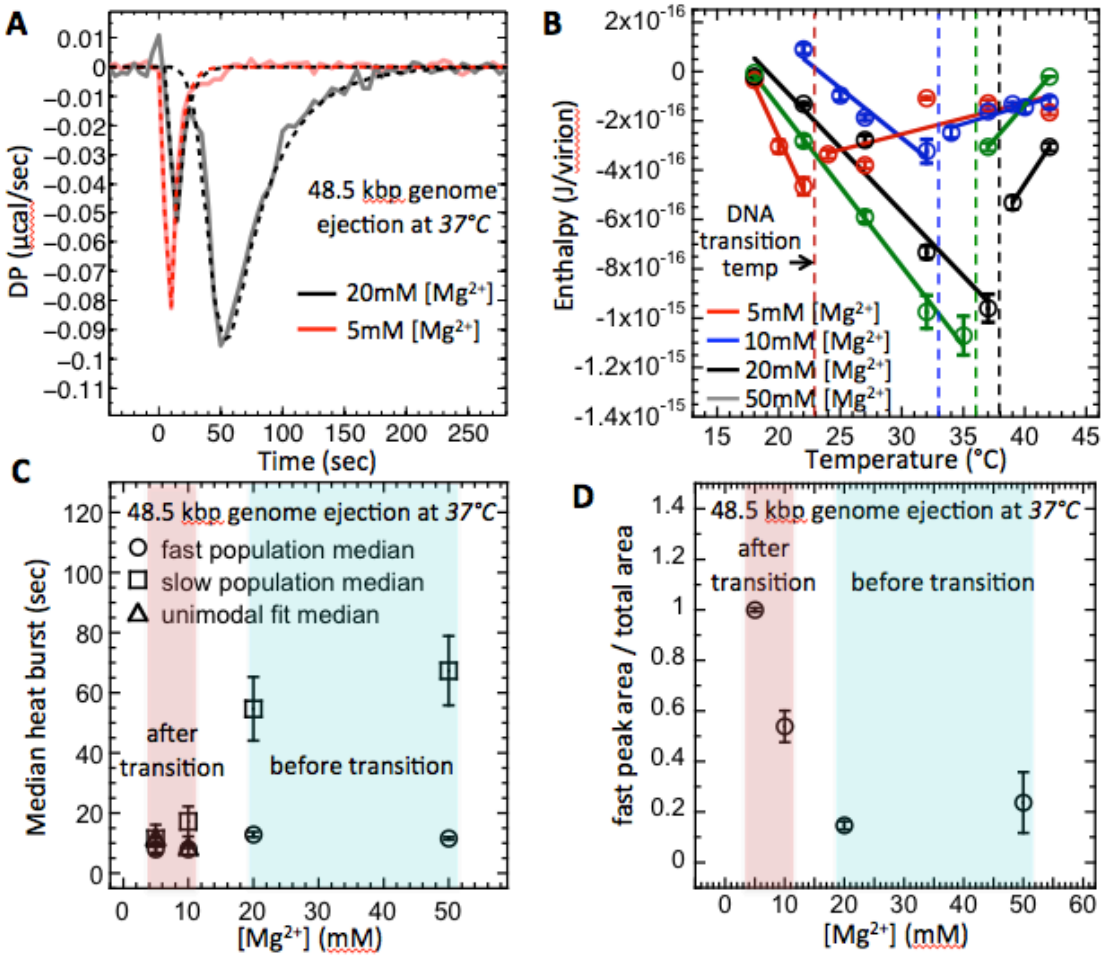

Figure 5.5 ITC data of genome ejection enthalpy for phages λ in various salt conditions. (A) Wild type λ virions with full length genome was titrated into LamB solution at T = 37°C in TM buffer containing 20mM (black curve) or 5mM (red curve) Mg^{2+}. Solid line: raw data; dotted line: peak deconvolution fit data (B) Phase diagram for wt λ in TM buffer with 5,10,20 and 50mM Mg^{2+}. (C) Peak deconvolution was done for titration curves in all 4 salt conditions at T = 37°C. peak position for fast and slow peaks were analyzed and mean values were calculated and plotted. Errors shown are the width of Gaussian distribution. For λ virions in 5 and 10mM Mg^{2+}, they are in a post-transition state; for λ virions in 20 and 50mM Mg^{2+}, they are in a pre-transition state. See phase diagram. (D) Peak area of the deconvoluted fast peak (corresponding to ejection enthalpy from the fast population) and overall enthalpy were derived and the ratio of the fast peak area divided by the total peak area were calculated for all salt conditions. Experiments were repeated for 3 to 5 times and the progressed standard error of the mean were plotted. Note that for 5mM Mg^{2+}, because the fast and slow peak completely merge, as indicated by (C), so the fast peak area/total area is indicated as 1 here.

As mentioned above, since the Mg-concentration affects DNA stress in the capsid, it should also strongly influence the transition temperature and resulting ejection dynamics of the encapsidated genome. Therefore, we investigate whether the physiologic Mg-concentrations provide optimum conditions for infectivity in vivo by facilitating synchronized fast genome ejection dynamics from majority of phage λ particles close to the temperature of infection (37 °C). Such a unique correlation between the Mg-concentration and dynamics of infectivity related to genome release would suggest that the intracapsid DNA transition is an important regulatory mechanism for viral replication.

In the first set of measurements, using ITC assay described above, we determine DNA transition temperatures for WT λ-DNA length phage in $MgCl_2$ Tris-buffer with $MgCl_2$ concentrations varied between 5 and 50 mM, see Figure 5.5B. After this, we investigate how switching DNA transition on and off by changing Mg-concentration affects the DNA ejection dynamics at physiologic temperature of 37 °C. The intracapsid DNA transition occurs at temperature T*, corresponding to a discontinuity in the linear dependence of ΔH_{ej} on temperature. Increasing the Mg-concentration will initially significantly reduce the strength of the interstrand repulsive interactions in the capsid due to the counterion screening of the negative charges between packaged DNA helices (*48*, *52*). However, we have previously shown that at DNA packing densities in phage l, the screening effect of Mg-ions will become progressively smaller due to the counter-ion saturation (*48*). As described above, DNA packaged in the capsid, has to reach the critical stress level which increases with increasing temperature until the structural transition relieving the genome stress occurs at T*. Thus, reducing the intra-capsid DNA stress by increasing Mg-ion concentration leads to an increase in T*. That is, a higher temperature is required to reach the critical DNA stress limit in order to overcome the energetic barrier triggering the structural genome transition. Figure 5.5B shows that the DNA transition temperature T* is at first significantly increased with

increasing Mg-concentration, from T*~22 °C at 5 mM $MgCl_2$ Tris-buffer to T*~37 °C at 20 mM $MgCl_2$ Tris-buffer. Between 20 and 50 mM MgCl2, T* remains essentially unchanged due to Mg-ion saturation at the DNA helices (*48*). While T* varies significantly with Mg^{2+} concentration, it is remarkable that the most favorable Mg-concentration for phage λ infection of E. coli (~10 mM) (*41*) triggers DNA transition in the capsid precisely at the physiologic temperature of infection (~37 °C). Figure 5.5B also shows that at 5 and 10 mM $MgCl_2$ and 37 °C the DNA in the λ capsid is entirely in a fluid-like state since DNA transition occurs at a significantly lower temperature. However, at 37 °C and concentration of Mg^{2+} ≥ 20 mM the DNA transition occurs close to this temperature and there will be a coexistence between phages with DNA packaged in both fluid- and solid-like states. Therefore, using time-resolved ITC, we investigate below how salt-conditions in the host solution influence the dynamics of DNA ejection from phage at physiologic temperature of infection at 37 °C.

Figure 5.5A shows DP titration curves describing dynamics of DNA ejection from WT λ-DNA phage at 37 °C. After the intra-capsid DNA transition has occurred in 5 MgCl2 Tris-buffer (T* ~23 °C) and packaged DNA is predominantly in a fluid-like state, the Figure shows only one fast population dynamics with one DNA ejection peak centered at ~11 s. In 20 mM $MgCl_2$ Tris-buffer the intracapsid DNA is at transition temperature (T* ~38 °C). Indeed, DP titration curve shows two phage population dynamics. The first peak with median average ejection time of ~12 s corresponds to phage population with DNA in a fluid-like state. The second peak has median time of ~54 s arising from phage with DNA packaged in a solid-like state (Table 5.2). Analogously to the ITC data analysis above, the median value, derived from the right skewed Gaussian fit to the DP titration curve, better reflects the average DNA ejection time than the smaller mode value. In Figure 5.5C, we plot median time values derived from the skewed Gaussian fits to the deconvoluted DNA ejection peaks for DNA ejection dynamics in 5-50 mM MgCl2 Tris-buffers at 37 °C.

Data shows that at all salt conditions where DNA in the capsid has undergone a transition and is in fluid-like state (5-10 mM $MgCl_2$), there is only one population of phage particles with fast DNA ejection dynamics around ~11 s. This ejection time corresponds to DNA translocation time from the capsid which suggests that ejections occur in a synchronized manner. At high Mg-concentrations (≥ 20 mM), there are always two DP peaks corresponding to fast and slow dynamics of DNA ejection. The slow ejection dynamics is associated with slower DNA translocation when DNA is a solid-like state as well as delays in initiation of DNA ejection (which we previously observed). This occurs due to high DNA-DNA sliding friction in the capsid for the population of phage particles with encapsidated DNA in a solid-like state.

Finally, in Figure 5.5D, we plotted the area fraction of the fast population dynamics peak compared to the total area of both fast and slow peaks (in those cases where slow peak is present). Figure nicely illustrates how intracapsid solid-to-fluid like DNA transition has a polarizing effect on DNA ejection dynamics. In the ionic conditions which turn the DNA transition on at 37 °C, the DNA ejection is fast and completes in ~11 s for a monomodal (unimodal) population of phage particles. This Mg-concentration of 10 mM is also shown to provide most efficient phage infection. Deviation from this conditions at higher Mg-concentrations leads to predominantly slow genome ejection dynamics with ejection times delayed 6-8 times (~60 s), suggesting reduced rate of the viral growth cycle and therefore less optimized infection conditions.

5.9 Conclusions

With this data, we show for the first time, that temperature regulated DNA transition in the capsid has a direct influence on the dynamics of initiation of DNA ejection process. Temperature is a parameter that is rarely varied in biophysical measurements on viruses. Yet, temperature is directly pertinent to the ability of

viruses to survive outside of their hosts and multiply within them. This data demonstrates that at ~22 °C, where many biophysical measurements on viruses are conducted, there is ~60% of phage particles with delayed DNA release process which can in turn have implication for the replication cycle affecting rate of mutations and limiting infectivity (e.g., some phages with the solid-like DNA state take 25 times longer to eject their DNA compared to the time for a single ejection). At the same time, at the temperature of the human host, 37 °C (since phage λ infects E. coli in the human gut), the structural DNA change leads to a more mobile genome inside the capsid, which facilitates synchronized and instantaneous initiation of DNA ejection into a cell during infection (*25*, *38*). This significant difference in phage ejection dynamics behavior should be considered when comparing in vitro versus in vivo measurements on phages often performed at different temperatures. This mechanism of temperature regulated DNA ejection dynamics from phage, provides a new paradigm of viral metastability, which was previously only attributed to the structural transformations in the nucleocapsid and/or surrounding lipid envelop in response to changes in the virion's environment (*53*). Virion metastability is one of the central concepts in virology (*53*). It implies that the virus, in order to successfully replicate, must be sufficiently stable to prevent spontaneous release of its genome outside the cell between infection events, and at the same time be unstable enough to release its genome during infection.

We can switch the DNA transition in phage λ on and off by directly affecting the interstrand repulsions, and consequently, the stress level of the encapsidated genome. We discovered for the first time that DNA ejection has a slower population at more stressed state tuned by ionic strength in the surrounding solutions. The slow population is switched off when encapsidated DNA is past the transition and in the fluid-like phase already. Since DNA transition markedly affects the ability of the virion to eject its DNA into a cell (*38*), these results demonstrate how variations in the extracellular ionic environment can lead to favorable as well as inhibiting conditions for infectivity.

References for Chapter 5

1. S. Bonhoeffer, R. M. May, G. M. Shaw, M. A. Nowak, Virus dynamics and drug therapy. *Proceedings of the National Academy of Sciences of the United States of America* **94**, 6971-6976 (1997).
2. J. M. Coffin, HIV population dynamics in vivo: implications for genetic variation, pathogenesis, and therapy. *Science* **267**, 483-489 (1995).
3. A. S. Perelson, A. U. Neumann, M. Markowitz, J. M. Leonard, D. D. Ho, HIV-1 dynamics in vivo: virion clearance rate, infected cell life-span, and viral generation time. *Science* **271**, 1582-1586 (1996).
4. Y. Lee, S. D. Eisner, J. Yin, Antiserum inhibition of propagating viruses. *Biotechnol Bioeng* **55**, 542-546 (1997).
5. E. L. Ellis, M. Delbruck, The Growth of Bacteriophage. *J Gen Physiol* **22**, 365-384 (1939).
6. R. Gallet, S. Kannoly, I. N. Wang, Effects of bacteriophage traits on plaque formation. *BMC Microbiol* **11**, 181 (2011).
7. S. Casjens, Prophages and bacterial genomics: what have we learned so far? *Mol Microbiol* **49**, 277-300 (2003).
8. S. R. Casjens, I. J. Molineux, Short noncontractile tail machines: adsorption and DNA delivery by podoviruses. *Adv Exp Med Biol* **726**, 143-179 (2012).
9. Y. Shao, I. N. Wang, Bacteriophage adsorption rate and optimal lysis time. *Genetics* **180**, 471-482 (2008).
10. M. Briggiler Marco, J. Reinheimer, A. Quiberoni, Phage adsorption and lytic propagation in Lactobacillus plantarum: could host cell starvation affect them? *BMC Microbiol* **15**, 273 (2015).
11. C. W. Baker *et al.*, Genetically Determined Variation in Lysis Time Variance in the Bacteriophage phiX174. *G3 (Bethesda)* **6**, 939-955 (2016).
12. Z. J. Storms, D. Sauvageau, Evidence that the heterogeneity of a T4 population is the result of heritable traits. *PloS one* **9**, e116235 (2014).
13. P. Grayson, L. Han, T. Winther, R. Phillips, Real-time observations of single

bacteriophage lambda DNA ejections in vitro. *Proceedings of the National Academy of Sciences of the United States of America* **104**, 14652-14657 (2007).

14. N. Chiaruttini *et al.*, Is the in vitro ejection of bacteriophage DNA quasistatic? A bulk to single virus study. *Biophysical journal* **99**, 447-455 (2010).
15. D. Van Valen *et al.*, A single-molecule Hershey-Chase experiment. *Current biology : CB* **22**, 1339-1343 (2012).
16. K. G. Freeman, M. A. Behrens, K. A. Streletzky, U. Olsson, A. Evilevitch, Portal Stability Controls Dynamics of DNA Ejection from Phage. *The journal of physical chemistry. B* **120**, 6421-6429 (2016).
17. E. Raspaud, T. Forth, C. Sao-Jose, P. Tavares, M. de Frutos, A kinetic analysis of DNA ejection from tailed phages revealing the prerequisite activation energy. *Biophysical journal* **93**, 3999-4005 (2007).
18. M. Schwartz, Reversible interaction between coliphage lambda and its receptor protein. *Journal of molecular biology* **99**, 185-201 (1975).
19. D. W. Bauer, A. Evilevitch, Influence of Internal DNA Pressure on Stability and Infectivity of Phage lambda. *Journal of molecular biology* **427**, 3189-3200 (2015).
20. M. M. Inamdar, W. M. Gelbart, R. Phillips, Dynamics of DNA ejection from bacteriophage. *Biophysical journal* **91**, 411-420 (2006).
21. I. J. Molineux, D. Panja, Popping the cork: mechanisms of phage genome ejection. *Nat Rev Microbiol* **11**, 194-204 (2013).
22. D. Lof, K. Schillen, B. Jonsson, A. Evilevitch, Forces controlling the rate of DNA ejection from phage lambda. *Journal of molecular biology* **368**, 55-65 (2007).
23. I. N. Wang, Lysis timing and bacteriophage fitness. *Genetics* **172**, 17-26 (2006).
24. T. Liu *et al.*, Solid-to-fluid-like DNA transition in viruses facilitates infection. *Proceedings of the National Academy of Sciences of the United States of America* **111**, 14675-14680 (2014).

25. U. Sae-Ueng *et al.*, Solid-to-fluid DNA transition inside HSV-1 capsid close to the temperature of infection. *Nature chemical biology* **10**, 861-867 (2014).
26. P. Grayson *et al.*, The effect of genome length on ejection forces in bacteriophage lambda. *Virology* **348**, 430-436 (2006).
27. D. Li *et al.*, Ionic switch controls the DNA state in phage lambda. *Nucleic acids research* **43**, 6348-6358 (2015).
28. A. Evilevitch, L. Lavelle, C. M. Knobler, E. Raspaud, W. M. Gelbart, Osmotic pressure inhibition of DNA ejection from phage. *Proceedings of the National Academy of Sciences of the United States of America* **100**, 9292-9295 (2003).
29. I. Ivanovska, G. Wuite, B. Jonsson, A. Evilevitch, Internal DNA pressure modifies stability of WT phage. *Proceedings of the National Academy of Sciences of the United States of America* **104**, 9603-9608 (2007).
30. M. Jeembaeva, B. Jonsson, M. Castelnovo, A. Evilevitch, DNA heats up: energetics of genome ejection from phage revealed by isothermal titration calorimetry. *Journal of molecular biology* **395**, 1079-1087 (2010).
31. M. de Frutos, L. Letellier, E. Raspaud, DNA ejection from bacteriophage T5: analysis of the kinetics and energetics. *Biophysical journal* **88**, 1364-1370 (2005).
32. A. Leforestier *et al.*, Bacteriophage T5 DNA ejection under pressure. *Journal of molecular biology* **384**, 730-739 (2008).
33. P. Dumas *et al.*, Extending ITC to Kinetics with kinITC. *Methods Enzymol* **567**, 157-180 (2016).
34. D. Burnouf *et al.*, kinITC: a new method for obtaining joint thermodynamic and kinetic data by isothermal titration calorimetry. *J Am Chem Soc* **134**, 559-565 (2012).
35. P. K. Purohit, J. Kondev, R. Phillips, Mechanics of DNA packaging in viruses. *Proceedings of the National Academy of Sciences of the United States of America* **100**, 3173-3178 (2003).
36. P. K. Purohit *et al.*, Forces during bacteriophage DNA packaging and ejection.

Biophysical journal **88**, 851-866 (2005).

37. H. G. Garcia *et al.*, Biological consequences of tightly bent DNA: the other life of a macromolecular celebrity. *Biopolymers* **85**, 115-130 (2007).
38. T. Liu *et al.*, Solid-to-fluid-like DNA transition in viruses facilitates infection. *Proc Natl Acad Sci U S A*, (2014).
39. K. J. Goodman, J. T. Brenna, Curve fitting for restoration of accuracy for overlapping peaks in gas chromatography/combustion isotope ratio mass spectrometry. *Anal Chem* **66**, 1294-1301 (1994).
40. E. Grushka, Characterization of exponentially modified Gaussian peaks in chromatography. *Analytical Chemistry* **44**, 1733-1738 (1972).
41. B. A. Fry, Conditions for the infection of Escherichia coli with lambda phage and for the establishment of lysogeny. *J Gen Microbiol* **21**, 676-684 (1959).
42. H. Gaussier, Q. Yang, C. E. Catalano, Building a virus from scratch: assembly of an infectious virus using purified components in a rigorously defined biochemical assay system. *J Mol Biol* **357**, 1154-1166 (2006).
43. J. E. Lusk, R. J. Williams, E. P. Kennedy, Magnesium and the growth of Escherichia coli. *J Biol Chem* **243**, 2618-2624 (1968).
44. F. C. Kung, J. Raymond, D. A. Glaser, Metal ion content of Escherichia coli versus cell age. *J Bacteriol* **126**, 1089-1095 (1976).
45. C. Hurwitz, C. L. Rosano, The intracellular concentration of bound and unbound magnesium ions in Escherichia coli. *J Biol Chem* **242**, 3719-3722 (1967).
46. W. C. Earnshaw, S. C. Harrison, DNA arrangement in isometric phage heads. *Nature* **268**, 598-602 (1977).
47. X. Qiu *et al.*, Salt-dependent DNA-DNA spacings in intact bacteriophage lambda reflect relative importance of DNA self-repulsion and bending energies. *Physical review letters* **106**, 028102 (2011).
48. A. Evilevitch *et al.*, Effects of salt concentrations and bending energy on the extent of ejection of phage genomes. *Biophysical journal* **94**, 1110-1120

(2008).

49. R. H. Davis, D. R. Morris, P. Coffino, Sequestered end products and enzyme regulation: the case of ornithine decarboxylase. *Microbiological reviews* **56**, 280-290 (1992).

50. W. Gibson, B. Roizman, Compartmentalization of spermine and spermidine in the herpes simplex virion. *Proc Natl Acad Sci U S A* **68**, 2818-2821 (1971).

51. K. Igarashi, K. Kashiwagi, Polyamines: mysterious modulators of cellular functions. *Biochemical and biophysical research communications* **271**, 559-564 (2000).

52. G. C. Lander *et al.*, DNA bending-induced phase transition of encapsidated genome in phage lambda. *Nucleic acids research* **41**, 4518-4524 (2013).

53. S. J. Flint, L. W. Enquist, V. R. Racaniello, A. M. Skalka, *Principles of Virology: Pathogenesis and Control*. (ASM Press, ed. 3rd, 2009), pp. 1028.

CHAPTER 6 OSMOTIC PRESSURE INHIBITS HSV-1 GENOME TRANSLOCATION INTO NUCLEUS

6.1 Abstract

Many double-stranded DNA viruses are highly pressurized. Upon confinement within the capsid, neighboring DNA strands experience repulsive electrostatic and hydration forces as well as bending stress due to curvature required of packaged DNA. This internal pressure was measured to be 20 atm in bacteriophage λ and 18 atm in type 1 herpes simplex virus (HSV-1). Existence of internal pressure has been verified as the major driving forces during genome ejection in infection process; Reduction of the intracapsid pressure by applying balancing osmotic pressure in the surrounding solutions of viral capsids result in suppression of DNA release. By mimicking intra-nuclear DNA translocation in a reconstituted system consist of isolated rat liver nuclei, cytosolic homogenate and purified HSV-1 capsids, we showed for the first time, DNA ejection in eukaryotic human virus into nucleoplasm can be completely inhibited by addition of osmolytes around the nuclei. This study also provides the first experimental prove that, the critical stage of viral infection in a sub-cellular organelle environment, is mechanically controlled. Results of this study provide insights on understanding physical evolution of viruses, how they mechanically evolved to adapt the surrounding environment and maximize the infection efficiency *in vivo*.

6.2 Introduction

In the case of many double-stranded DNA viruses, the capsids are highly pressurized. Encapsidated DNA is strongly bent and tightly packaged, giving rise to high bending and repulsion forces. Furthermore, this extreme packing density removes water molecules from the viral DNA surface and causes additional repulsive hydration forces (*1*). The rigid protein shell of viral capsids therefore

resist a significant force per-unit-area value, known as the intra-capsid pressure (*2*). Existence of intra-capsid pressure was addressed theoretically as early as 1970s (*3*) and first proved in bacteriophage λ in 2003 (*4*). Recent work also demonstrated presence of inter pressure in human herpes simplex virus type 1 (HSV-1). Both measured the pressure to be tens of atmospheres. In both HSV-1 and λ, DNA occupies ~ 60% of the internal capsid volume. The internal capsid size of HSV-1 is about 5.8 times of that in λ; The inter-DNA strand spacing is also larger in HSV-1 capsid than in λ (3.2 nm compared to 1.7 nm). These geometric constrain result in a lower intra-capsid pressure in HSV-1 than λ due to smaller bending and repulsive electrostatic forces of viral DNA molecule. The pressure was measured to be 18 atm in HSV-1 and 20 atm in λ (*4*, *5*).

Post infection, HSV-1 capsids are transported from the plasma membrane to the nucleus along microtubules (might be dynein-mediated) and start to accumulate on the nuclear membrane at 1-2 hour post-adsorption to the cell (*6*). Nuclear pore complexes (NPCs) are the target sites for HSV-1 capsid docking and DNA translocation (*6*, *7*). The diameter of NPC is ~ 120 nm on the cytoplasmic-side surface (*8*), in comparable dimension to the size of HSV-1 capsids (125 nm). Binding of HSV-1 capsid was shown to occur in a distinct orientation with one of the five-fold axis on capsid facing the NPC at a distance of ~50 nm away (*6*, *9*, *10*). The binding interactions between capsids and NPC are highly specific. HSV-1 protein pUL25, which arrayed around pentons on the capsid (*11*, *12*), was shown to interact with its nuclear receptor, nucleoporin CAN/Nup214 and mediate docking of HSV-1 capsid to the nuclear membrane (*13*).

After docking, HSV-1 DNA is quickly ejected into the nucleoplasm, the empty, NPC-bound capsids were eventually released back into cytosol (*6*, *7*, *10*). Previous works showed HSV-1 were capable of ejecting a fraction of their genome (~20%) into nuclei independent of metabolic energy (in the absence of ATP) (*10*). It was not

yet known how intra-capsid pressure contributes to energy for translocation. In this work, we places for the first time, the observation of mechanical DNA pressure inside viral capsids in the biological context of Herpes infection; We tested the role of osmotic pressure in viral DNA ejection in a reconstituted system made of isolated rat liver nuclei, cytosolic mixture and purified HSV-1 capsids. The reconstituted solution system encompassed the necessary and sufficient components for efficient HSV-1 DNA ejection into nucleus. This system was placed at physiological temperature (37°C) for half an hour, then DNA samples from nucleoplasm, nuclei-bound capsids, free capsids and extra-nuclear fluid were separately extracted and assayed by quantitative PCR analysis for HSV-1 DNA contents. Both iso-osmotic and hyper-osmotic buffer conditions were tested using this system in search for pressure tuning of intra-nuclear DNA ejection. We found that in iso-osmotic conditions, an average of 98.3% of the nuclei-bound capsids have ejected their DNA into the nucleoplasm. When increasing the osmotic pressure to 18 atm by addition of 30% polyethylene glycol with molecular weight 8000 g/mol (PEG-8k) to the solution, the percentage of ejecting, nuclei-bound capsids reduced to 0.2%. This arresting result directly revealed the vital role of external osmotic pressure on DNA ejection into nucleus. Furthermore, we examined the role of osmolarity on DNA ejection by supplement of a different osmolyte, Dextran with molecular weight of 155k g/mol (Dextran-155k), and confirmed that the suppression of DNA ejection depends on the external osmotic pressure only, not on the nature of the osmolyte. This work provides the first experimental evidence on criticality of mechanical forces to viral capsid DNA - nucleoplasm translocation process in a reconstructed, sub-cellular environment mimic system.

6.3 Materials and methods

6.3.1 HSV-1 capsid, rat liver nuclei isolation, BHK cytosol prep

Purification of HSV-1 capsids were described previously (*5*). African green monkey kidney cells (Vero) were infected with HSV-1 KOS strain or HSV-1 (Kos)-

RFP (HSV-1 KOS virus that expresses RFP conjugated to the capsid protein VP26, gift from Fred Homa, University of Pittsburgh) at a multiplicity of infection (MOI) of 5 pfu/cell for 20 h at 37 °C. Cells were collected, pelleted and resuspended in 20mM Tris buffer (pH 7.5) on ice for 20 min and lysed by addition of 1.25% (v/v) Triton X-100 (Alfa Aesar) for 30 min on ice. Lysed cells were centrifuged at 2000 rpm for 10 min and the nuclei pellets were resuspended with 1x protease inhibitor cocktail (Complete; Roche) added. Nuclei were disrupted by sonication for 30 s and loaded onto TNE sucrose gradient at 24 k rpm for 1 h. The C-capsid band was isolated by side puncture, diluted in TNE buffer and centrifuged at 24 k rpm for an additional 1 h. Capsids were resuspended in a preferred capsid binding buffer (CBB: 20 mM HEPES-KOH with pH of 7.3, 80 mM K-acetate, 2 mM DTT, 1mM EGTA, 2mM Mg-acetate, 1mM PMSF, and 1X CLAP cocktail).

Nuclei from rat liver were isolated as adapted from previously described protocol (*10*, *14*). Livers were chopped, grinded then fileted through a metal mesh in 0.25M STKM buffer (0.25 M sucrose, 25 mM HEPES-KOH pH 7.4, 25 mM KOAc, 5mM MgCl2, 0.1mM EDTA, 1mM PMSF, 1X CLAP cocktail and 1 mM DTT). Samples were treated by centrifugation at 1000 g for 10 min and resuspended in 0.25 M STKM solution with 1x protease inhibitor cocktail (complete; Roche). The pellets were then homogenized 20 times using a Dounce homogenizer on ice. The homogenate was centrifuged at 1000 g for 10 min at 4°C.

Nuclei pellets were resuspended in 0.25M STKM buffer and mixed with approximately double volume 2.3 M STKM buffer to raise the sucrose concentration to 1.6M. Nuclei were then separated from the cytoplasmic components by underlaying the homogenate with 2.3 M STKM buffer followed by centrifugation in a Beckman SW28 rotor at 25 k rpm for 40 min at 4 °C. The white nuclear pellets were harbested and resuspended in 0.25 M STKM and re-homogenized with Dounce for 3 strokes. Homogenate were underplayed with 30% STKM and centrifugated at 2000

rpm for 10 min. Pellets were resuspended in 0.25 M STKM, pelleted and frozen in liguid nitrogen and store at –80^{o}C for long term storage.

The cytosol was separately prepared using BHK-21 cells (ATCC CCL-10). Cells were grown to confluent in 245x245mm plates and collected from the plates by addition of 0.25% trypsin/EDTA (ThermoFisher Scientific). Collected cells were washed with KEHM buffer (50 mM KCl, 10 mM EGTA, 50 mM Herpes, pH 7.4, 2 mM $MgCl_2$) and kept on ice. Cells were then resuspended in KEHM buffer supplement with 1 mM DTT and 1x protease inhibitor (complete; Roche) at the volume of 5mL KEHM per 10^9 cells. Resuspended cells were broken using EMBL 8.020mm cell cracker homogenizer with ball sizes 8.010, 8.008 or 8.004nm, then spin at 3000 rpm, 4^{o}C for 15 min to remove the intact cells and nuclei. The supernatant was re-spin at 80,000 rpm (267,000 g), 4^{o}C for 30 min and only the supernatant was kept as the purified cytosol. The cytosol was frozen in liguid nitrogen and store at –80^{o}C for long time storage.

6.3.2 Reconstituted Nuclei-capsid system

An in vitro viral HSV-1 DNA translocation system was built in which HSV-1 genome was released into nucleoplasm in a homogenate solution mimicking cytoplasm environment. In a typical 500 µL scale system, 8×10^5 counts of rat liver cell nuclei was incubated with approximately 10^9 counts of viruses on ice for 10min in CBB buffer as previously described (*10*) containing: (i) BHK cell cytosol (final concentration reading about 2.5 mg/mL protein contents) (ii) 1 mg/mL BSA (iii) ATP regeneration system composed of 5mM creatine phosphate (Sigma), 20 U of creatine phosphokinase (Sigma), 1mM ATP, 0.2 mM GTP. Then osmolytic solution of PEG-8k (or water in control sample) was added to make up a total of 500µL system. Final osmolytes in the solution reaches a concentration of 30% w/w. The system is incubated 37°C for 30min then transferred on ice for a minimum of 10min.

6.3.3 Fluorescence imaging

For fluorescence microscopy, both unlabeled and the RFP-labeled HSV-1 capsids (strain name, gift from Dr. Fred Homa) were used. For unlabeled HSV-1 C-capsid, it is prestained by YOYO-1 iodide (ThermoFisher Scientific). After incubation as described, the buffer system containing purified HSV capsids and nuclei were loaded onto cover-slips. For RFP-capsid incubation, 1000x diluted Syto13 were added to stain viral and nuclear DNA (*15*). For YOYO-1 stained c-capsids incubation, Hoechst 33342 (ThermoFisher Scientific) were used nuclear DNA. Overlay of the confocal 488 (for syto13 emitted signal) and 560 (for RFP emitted signal) channels show the localization of viral capsid onto the nucleus. For estimating of total viral number attached to nuclei, a z-stack were done through the nuclear volume and 3-D reconstruction of the nuclei were done by Imaris.

6.3.4 Electron microscopy

After nuclei-capsid binding incubation as described earlier, the samples were washed once with CBB buffer at 1000 rpm for 5 min, then fixed with 2% gluteraldehyde in phosphate buffered saline (PBS) 1 to 3 hr, followed by 1 hr incubation with 1% osmium tetroxide in PBS. Samples were dehydrated by a graded ethanol series and propylene oxide, embedded in Epon, and further contrasted with lead citrate and uranyl acetate.

6.3.5 Capsid pull-down assay

After capsid-nuclei incubation, the system was centrifuged at 3k rpm to spin down the capsid-associated nuclei. Nuclei pellet was washed twice in CBB buffer at 4°C to remove excessive osmolytes in the pellet (low temperature and placement of the sample on ice at all times were required to minimize DNA ejections after the incubation stage). The pellet was then resuspended and incubated for 20 min in 1x reticulocyte standard buffer (RSB: 10mM Tris of pH 7.5, 10mM KCl, 1.5mM MgCl2, 0.5% NP-40 substitute) for nuclear membrane lysis. The supernatant was collected

separately as the extranuclear solution.

Both extra-nuclear supernatant solution and lysed nuclear pellet were then incubated with 5μL anti-HSV1/2 ICP5/UL19 antibody (from Bernard Roizman lab) for overnight at 4°C. 50μL 50% Protein A bead slurry (Sigma-Aldrich P1406) was added to each samples to capture viral capsid-antibody complex on the next day. Protein A bead complex was collected by low speed centrifugation (1500 rpm, 5 min). The supernatant was collected as capsid-free part (sample b and d in Figure 3). In parallel, the pelleted beads parts were re-suspended in Proteinase K solution to digest the capsid and let viral DNA diffuse into the solution (sample a and c in Figure 3). Then all the sample solutions were phenol-chloroform treated and DNA was ethanol precipitated at re-suspended in clean water.

This in vitro assay successfully parted HSV-1 DNA into four samples: (a) HSV genome from those capsids unbound or failed to dock onto nuclear pore complex. (b) Free HSV DNA in the extra-nuclear solution due to contamination or broken capsids. (c) HSV DNAs still sustained inside the nuclear-associated capsids within the time frame of experimental incubation. (d) HSV genomes that are successfully ejected into nucleoplasm.

Quantification of each part of traces of viral genome in the in vitro translocation system was crucial to understand the efficiency of viral genome release in our reconstructed system. Extracted DNAs from sample a, b, c, d were quantified by real-time PCR analysis for DNA level by custom TaqMan assays. Viral genes VP16 and ICP0 were quantified with primers and probe sequences (from Bernard Roizman lab). The assays were performed using a StepOnePlus system (Applied Biosystems) and were analyzed with software provided by the supplier. Viral gene copies were calculated with comparison to amplification from HSV-1 DNA with known copy numbers.

6.4 HSV-1 C-capsids docking to NPC

A cell-free system was reconstituted to mimic the in vivo HSV-1 DNA ejection into nucleus inside the cytoplasm (*10*, *16*). Purified nuclear C-capsids were incubated with isolated rat liver nuclei (*14*), in presence of BHK cell cytosol (*10*). To maximize HSV-1 binding events per nuclei, C-capsids were added in abundance relative to nuclei (~1200:1 ratio). Importin β was the only cytosolic factor known to be sufficient and necessary for HSV-1 capsid binding, depletion of Importin β result in inhibition of nuclei binding events (*10*). In our system, no purified importin β was separately appended; thus the cytosol homogenate was a critical component for the capsid-binding assay. In addition, a creatine phosphokinase (CPK), phospho-creatine (PC) based ATP-regeneration system was supplemented to the system. Although binding of the HSV-1 capsids to nuclei was found to be independent of energy in the form of ATP, the subsequent DNA ejection step was found to be ATP-dependent (*10*). Supplementation of ATP-regeneration system was shown to enhance the DNA ejection efficiency about three-fold (10).

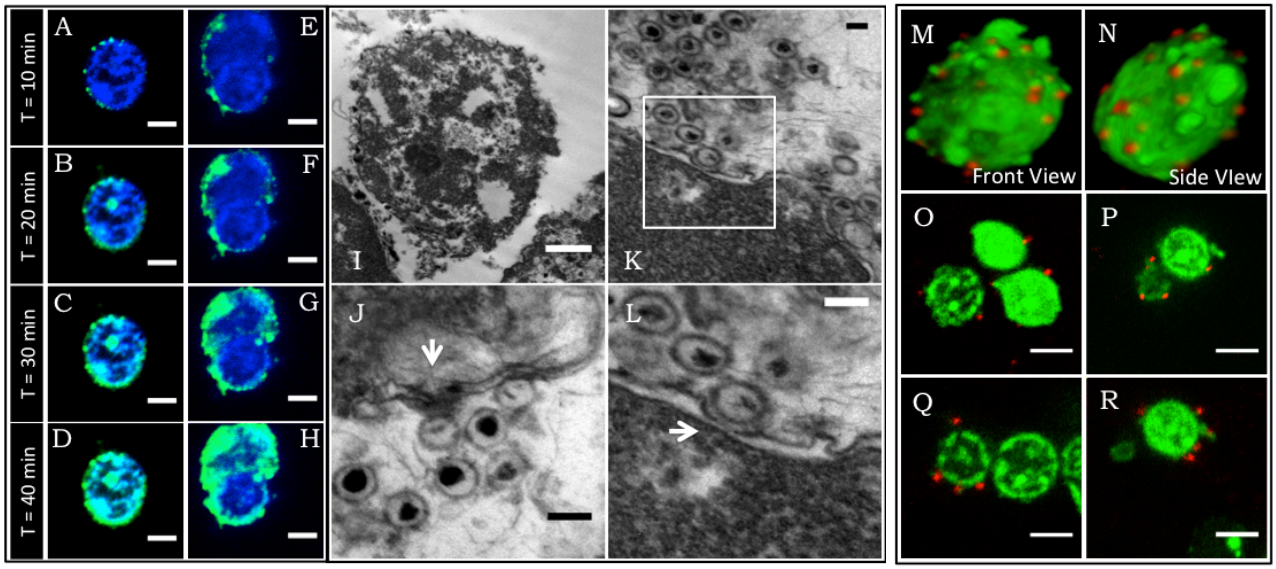

Figure 6.1: HSV C-caspids docking to nucleus, observed both by fluorescence and electron microscopy. All fluorescence images were obtained by spinning disk confocal microscopy, nuclei DNA stained by Hoechst (blue) and capsid DNA labeled by YOYO-1 (green). Columns (A) through (D), (E) through (H) are two different examples. Each nuclei sample was pre-incubated with HSV-1 capsids for 10 min before imaging, so T starts at 10

min. (I) through (L) are the electron microscopy observation of our incubation system. (I) shows the full view of a nuclei bound with many viruses on its surface (J) is the zoom in of the nuclei membrane where an empty capsid bound to NPC is clearly visible here (indicated by arrow head). We can see some filled, non-ejected caspids around competing for the binding spots on membrane. (K) Another view of capsids associated nuclear membrane, (L) Zoom in of the boxed region in (K), nuclear pore structure indicated by arrow head. Scale bar, (A-H): 5μm. (I): 1μm (J-L): 100nm. (M-R): **HSV RFP C-caspids binding to nucleus, observed both by confocal fluorescence microscopy.** Nuclei DNA stained by Syto13 (green) and viral capsids labeled by RFP (red). (M) and (N) shows the 3D reconstruction of an example capsids-bound nuclei from confocal slices scanning through the whole nucleus volume in z-directions. (M): front (N): side view of the same nucleus. (Q) through (R) are the confocal z-sections of example nuclei. Scale bar in (Q-R): 5μm.

Tegument proteins were implicated to be critical for nuclear trafficking (interaction with the dynein motor), docking and binding (*6*). After HSV cell-entry, some of the capsid-associated tegument proteins were released into the peripheral cytoplasm while others remain tightly attached. Removal of teguments, either by mild trypsinization (*10*) or by microinjection of specific tegument protein VP1/2 (UL36) antibodies (*17*) show reduced level of HSV-1 binding. However in our system, we allow for a 30-40 min incubation time frame for capsids binding, we found that using un-tegumented C-capsids are sufficient for our assay. Later confirmed by qPCR results, more than 90% of the C-capsids in the system are, or have been nuclei-bound (Table 1).

Previous *in vitro* HSV-1 binding assay indicate optimized binding condition for capsid-nuclei at 37 °C for 40 min (*10*). We observed efficient capsid docking events onto nuclear membrane as early as 10 min and within 40 min, nuclear surfaces were majorly covered with C-capsid signal (Figure 6.1, panel A-F). To help visulazation, our C-capsids were labeled with YOYO-1 DNA dye. One drawback using DNA dye is that these dye molecules would stain nuclear DNA as well. Localization of these dye molecules inside the nucleus (Figure 6.1, panel D, H) may either come from ejected viral DNA or freshly stained heterochromatin DNA.

In the assay, the purified C-capsids were pre-stained in YOYO-1, then washed 2-3 times to get rid of the additional dye in the capsid buffer before incubation with the nuclei. YOYO-1 is a DNA intercalation dye, and dissociation half time for similar dyes was found on tens of ms (millisecond) scale (*18*). Which means upon bathing with nuclei, there will always be free YOYO dyes available in the buffer, which came off from the capsid DNA. These free YOYO dyes have a greater tendency to stain the less-packaged heterochromatin DNA. Though the binding of YOYO to the nucleus is much more time-consuming. The intercalation time constant for free YOYO-1 in the range of our assay was measured to be longer than 5 min (*19*). Shown in the fluorescence imaging results, the gradual appearance of YOYO signal in the nucleoplasm in a visible level starts at about 30 min post-incubation. And by T = 40 min, roughly half of nucleoplasm were stained by YOYO-1, indicated by co-localization with Hoechst dye.

EM imaging of our *in vitro* HSV-nucleus system confirms that bound capsids are docked onto the NPC structure on the nuclear membrane (Figure 6.1I-L). In EM studies, we observed a layer of capsids in proximity of the nuclear membrane (Figure 6.1I, 1H) since no strict stripping of unbound capsids were done for EM sample preparation. EM samples require maximized nuclei preservation, compared to fluorescence imaging, in which less rigorous standards of the nuclei are for imaging purposes thus we can apply excessive washing to remove all the unbound capsids from proximity of the nucleus. Shown in EM, most NPC-docked capsids are empty after 30 min incubation time while the unbound capsids in proximity remains DNA filled (Figure 6.1I-J). Dense patches of heterochromatin are normally seen all over the inner membrane side except around the NPC to leave a "pathway" for nuclear transport (*20*). Positions of NPC were confirmed in our EM images by association with absence of heterochromatin on the nucleoplasm side (Figure 6.1K-L).

The fluorescence imaging result in Figure 6.1, panel A-H shows good binding statistics of C-capsids to nucleus, though counting individual capsids are un-achievable with YOYO-stained capsids, especially when they start to stain the chromatin DNA In mammalian cells. Number of pore complexes on the nuclear membrane ranges anywhere from 1000 to 5000 per nucleus depending on the cellular type (*21*), which all could be potential sites for capsid binding. Additionally, after nuclear docking and DNA ejection, empty capsids were eventually released back into cytosol (*6*, *7*, *10*), leaving new available sites for capsid binding. The good binding statistics was later confirmed by quantitative PCR (qPCR) results, more than 90% of the C-capsids in our reconstituted system were shown to be, or have been nuclei-bound (Table 6.1). The fact that most of the capsids are associated with nuclear membrane is likely due to time scale of the experiment, where in fluorescence and electron microscopy, only one time-point was recorded. However all the capsids that have ejected DNAs into the nucleoplasm within the whole incubation time frame was recorded by non-imaging method.

To better visualize individual capsids on the nuclei, we later used C-capsids purified an HSV-1-KOS strain with small capsid protein VP26 tagged with RFP (gifted from F. Homa, University of Pittsburgh). Unfortunately, these capsids were displayed a significant reduction in binding capacity to nuclei (Figure 1M-R). VP26 was shown to mediate HSV-1 capsid binding to cytoplasmic dynein (*22*), thus critical for nuclear localization. However in our cell-free bathing system, cytoskeleton plays a minimum role in capsid localization. One HSV-1 capsid can harbor up to 900 copies of VP26 as it decorates on the tip of every hexons (*23*, *24*), protrusions of RFP protein everywhere on the capsid surface may have well interfered with the binding capacity to the nucleus through a none-specific interaction mechanism. We observed in each confocal cross-section, there is consistently 2 to 6 DNA filled capsids bind to each nuclei (Figure 6.1, panel O-R). 3D reconstruction from

continuous confocal slices estimated an average total of 30 to 50 RFP-capsids per nuclei (Figure 6.1M, 1N). These results unfortunately do not reflect true binding statistics of non-RFP labeled capsids (which we used for the quantification assay) as discussed.

6.5 Nuclear morphology and integrity in hyper-osmotic conditions

Now that we verified in our reconstructed cell-free system, viral capsids can successfully dock onto NPC on the nuclear membrane. We next confirmed that the nucleus remains in biologically competent condition upon addition of osmolytes. Figure 6.2 shows nuclei retained their morphology under osmotic pressure by PEG-8k or Dextran-155k. The interior of nuclei remains intact and structured, seen by differential interference contrast microscopy (DIC, first row panel in Figure 6.2). The total number of good nuclei remains unchanged as well (data not shown). The sub-nuclear structure of heterochromatin DNA was essentially unchanged upon addition of osmolytes, as visualized by Hoechst stain (second row panel in Figure 6.2). However we observed a slight shrink in nuclear size with presence of increasing osmolytes concentration. Studies show under hyper-osmotic stress, the nucleus size shrinks and assumes a more convoluted shape (*25-27*). In the hyper-osmotic range, the nucleus volume decrease in a linear pattern with decreased inverse normalized osmolarity (*25*). Previous results also indicate under hyper-osmotic conditions, distribution of Hoechst dye would become more heterogeneous due to altering in chromatin condensation (*26*). In our experimental condition, the change in distribution of Hoechst dye was not observable.

Osmotic pressure was know to play a role on nucleus transport, under hyper-osmotic stree, the rate of nuclear transport increased using passive diffusing nuclear cargo (*26*). Further studies show this rate change was mainly due to the decrease in the nuclear volume, resulting in a shorter effective diffusion distance. The nuclear permeability remains unchanged up to 480 mOsm (*26*). For our 30% PEG-8k (w/w)

solution, osmolarity is around 38.5 mOsm and for 30% Dextran-155k (w/w) solution, osmolarity is around 1.9 mOsm. This confirmation of nuclei integrity and functionality with addition of osmolytes is critical for our next step in the assay to monitor DNA ejection into nucleus under osmotic pressure.

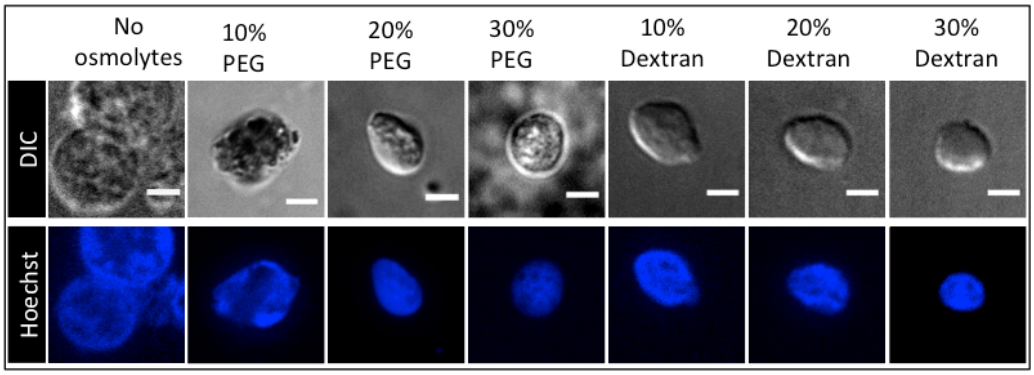

Figure 6.2: Osmotic pressure on nuclei function and morphology. Nuclei suspended in CBB buffer with 0% - 30% Osmolytes (PEG-8k or Dextran-155k) in surrounding. Nuclei were imaged by DIC shown in first row, we can see the nuclei morphology remained well up to 30% Dextran. Nuclear DNA were stained by Hoechst 33342 and shown in second row. Scale bar in all images: 3 μm

6.6 Quantification of viral DNA traces in the reconstituted system

Next, we quantified the capsid binding and DNA ejection efficiency, with being capable to track all traces of viral DNA in the reconstituted system. We carefully designed an incubation - pull down - qPCR assay for this purpose. After the HSV-1 C-capsid-nuclei incubation as previously described, the nuclei and extra-nuclear fluid were separated via low-speed centrifugation. The nuclei pellet sample was then re-suspended in surfactant (NP-40) containing buffer to break nuclear membrane. Nucleoplasm contents were thus released into the solution. A pull-down assay using anti-HSV1/2 ICP5/UL19 antibody and protein A beads were then performed to extract all the capsids away (along with those non-ejected, encapsidated viral DNAs). Any viral DNA traces left in the upper supernatant (sample-d) are from the intra-nuclear part. The pulled-down part (capsid pellets) was then treated with protease K to cut the protein-A beads off and digest the capsid shell, encapsidated

viral DNA part (sample-c) was then extracted using phenol-chloroform method. For the extra-nuclear fluid separated in the first centrifugation step, the same pull-down assay was performed to sediment all the non-nuclei associated capsids bound by HSV-1 antibody. This part of unbound capsids was quantified as sample-a. Any traces of free, non-encapsidated viral DNA in the extra-nuclear fluid is quantified as sample-b.

In the end, we successfully isolated viral DNA samples by: (a) free, non-capsid associated viral DNA (known as the contamination part) in the extra-nuclear fluid; (b) viral DNA from unbound capsids; (c) viral DNA from nuclear-membrane associated, but non-ejected particles; (d) viral DNA successfully translocated into nucleoplasm. Following the experimental flow, after we effectively isolated viral DNA samples (a), (b), (c), (d) (Figure 6.3A), we quantified HSV-1 gene copies in each sample using real-time qPCR analysis by custom TaqMan assays. Primers complimentary to VP16/UL48 and ICP0 sequences (located within IRL-IRS region) were chosen to estimate HSV-1 DNA copy numbers within our samples (Table 6.1).

Table 6.1 Quantification of HSV-1 DNA copy number in the *in vitro* genome translocation system by qPCR

marker	osmolyte concentration (w/w %)		Part a: viral DNA from unbound capsids	Part b: free viral DNA in the extra-nuclear fluid	Part c: non-ejected viral DNA	Part d: ejected viral DNA in the nucleoplasm	Control*: DNA detected after treating with Dnase I	Total copy number: (a+b+c+d)
	Dextran - 155k	PEG - 8k	Copy number (**×10^7**)					
ICP0	0	0	0.506 ± 0.176	15.093 ± 0.866	4.371 ± 0.332	186.543 ± 99.970	0.922 ± 0.068	206.51 ± 99.97
	30	0	1.903 ± 0.115	1.157 ± 0.097	3.447 ± 0.126	2.360 ± 0.231		8.87 ± 0.30
	0	30	0.022 ± 0.001	0.005 ± 0.000	560.646 ± 218.366	0.883 ± 0.043		561.56 ± 218.37
VP16	0	0	5.982 ± 0.698	57.966 ± 1.800	42.577 ± 8.205	4527.282 ± 3336.223	8.584 ± 0.816	4633.8 ± 3335.8
	30	0	37.684 ± 1.123	13.303 ± 2.998	63.063 ± 10.621	21.532 ± 6.196		135.58 ± 12.706
	0	30	0.124 ± 0.008	0.187 ± 0.136	5434.512 ± 4161.112	12.336 ± 2.068		5447.2 ± 4161.1

* A control is set up to detect the pull-down efficiency and qPCR background levels. In the control, an equivalent sample of Part b was prepared, then incubated with Dnase I at 37°C for 30 min to digest all the free DNA in the sample. The ICP0 and VP16 detected in the control sample is an indication of both traces of encapsidated DNA left (due to insufficient pull-down efficiency) and qPCR base level signal due to contamination.

When no osmolyte was introduced into the system, the vast majority of HSV-1 DNA isolated are intra-nuclear (sample-d in Figure 6.3A) after 30 min incubation time at 37°C and 95.5 ± 4.4% of the total capsids have been nuclei-bound (Figure 6.3B, 6.3C, 6.3D). Only a very small fraction is from the un-nuclei associated capsids (0.1 - 0.2%, sample-a in Figure 6.3A) or in free form in extra-nuclear fluid (less than 7%, part b in Figure 6.3A). By looking at percentage of intranuclear viral DNA copy number (sample-d) versus the total nuclei-associated viral copy number (sample-c + sample-d), we calculated that (98.4 ± 0.9) % of those nuclei-associated viral particles released their DNA into the nuclei during the 30 min time frame (Figure 6.3E). For any viral DNA that was not successfully ejected into the nuclei (ejected into extra-nuclear fluid instead), they will contribute to part b copy number instead.

As discussed earlier, sample-b consists free, non-encapsidated DNA (including contaminant DNA) in the extra-nuclear fluid. However, for any capsids that fail to be pulled and precipitated out from the supernatant, their encapsidated DNA contribute to sample-b as well. This fraction of sample-b is DNase-protective as the protein shell is non-permeable to DNase. By adding DNase I to sample b, we can quantify this encapsidated DNA part, which relates to those noon-successfully pulled capsids. Results show that this part only represented 1-6% of sample-b DNA.

6.7 Osmotic suppression of HSV-1 DNA ejection into the nuclei

Both ICP0 and VP16 qPCR results indicate that introduction of osmolytes did not interfere with our assay efficiency of DNA extraction. With presence or absence of 30% PEG, the total amount of DNA recovered from the assay (sum of DNA copy numbers from sample-a,b,c,d in Figure 6.3B) approximately equals. This is

important to show that quantity change of intra-nuclear DNA as we examined later (sample d) was not due to the change in total DNA extracted because of osmolytes. One thing to notice is that the DNA copy numbers in VP16 is in general one order of magnitude higher than that observed in ICP0 is due to the difference in qPCR efficiency because of primer-gene interactions.

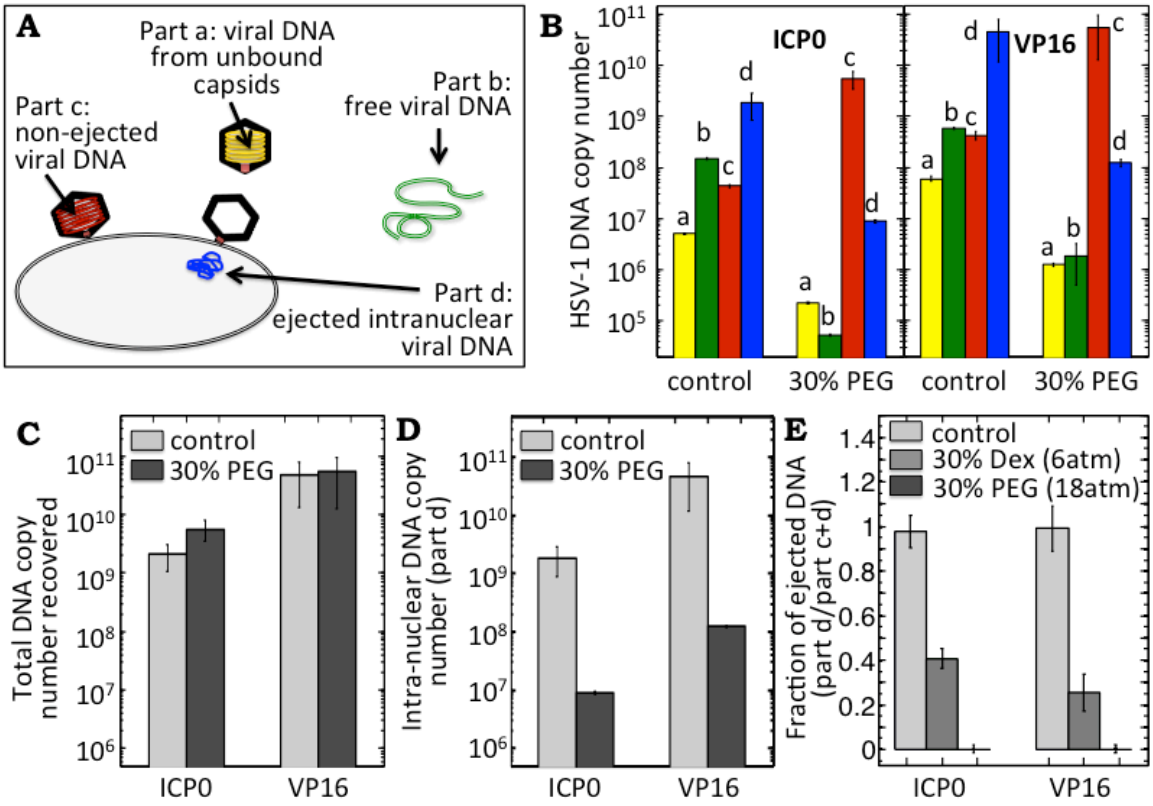

Figure 6.3 Track of DNA quantity in the reconstituted system. (A) Illustration of different DNA samples in the system. (B) Absolute HSV DNA copy number calculated from each DNA samples from the assay described in figure 4. Copy numbers were quantified by real time qPCR method. Coy numbers were obtained based on standard curve set by serial diluted wild type HSV-1 DNA with known copy numbers. Primers based on ICP0 (upper panel) and VP16 (lower panel) sequences were both used for quantification of HSV genes. (C) Total amount of DNA recovered from this assay, with presence or absence of osmolytes. Note that number in (C) is a summation of numbers from a,b,c,d samples. (D) Intra-nuclear viral DNA copy number, corresponding to part d in (B). (E) Ratio of intra-nuclear viral DNA copy (c) divided by total copy number of nuclei-associated viral DNAs (c+d). This is c/c+d and indicating efficiency of DNA ejection from nuclei-bound HSV-1s. Error bar in (B) and (D) are

standard derivations in copy numbers from 3 PCR reactions repeated at exactly the same conditions. Error bar in (C) and (E) are progressed standard derivations by using $\sigma(\sum a,b,c,d) = \sqrt{\sigma_a^2 + \sigma_b^2 + \sigma_c^2 + \sigma_d^2}$

* In all figures: control, no osmolytes, 30% PEG, with 30% PEG-8k, 30% Dex, with 30% w/w Dextran-155k.

With addition of 30% PEG-8k, the percentage of total nuclei-associated capsids. (sample-c + sample-d) slightly increased, from 95.5 ± 4.4 % to 99.9 ± 0.0 % . In parallel with the result that unbound en-capsidated and free viral DNA in extranuclear fluid (sample-a, b) decreased upon addition of PEG. This observation was likely due to the crowding effect of PEG, that osmolytes condense capsids around nuclei, thus enhancing the binding efficiency of capsids to nuclear membrane.

We can see that upon addition of 30% PEG-8k (18 atm), the nuclear membrane bound, non-ejected viral copy numbers (sample-c) dramatically increased in parallel with a significant drop of the intra-nuclear viral DNA (sample-d). The intra-nuclear viral DNA (sample-d) is of our most interests. Quantification of this sample gives us idea about viral translocation efficiency into the nucleoplasm. We can see in Figure 4D, the amount of successfully ejected DNA into nucleoplasm dropped 99% with presence of PEG-8k. This striking decrease indicates a strong effect of osmolytes on DNA ejection. Earlier work done by the groups shows that PEG-8k at concentration of 30% w/w (corresponding to 18 atm, Figure 6.3E) lead to complete suppression of genome release in a nuclear-free solution system by trypsin induced DNA ejection (*5*). This work confirms that in the reconstructed nuclei system where capsids are docked onto NPC, osmolytes again powerfully inhibits genome translocation into the nucleoplasm.

Figure 6.3E shows the fraction of DNA ejected of the total nuclei-associated viral particles, sample-d/ (sample-c + sample-d). We can see that with presence of 30% PEG, less than 0.3% percentage of DNA were ejected, which confirms a strong inhibition of DNA release due to osmotic pressure. To verify that this inhibition effect were non-osmolyte specific, we also repeated the experiment with presence of 30% dextran-155k, which can build an osmotic pressure of around 5.6 atm around in the extra-nuclear fluid. Viscosity of dextran 155k increased linearly with increasing concentration. For dextran 155k, 30% is the highest working

concentration we can achieve. We can see that at this lower pressure, an average of 33% DNA were successfully ejected into the nucleoplasm. As shown later in the results, this correlates well with the in vitro, nuclei-free system of ejected DNA length portion at 5.6 atm (Figure 6.4).

6.8 HSV-1 DNA ejection lengths with increasing external osmotic pressure in a nuclei-free system

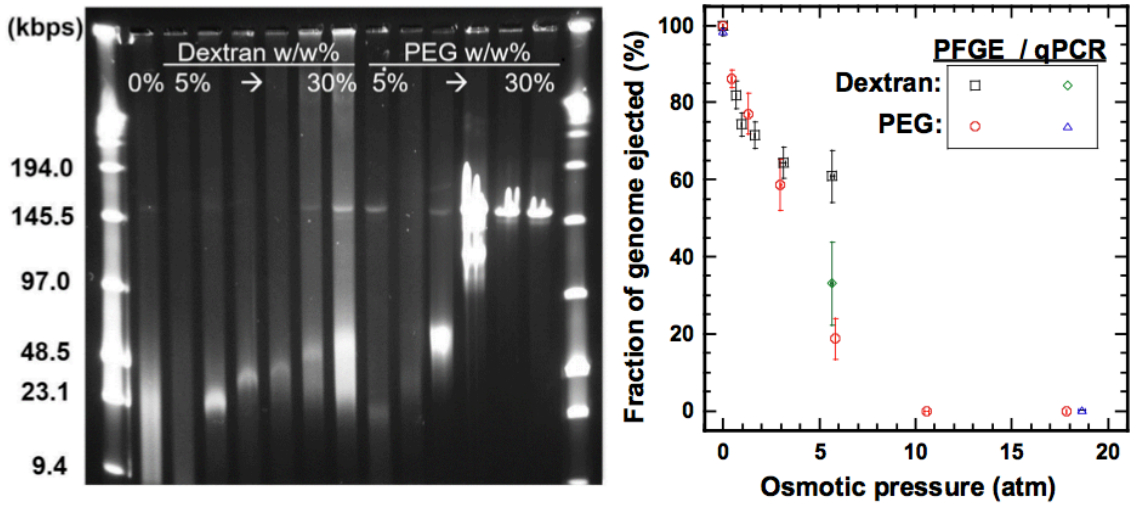

Figure 6.4: Osmotic pressure on HSV DNA ejection in a nuclear-free system (A) Pulse field electrophoresis (PFGE) of ejected DNA fragments after osmotic inhibition by PEG-8k and Dextran-155k (B) plot of ejected DNA fraction vs. increasing osmotic pressure, result both by PFGE and by qPCR.

To confirm the osmotic pressure effect on ejected DNA length in HSV-1 in our buffer system (with different ionic condition than previously published (*5*)), we repeated the experiments using pulse-field electrophoresis (PFGE) to measure the (non-) ejected length of DNA fragments with increasing PEG 8000 concentration (*5*). Similar experiments were also done with Dextran-155k. In this assay, the DNA ejection from HSV-1 was triggered with trypsin, followed with DNase I treatment, and the non-ejected DNA within capsids was then extracted by SDS and protease K treatment and loaded onto PFGE for gel analysis. Figure 6.4 shows that the presence

of 25% PEG w/w would completely suppressed DNA ejection, which corresponds to an internal pressure of ~11 atm within HSV-1 capsids balanced by an external osmotic pressure of equal magnitude.

Previous results show that encapsidated viral DNA pressure is dependent on cat-ion ionic strength of the sitting buffer (*4*, *28-31*). HSV-1 genome pressure was measured to be 18 atm in TM buffer (50 mM Tris, 10 mM MgSO4, pH7.4) with ionic strength of 0.02 M (*5*). In this assay, the ionic strength of CBB buffer is 0.054 M, about 2.5 fold of that in TM buffer. Additional cations in solution help in screening viral DNA surface charge, thus reducing inter-strand repulsions and lowered the encapsidated DNA pressure. Dextran-155k was shown to have similar inhibition effect at concentrations up to 30% (which corresponds to 5.6 atm). The fact that in our isolated-nuclei assay, a mean of 33% DNA was ejected with 30% Dextran (average value from ICP0 and VP16 result) and 0.2% DNA were ejected with 30% PEG correspond well with these nuclei-free assay result.

6.9 Conclusions

Internal genome pressure was known to exist inside HSV-1 capsid. This result demonstrates for the first time, that genome ejection from HSV-1 to nucleus can be completely suppressed by varying external osmotic pressure. An in vitro system was reconstituted to monitor the HSV-1 DNA ejection into isolated nucleus. The reconstituted system allowed introducing osmolarity into the extra-nuclear environment, thus investigating the effects of osmotic pressure on viral genome ejection. The nuclear morphology and sub-nuclear chromosomal DNA structure were proved to be preserved under osmotic pressure up to 18 atm. We found striking results that DNA ejection into nucleoplasm was reduced 99% under osmotic pressure of 18 atm. This research shed light on future studies of how viral DNA ejects in vivo and suggest a common mechanism for viral infection in double-stranded DNA viruses.

References for Chapter 6

1. D. C. Rau, B. Lee, V. A. Parsegian, Measurement of the Repulsive Force between Poly-Electrolyte Molecules in Ionic Solution - Hydration Forces between Parallel DNA Double Helices. *P Natl Acad Sci-Biol* **81**, 2621-2625 (1984).
2. A. Cordova, M. Deserno, W. M. Gelbart, A. Ben-Shaul, Osmotic shock and the strength of viral capsids. *Biophysical journal* **85**, 70-74 (2003).
3. S. C. Riemer, V. A. Bloomfield, Packaging of DNA in bacteriophage heads: some considerations on energetics. *Biopolymers* **17**, 785-794 (1978).
4. A. Evilevitch, L. Lavelle, C. M. Knobler, E. Raspaud, W. M. Gelbart, Osmotic pressure inhibition of DNA ejection from phage. *Proceedings of the National Academy of Sciences of the United States of America* **100**, 9292-9295 (2003).
5. D. W. Bauer, J. B. Huffman, F. L. Homa, A. Evilevitch, Herpes virus genome, the pressure is on. *J Am Chem Soc* **135**, 11216-11221 (2013).
6. B. Sodeik, M. W. Ebersold, A. Helenius, Microtubule-mediated transport of incoming herpes simplex virus 1 capsids to the nucleus. *J Cell Biol* **136**, 1007-1021 (1997).
7. W. Batterson, D. Furlong, B. Roizman, Molecular genetics of herpes simplex virus. VIII. further characterization of a temperature-sensitive mutant defective in release of viral DNA and in other stages of the viral reproductive cycle. *Journal of virology* **45**, 397-407 (1983).
8. K. Bodoor *et al.*, Function and assembly of nuclear pore complex proteins. *Biochem Cell Biol* **77**, 321-329 (1999).
9. S. Cohen, S. Au, N. Panté, How viruses access the nucleus. *Biochimica et Biophysica Acta (BBA) - Molecular Cell Research* **1813**, 1634-1645 (2011).
10. P. M. Ojala, B. Sodeik, M. W. Ebersold, U. Kutay, A. Helenius, Herpes simplex virus type 1 entry into host cells: reconstitution of capsid binding and uncoating at the nuclear pore complex in vitro. *Molecular and cellular biology*

20, 4922-4931 (2000).

11. J. F. Conway *et al.*, Labeling and localization of the herpes simplex virus capsid protein UL25 and its interaction with the two triplexes closest to the penton. *Journal of molecular biology* **397**, 575-586 (2010).
12. U. Sae-Ueng *et al.*, Major capsid reinforcement by a minor protein in herpesviruses and phage. *Nucleic acids research* **42**, 9096-9107 (2014).
13. D. Pasdeloup, D. Blondel, A. L. Isidro, F. J. Rixon, Herpesvirus capsid association with the nuclear pore complex and viral DNA release involve the nucleoporin CAN/Nup214 and the capsid protein pUL25. *Journal of virology* **83**, 6610-6623 (2009).
14. G. Blobel, V. R. Potter, Nuclei from rat liver: isolation method that combines purity with high yield. *Science* **154**, 1662-1665 (1966).
15. S. Loret, N. El Bilali, R. Lippé, Analysis of herpes simplex virus type I nuclear particles by flow cytometry. *Cytometry Part A* **81A**, 950-959 (2012).
16. G. Remillard-Labrosse, G. Guay, R. Lippe, Reconstitution of herpes simplex virus type 1 nuclear capsid egress in vitro. *Journal of virology* **80**, 9741-9753 (2006).
17. A. M. Copeland, W. W. Newcomb, J. C. Brown, Herpes simplex virus replication: roles of viral proteins and nucleoporins in capsid-nucleus attachment. *Journal of virology* **83**, 1660-1668 (2009).
18. M. Eriksson, H. J. Karlsson, G. Westman, B. Akerman, Groove-binding unsymmetrical cyanine dyes for staining of DNA: dissociation rates in free solution and electrophoresis gels. *Nucleic acids research* **31**, 6235-6242 (2003).
19. M. Reuter, D. T. Dryden, The kinetics of YOYO-1 intercalation into single molecules of double-stranded DNA. *Biochem Biophys Res Commun* **403**, 225-229 (2010).
20. B. Alberts, *Molecular biology of the cell*. (Garland Science, New York, ed. 4th, 2002), pp. xxxiv, 1548 p.

21. G. G. Maul, L. Deaven, Quantitative determination of nuclear pore complexes in cycling cells with differing DNA content. *J Cell Biol* **73**, 748-760 (1977).
22. M. W. Douglas *et al.*, Herpes simplex virus type 1 capsid protein VP26 interacts with dynein light chains RP3 and Tctex1 and plays a role in retrograde cellular transport. *The Journal of biological chemistry* **279**, 28522-28530 (2004).
23. F. P. Booy *et al.*, Finding a needle in a haystack: detection of a small protein (the 12-kDa VP26) in a large complex (the 200-MDa capsid of herpes simplex virus). *Proceedings of the National Academy of Sciences of the United States of America* **91**, 5652-5656 (1994).
24. C. H. Nagel, K. Dohner, A. Binz, R. Bauerfeind, B. Sodeik, Improper tagging of the non-essential small capsid protein VP26 impairs nuclear capsid egress of herpes simplex virus. *PloS one* **7**, e44177 (2012).
25. J. D. Finan, K. J. Chalut, A. Wax, F. Guilak, Nonlinear osmotic properties of the cell nucleus. *Ann Biomed Eng* **37**, 477-491 (2009).
26. J. D. Finan, H. A. Leddy, F. Guilak, Osmotic stress alters chromatin condensation and nucleocytoplasmic transport. *Biochem Biophys Res Commun* **408**, 230-235 (2011).
27. J. D. Finan, F. Guilak, The effects of osmotic stress on the structure and function of the cell nucleus. *J Cell Biochem* **109**, 460-467 (2010).
28. A. Evilevitch *et al.*, Effects of salt concentrations and bending energy on the extent of ejection of phage genomes. *Biophysical journal* **94**, 1110-1120 (2008).
29. T. Liu *et al.*, Solid-to-fluid-like DNA transition in viruses facilitates infection. *Proceedings of the National Academy of Sciences of the United States of America* **111**, 14675-14680 (2014).
30. U. Sae-Ueng *et al.*, Solid-to-fluid DNA transition inside HSV-1 capsid close to the temperature of infection. *Nature chemical biology* **10**, 861-867 (2014).
31. D. Li *et al.*, Ionic switch controls the DNA state in phage lambda. *Nucleic acids*

research **43**, 6348-6358 (2015).

CHAPTER 7 SUMMARY AND CONCLUSIONS

Genome release constitutes a major part in viral infection and replication cycles. The genome translocation process in double-stranded DNA viruses was studied extensively in the previous biophysical work (Chapter 1): from frictional and pressure-driven forces controlling ejection step (*1-6*); to ejection kinetics studied by bulk (*2*, *4*, *6-10*) and single-particle (*11-13*) approaches; to more recent studies in our group on relationship between DNA phases/states and genome release efficiency (*14-16*). Studies from these researches provide deep insights into how viral particles gain the capability to release its genome in extreme efficiency *in vivo*. As the interest is in the general physical characteristics, many discoveries made were directly applicable to other viral systems of diverse evolutionary origin and have been confirmed in multiple viral strains. For example, one principal breakthrough in the field was the existence of internal pressure. It was learnt as early as in 1970s that viral DNA adopts an extraordinarily ordered and dense-packed structure inside the capsid (*17-20*). It has been postulated for a long time that this extremely compact structure stores an enormous energy inside. It was first experimentally proved in 2003 that this stored internal energy exhibits a large pressure against capsid wall and serves as the driving force during DNA translocation step (*1*). Subsequent studies have been done on other phages (*6*, *9*, *10*) and in 2013 it was first confirmed in eukaryotic viruses (HSV-1) that internal pressure of similar magnitude exists and decrease of this en-capsidated pressure by applying osmolytes around the capsids can lead to complete inhibition of genome release (*21*).

All these work shed lights on how viruses work during infection and provide insights onto next-generation anti-viral medicine development. However, lots of questions remain unanswered in the field. For example, how could viral genome

packaged at crystal density gain high mobility during infection? In this thesis, we discovered a solid-to-fluid DNA transition in the viral genome. This transition provides flexibility and packing defects in the core region of a well-packed intracapsid DNA molecule, which gains the DNA polymer more fluidity. This crucial transition is only switched on when viral particles are under physical environments optimized for infection purposes (Chapter 3 and 4). The experiments presented relied on a range of techniques including isothermal titration calorimetry, solution small-angle x-ray scattering, fluorescence and electron microscopy, capsid pull-down and real-time quantitative PCR assays (Chapter 2). A large portion of this dissertation focused on the intracapsid DNA state and how it relates the genome ejection efficiency. These efforts focused on setting up *in vitro* assays to investigate how physical parameters such as temperature and ionic strength, osmotic pressure (Chapter 6) regulate genome ejection (Chapter 5).

With all the previous fundamental work and understandings of the viral ejection machinery, we eventually set up a reconstructed cell nuclei system using isolated rat liver cell nuclei and cytosol homogenate, along with some other critical host cell factors (with reference to work in (*22*, *23*)). We investigated genome ejection efficiency by adding purified HSV-1 C capsids with absence or presence of high concentration osmolytes. The results show that when osmolytes are introduced into this reconstructed system, genome releases from C capsids are reduced as much as 99%. This striking observation confirms our understanding of how internal pressure serve as the main driving force during genome translocation in viral infection.

With all the discoveries made in this thesis, we hope it could trigger more extensive studies on viruses from different origins, or deeper understanding of how physical parameters regulate genome ejection process. For example, the concept of inter-DNA strand frictional force was mentioned in Chapter 3, we are looking for

more thought-provoking mechanism discussions of the nature of this frictional force and how it plays an essential role as the internal pressure in genome ejection machinery. With all these being said, we hope that studies in this thesis can ignite bigger sparks on physical virology, and results can be applied in more biologically profound contexts, with the aim to understand better what is really happening *in vivo*.

References for Chapter 7

1. A. Evilevitch, L. Lavelle, C. M. Knobler, E. Raspaud, W. M. Gelbart, Osmotic pressure inhibition of DNA ejection from phage. *Proceedings of the National Academy of Sciences of the United States of America* **100**, 9292-9295 (2003).
2. P. Grayson *et al.*, The effect of genome length on ejection forces in bacteriophage lambda. *Virology* **348**, 430-436 (2006).
3. I. Ivanovska, G. Wuite, B. Jonsson, A. Evilevitch, Internal DNA pressure modifies stability of WT phage. *Proceedings of the National Academy of Sciences of the United States of America* **104**, 9603-9608 (2007).
4. D. Lof, K. Schillen, B. Jonsson, A. Evilevitch, Forces controlling the rate of DNA ejection from phage lambda. *Journal of molecular biology* **368**, 55-65 (2007).
5. A. Evilevitch *et al.*, Effects of salt concentrations and bending energy on the extent of ejection of phage genomes. *Biophysical journal* **94**, 1110-1120 (2008).
6. M. de Frutos, L. Letellier, E. Raspaud, DNA ejection from bacteriophage T5: analysis of the kinetics and energetics. *Biophysical journal* **88**, 1364-1370 (2005).
7. E. Raspaud, T. Forth, C. Sao-Jose, P. Tavares, M. de Frutos, A kinetic analysis of DNA ejection from tailed phages revealing the prerequisite activation energy. *Biophysical journal* **93**, 3999-4005 (2007).
8. C. Sao-Jose, M. de Frutos, E. Raspaud, M. A. Santos, P. Tavares, Pressure built by DNA packing inside virions: enough to drive DNA ejection in vitro, largely insufficient for delivery into the bacterial cytoplasm. *Journal of molecular biology* **374**, 346-355 (2007).
9. A. Leforestier *et al.*, Bacteriophage T5 DNA ejection under pressure. *Journal of molecular biology* **384**, 730-739 (2008).
10. W. M. Gelbart, C. M. Knobler, Pressurized Viruses. *Science* **323**, 1682-1683 (2009).
11. S. Mangenot, M. Hochrein, J. Radler, L. Letellier, Real-time imaging of DNA

ejection from single phage particles. *Current biology : CB* **15**, 430-435 (2005).
12. D. N. Fuller *et al.*, Measurements of single DNA molecule packaging dynamics in bacteriophage lambda reveal high forces, high motor processivity, and capsid transformations. *Journal of molecular biology* **373**, 1113-1122 (2007).
13. P. Grayson, L. Han, T. Winther, R. Phillips, Real-time observations of single bacteriophage lambda DNA ejections in vitro. *Proceedings of the National Academy of Sciences of the United States of America* **104**, 14652-14657 (2007).
14. T. Liu *et al.*, Solid-to-fluid-like DNA transition in viruses facilitates infection. *Proceedings of the National Academy of Sciences of the United States of America* **111**, 14675-14680 (2014).
15. U. Sae-Ueng *et al.*, Solid-to-fluid DNA transition inside HSV-1 capsid close to the temperature of infection. *Nature chemical biology* **10**, 861-867 (2014).
16. D. Li *et al.*, Ionic switch controls the DNA state in phage lambda. *Nucleic acids research* **43**, 6348-6358 (2015).
17. W. Earnshaw, S. Casjens, S. C. Harrison, Assembly of the head of bacteriophage P22: x-ray diffraction from heads, proheads and related structures. *Journal of molecular biology* **104**, 387-410 (1976).
18. L. C. Gosule, J. A. Schellman, Compact form of DNA induced by spermidine. *Nature* **259**, 333-335 (1976).
19. W. C. Earnshaw, S. C. Harrison, DNA arrangement in isometric phage heads. *Nature* **268**, 598-602 (1977).
20. M. Feiss, R. A. Fisher, M. A. Crayton, C. Egner, Packaging of Bacteriophage-Lambda Chromosome - Effect of Chromosome Length. *Virology* **77**, 281-293 (1977).
21. D. W. Bauer, J. B. Huffman, F. L. Homa, A. Evilevitch, Herpes virus genome, the pressure is on. *J Am Chem Soc* **135**, 11216-11221 (2013).
22. P. M. Ojala, B. Sodeik, M. W. Ebersold, U. Kutay, A. Helenius, Herpes simplex virus type 1 entry into host cells: reconstitution of capsid binding and

uncoating at the nuclear pore complex in vitro. *Molecular and cellular biology* **20**, 4922-4931 (2000).

23. K. Rode *et al.*, Uncoupling uncoating of herpes simplex virus genomes from their nuclear import and gene expression. *Journal of virology* **85**, 4271-4283 (2011).